

# **Durability Over Time of Skin Used for JAMA–JARI Pedestrian Headform Impactor Measured by Biofidelity Certification Testing**

**Yasuhiro Matsui**

Japan Automobile Research Institute

**Masaaki Tanahashi**

Japan Automobile Manufacturers' Association, Inc.

Japan

Paper Number 05-0007

## **ABSTRACT**

Head injuries are the most common cause of pedestrian deaths in car–pedestrian accidents. To reduce the severity of such injuries, the ISO, IHRA and Japan MLIT proposed subsystem tests in which a headform impactor is impacted upon a car bonnet top. JAMA and JARI have developed the headform impactors in compliance with the ISO standard, the IHRA recommendation and the Japan MLIT safety regulation. The impactor consists of the core and skin. Since the skin is made of nonferrous material, the stiffness of the skin would be changed due to time elapse. The stiffness of the skin was confirmed by assessing the peak resultant acceleration of the gravity center measured in the biofidelity certification test, the so-called drop certification test. The ISO, IHRA and Japan MLIT specified the corridor of the peak acceleration impact must range from 245 to 300 G for a child headform impactor. In the present study, the newly developed skin durability over time at 0 month, 13, 16, 19, 22, 25, 28 and 31 months after manufacture was investigated in a room either with or without control of temperature and humidity. The results indicated that the peak acceleration impact using the two skins immediately after manufacture was 270 G. The peak acceleration of 287 G using the skin kept in a room with control of temperature and humidity increased 17G at 31 months after manufacture. The peak acceleration impact of 288 G using the skin kept in a room without control of temperature and humidity increased 18 G at 31 months after manufacture. The respective increases of 17 G and 18 G correspond to 31% and 33% of the range of certification test corridor (55 G), respectively. These results indicate that if the acceleration is close to the middle of the drop certification corridor (272.5 G) immediately after purchase by a testing facility, the skin is available for pedestrian impact test use with a storage period of at least 31 months. The results also suggest that if the acceleration is close to the upper limit of the drop certification corridor (300 G), the skin expiration time may be drawing very near. The findings also indicated temperature and humidity did not significantly affect the skin durability over time.

## **INTRODUCTION**

Head injuries are the most common cause of pedestrian deaths in car–pedestrian accidents, and countermeasures against them are of the highest priority in traffic safety strategy [1]. The key element in this strategy is improvement of the safety performance of the car front. To reduce the severity of pedestrian head injuries in bonnet top contacts, the International Organization for Standardization (ISO) [2][3] and International Harmonized Research Activities (IHRA) [4] have proposed subsystem tests in which a headform impactor is impacted upon a car bonnet top. The ISO and IHRA have specified the biofidelity requirements for the headforms in terms of the peak value of the resultant centre of gravity (CG) acceleration measured in biofidelity certification tests (hereafter referred to as the drop certification test).

In 2004, the Japan Ministry of Land, Infrastructure and Transport (Japan MLIT) officially announced the Japanese safety regulation for the evaluation of car–front safety performance in terms of pedestrian head protection. The Japanese standard requires headform impactors to be in compliance with the IHRA specification. The IHRA required the specification of headform impactor for mass, diameter, moment of inertia, location of center of gravity, seismic mass location of accelerometer, first natural frequency and resultant acceleration in the biofidelity certification test as listed in Table 1. The same table also indicates that any impactor built according to the IHRA proposal [5] fulfills the ISO specifications [2][3]. The Japan Automobile Manufacturers' Association (JAMA) and the Japan Automobile Research Institute (JARI) have thus far jointly developed headform impactors which are compliant with the ISO/IHRA/Japan MLIT requirements (hereafter referred to as the JAMA–JARI headform impactor) [6]. The JAMA–JARI headform impactor consists of the core (sphere and baseplate) and the skin which is made of polyvinyl chloride (PVC) (Figure 1). Skin stiffness was confirmed by assessing the peak resultant acceleration of the gravity center measured in the drop certification test. Since the skin material is nonferrous, the skin impact durability and

Table 1 Pedestrian headform impactor measurement parameters required by ISO, IHRA, Japan MLIT, and parameters measured in present and other [6, 7] studies

Measured parameter	Required by			Investigation
	ISO	IHRA	Japan MLIT	Prototype JAMA-JARI headform
1) Mass	✓	✓	✓	Reference [6]
2) Diameter	✓	✓	✓	
3) Moment of inertia		✓	✓	
4) Location of centre of gravity	✓	✓	✓	
5) Seismic mass location of accelerometer		✓	✓	
6) First natural frequency		✓	✓	
7) Resultant acceleration in biofidelity test (drop test)	✓	✓	✓	
8) Shore hardness of skin				Reference [7]
9) Quasi-static compression characteristic of skin				
10) Resultant acceleration in high velocity certification test				
11) Impact durability of skin				Present study
12) Durability over time of skin				

ISO: International Organization for Standardization  
 IHRA: International Harmonized Research Activities  
 Japan MLIT: Japan Ministry of Land, Infrastructure and Transport

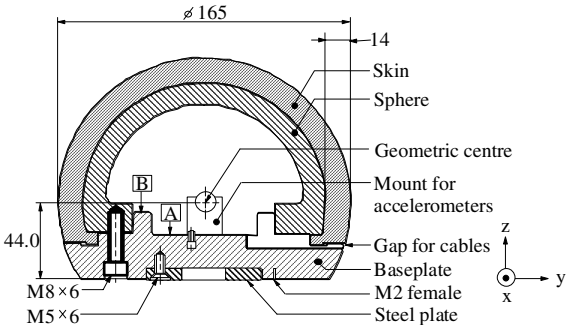


Figure 1. Schematic design of JAMA-JARI child headform impactor (unit: mm).

skin durability over time should be clarified. Matsui et al. [7] investigated some skin characteristics (see Table 1: measured parameters from eighth to eleventh) used for the JAMA-JARI headform impactor, which involves the skin impact durability against a car bonnet. This result indicated that when the drop certification test was run following a total of 50 impacts of the JAMA-JARI headform impactor against the car bonnet, the peak resultant acceleration decreased a mean 13 G. However, the durability over time of the skin used for the JAMA-JARI headform impactor has not been investigated to date, since a certain time must elapse after the development of the skin. Therefore, the aim of the present study is to clarify the durability over time of the skin used for JAMA-JARI headform impactors (see Table 1: twelfth measured parameter). The present study first discussed the suitable method for the durability over

time of the skin, and second investigated the durability over time of newly developed skin for 31 months after manufacture.

## METHOD

### Verification of Biofidelity Certification Test

The purpose of this section is to determine a suitable method to measure the skin durability over time. A drop certification test was utilized by ISO/IHRA/Japan MLIT (Figure 2) to investigate scatter in drop certification testing, scatter in skin reproducibility and recovery of skin after impact by means of the JAMA-JARI child headform impactor.

### Scatter in drop certification testing

The drop certification test setup was shown in Figure 2. The headform impactor was dropped by instant release from a height of 376 mm onto a rigidly-supported, flat horizontal steel plate (55 mm thick and 610 mm<sup>2</sup>) with a clean dry surface using a drop angle of 60°, i.e., close to the mean drop angle proposed by the ISO (54°) and category 1 of the IHRA (65°). To investigate possible scatter in the drop certification testing, we performed fifteen repeated tests of the headform impactor. One newly manufactured skin was employed. The skin was not removed from the sphere of the headform impactor during the present investigation. The impact point of the skin surface was the same throughout all fifteen tests. The time interval of each test was 24 hours to avoid the possible effect of delayed recovery of skin after impact on the present test results. To avoid the

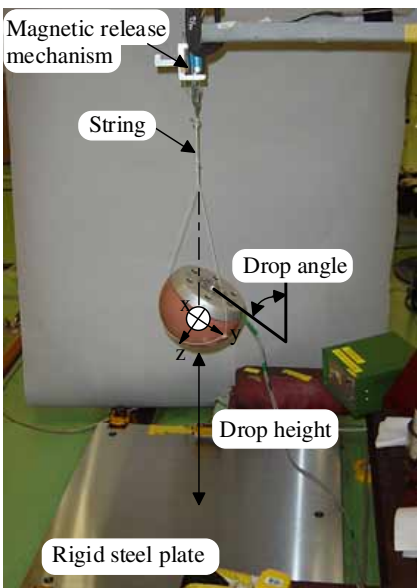


Figure 2. Drop certification test setup.

possible effect of temperature on the skin stiffness, the skin was left in the test room for 24 hours before the first test. The room had a constant temperature of about 21.4°C.

In the present research, three ENDEVCO type 7264B accelerometers [8] were employed. In the process of acceleration recording, each datum measured by the accelerometer was sampled at 10 kHz, and batch data processing was performed with a channel filter class (CFC) 1000. The results of the drop certification test were assessed by means of the peak resultant acceleration calculated from three axis accelerations. The standard deviation of the 15 peak resultant acceleration was calculated.

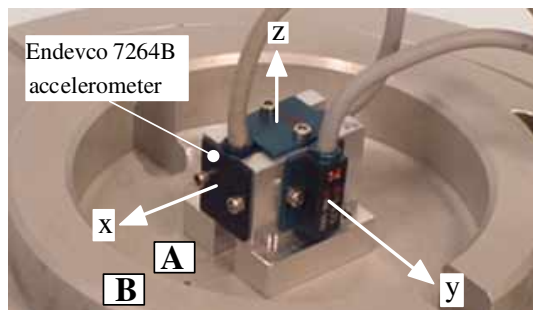


Figure 3. Accelerometers mounted on JAMA-JARI headform impactor.

#### Scatter in skin product repeatability

To investigate possible scatter in skin product repeatability, the drop certification tests were performed for the headform impactor employing nine newly manufactured skins. The headform impactor was rotated 120° around z-axis after each test. Therefore, three locations on one skin were impacted as shown in Figure 4. The time interval of each test was 24 hours. The standard deviation of 27 impact test results (3 impact locations for 9 skins) was calculated.

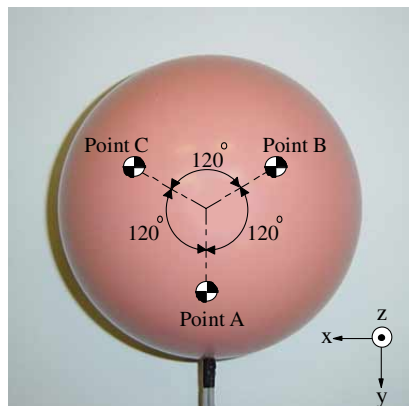


Figure 4. Impact points (View from top).

#### Recovery of skin after impact

To investigate the recovery of skin after impact, the drop certification tests were performed for the headform impactor employing one newly manufactured skin. The point A (Figure 4) was impacted 4 times, repeatedly. The time interval of each impact test was put at 24, 6 and 2 hours, respectively. On the contrary, the test results will appear in the order of 0, 2, 6 and 24 hours. Point B (Figure 4) was also impacted 4 times using the same procedure employed for the investigation at point A. The presently employed skin was not removed from the sphere of the headform impactor during this investigation.

#### Skin Durability Over Time

To investigate the skin durability over time, the drop certification tests were performed for the child headform impactor employing two newly manufactured skins. The headform impactor in which each skin was equipped was kept in a room either with or without control of temperature and humidity to investigate the effect of atmosphere on skin durability over time. The investigation period was 31 months after factory shipping. The temperature and humidity over a day in a room with control of temperature and humidity, where one skin (hereafter referred to as skin A) has been kept in are shown in Figure 5. The temperature and relative humidity were controlled at  $21.4 \pm 0.8^\circ\text{C}$  and  $45 \pm 15\%$  for 31 months, respectively.

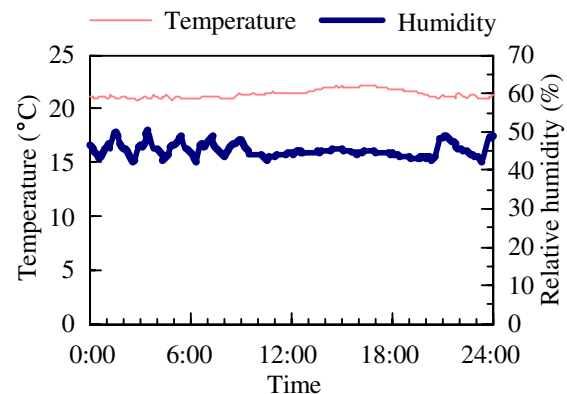


Figure 5. Temperature and humidity over a day in a room with control of temperature and humidity where skin A was kept.

The temperature over one year in a room without control of temperature and humidity, where another skin (hereafter referred to as skin B) has been kept, is shown in Figure 6. The highest temperature (36°C) was recorded in August, and the lowest (4°C) in December. The humidity over one year in room without control of temperature and humidity where

skin B has been kept is shown in Figure 7. The highest relative humidity (81%) was recorded in July, and the lowest (8%) in March. Overall, a relative high

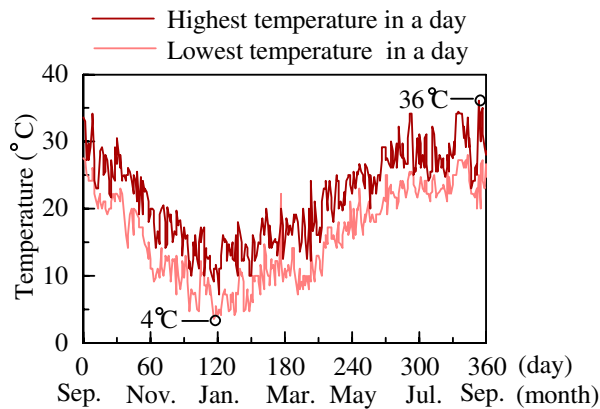


Figure 6. Temperature over one year in a room without control of temperature and humidity where skin B was kept.

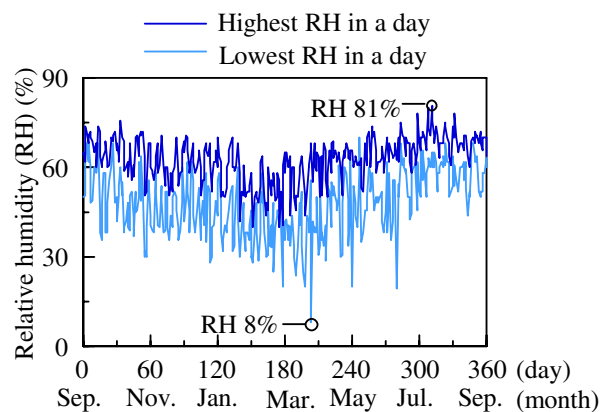


Figure 7. Humidity over one year in a room without control of temperature and humidity where skin B was kept.

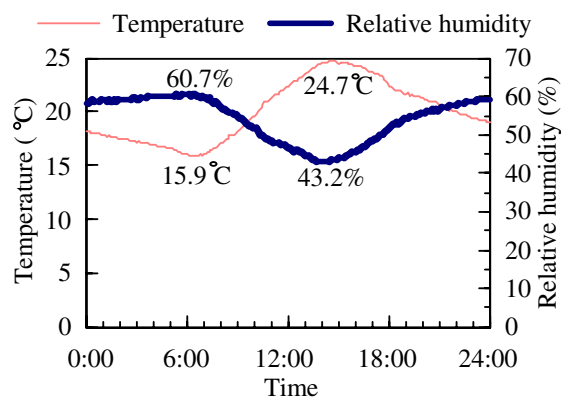


Figure 8. Temperature and humidity over one day in a room without control of temperature and humidity where skin B was kept.

humidity of sometimes over 70% was frequently observed during the monsoon months of June and July. On a day in October, the temperature ranged from 15.9°C to 24.7°C and the humidity from 43.2% to 60.7% (Figure 8). Therefore, skin B was stored in the condition in which the temperature and humidity always ranged widely over 31 months.

The drop certification tests were performed for the child headform impactor at 0 month, 13, 16, 19, 22, 25, 28 and 31 months after manufacture. Skin B was put in the test room for 24 hours before the test. The room had a constant temperature of about 21.4°C.

The headform impactor was rotated 120° around z-axis after each test, so three locations on one skin were impacted as shown in Figure 4. Based on the results obtained through preliminary investigations, the time interval of each test was put at 2 hours, and the skins were not removed from the spheres of the headform impactor during this investigation (31 months).

## RESULTS

### Verification of Biofidelity Certification Test

#### Scatter in drop certification testing

The peak resultant acceleration measured by fifteen drop certification tests employing one newly manufactured skin is shown in Table 2. The mean peak resultant acceleration was 272.7 G, which corresponds to the middle of the drop certification corridor (272.5 G). The standard deviation was 3.6 G, while the coefficient of variance was 1.3%. Thus, there was good repeatability.

Table 2 Peak resultant accelerations measured from fifteen drop certification test for one newly manufactured skin (time interval of each test was 24 hours)

Peak resultant accel. (G)					
n=15			Mean	SD	CV (%)
268	268	275	272.7	3.6	1.3
271	277	276			
268	277	271			
273	277	271			
276	268	274			

#### Scatter in skin product repeatability

The peak resultant accelerations measured from twenty-seven drop certification tests employing nine newly manufactured skins are shown in Table 3. The mean peak resultant acceleration was 268.0 G, the standard deviation 2.4 G with a coefficient of variance of 0.9%.



When we focused on the standard deviation obtained in the previous section on “scatter in drop certification testing,” it was higher (3.6 G) than the standard deviation obtained in the present section on “scatter in skin product repeatability” (2.4 G). Therefore, we should focus on the scatter in drop certification testing, since it was higher than that in skin product repeatability. Approximately 95% of the scatter in the drop certification testing was calculated to be 7.2 G (2\*SD). The 95% scatter (7.2 G) corresponds to 26% of the half range (27.5 G) of the biofidelity certification test corridor (55 G) proposed by ISO/IHRA/Japan MLIT. Thus, scatter did not have a significant influence on the drop certification test results. Therefore, the test condition in the previous section was employed for the section on “investigation of skin durability over time,” where the skin was not removed from the sphere of the headform impactor during the investigation.

Table 3 Peak resultant accelerations measured from drop certification test for nine newly manufactured skins (time interval of each test was 24 hours)

Skin	Peak resultant accel. (G)					
	Point A	Point B	Point C	Mean	SD	CV (%)
#1	270	265	264	266.3	3.2	1.2
#2	270	267	268	268.3	1.5	0.6
#3	270	268	271	269.7	1.5	0.6
#4	269	266	266	267.0	1.7	0.6
#5	269	272	265	268.7	3.5	1.3
#6	263	268	270	267.0	3.6	1.4
#7	269	269	268	268.7	0.6	0.2
#8	266	267	272	268.3	3.2	1.2
#9	266	266	271	267.7	2.9	1.1
Total				268.0	2.4	0.9

### **Recovery of skin after impact**

The peak resultant accelerations measured by four drop certification tests at different time intervals at impact point A of one newly manufactured skin are shown in Table 4. The differences in peak resultant acceleration measured between the initial and repeated tests performed at 2, 6 and 24 hours were 1 G, 1G and 3 G, respectively.

Regarding the results measured at impact point B, the differences in peak resultant acceleration measured between the initial and repeated tests performed at 2, 6 and 24 hours were 0 G, 1G and 4 G, respectively (Table 5).

These results indicated that 2 hours is sufficient for skin recovery after the impact. Thus, the present study employed 2 hours as the time interval for the three drop certification tests (impact points A, B and C as shown in Figure 4) for skin durability over time.

Table 4 Peak resultant accelerations for different time intervals at impact of point A

Time interval	Peak resultant accel. (G)	
	Measured	Difference
Initial	268	-
2 hours	267	-1
6 hours	267	-1
24 hours	271	3

Table 5 Peak resultant accelerations for different time intervals at impact of point B

Time interval	Peak resultant accel. (G)	
	Measured	Difference
Initial	271	-
2 hours	271	0
6 hours	270	-1
24 hours	267	-4

### **Skin Durability Over Time**

The peak resultant accelerations measured at 0 month, 13, 16, 19, 22, 25, 28 and 31 months after manufacture of skin A and B are shown in Tables 6 and 7 and Figures 9 and 10. Note that the headform impactor with skin A was kept in a room with control of temperature and humidity and the headform impactor installing skin B was kept in a room without control of temperature and humidity.

The results indicated that the peak resultant acceleration measured using the two skins immediately after manufacture was 270 G. The peak resultant acceleration of 279 G measured using the skin A increased 9 G at 13 months after manufacture, while the peak resultant acceleration of 275 G measured using the skin B increased 5 G at 13 months after manufacture. The increase of 9 G and 5 G correspond to 16% and 9% of the range of the certification test corridor (55 G), respectively.

The peak resultant acceleration of 287 G measured using the skin A increased 17 G at 31 months after manufacture, while the peak resultant acceleration of 288 G measured using the skin B increased 18 G at 31 months after manufacture. The increases of 17 G and 18 G correspond to 31% and 33% of the range of the certification test corridor (55 G), respectively. These results indicate that if the acceleration is close to the middle of the drop certification corridor (272.5 G) immediately after purchase by a testing facility, the

Table 6 Peak resultant accelerations measured using skin A kept in a room with control of temperature and humidity

Time (month)	yy/mm	Results				
		Impact point	Peak resultant accel. (G)			
			Measured	Mean	Increase from 0 month	SD
0	2002 Aug.	A	272	270	0 (0%)	1.7
		B	269			
		C	269			
13	2003 Sep.	A	279	279	9 (16%)	0.0
		B	279			
		C	279			
16	2003 Dec.	A	281	279	9 (16%)	2.0
		B	279			
		C	277			
19	2004 Mar.	A	280	283	13 (24%)	3.6
		B	287			
		C	282			
22	2004 Jun.	A	280	283	13 (24%)	3.5
		B	283			
		C	287			
25	2004 Sep.	A	282	284	14 (25%)	1.5
		B	284			
		C	285			
28	2004 Dec.	A	284	287	17 (31%)	2.5
		B	287			
		C	289			
31	2005 Mar.	A	284	287	17 (31%)	2.3
		B	288			
		C	288			

\*( ) represents ratio of increased peak resultant acceleration from 0 month to the range of the ISO/IHRA/Japan MLIT corridor (55 G)

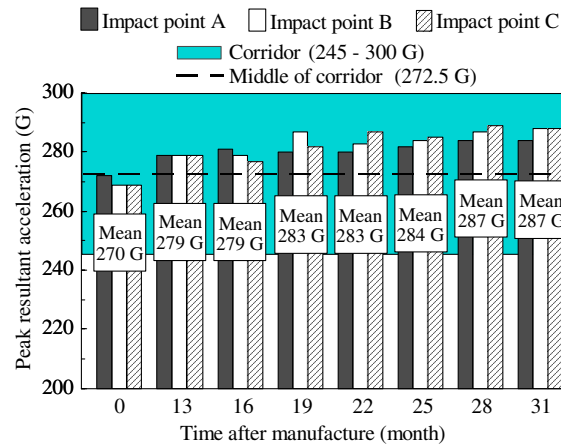


Figure 9. Peak resultant accelerations measured using skin A kept in a room with control of temperature and humidity.

skin can be available for use in a pedestrian impact test with a storage period of at least 31 months (2 years and 7 months). These results also suggest that if the acceleration is close to the upper limit of the drop certification corridor (300 G) immediately after purchase by a testing facility, the skin expiration time

Table 7 Peak resultant accelerations measured using skin B kept in a room without control of temperature and humidity

Time (month)	yy/mm	Impact point	Results			
			Peak resultant accel. (G)			
			Measured	Mean	Increase from 0 month	SD
0	2002 Aug.	A	272	270	0 (0%)	2.1
		B	269			
		C	268			
13	2003 Sep.	A	273	275	5 (9%)	3.2
		B	279			
		C	274			
16	2003 Dec.	A	278	280	10 (18%)	1.5
		B	280			
		C	281			
19	2004 Mar.	A	280	283	13 (24%)	3.8
		B	281			
		C	287			
22	2004 Jun.	A	280	284	14 (25%)	3.5
		B	286			
		C	286			
25	2004 Sep.	A	283	285	15 (27%)	2.1
		B	286			
		C	287			
28	2004 Dec.	A	283	288	18 (33%)	4.0
		B	290			
		C	290			
31	2005 Mar.	A	284	288	18 (33%)	3.2
		B	289			
		C	290			

\*( ) represents ratio of increased peak resultant acceleration from 0 month to the range of the ISO/IHRA/Japan MLIT corridor (55 G)

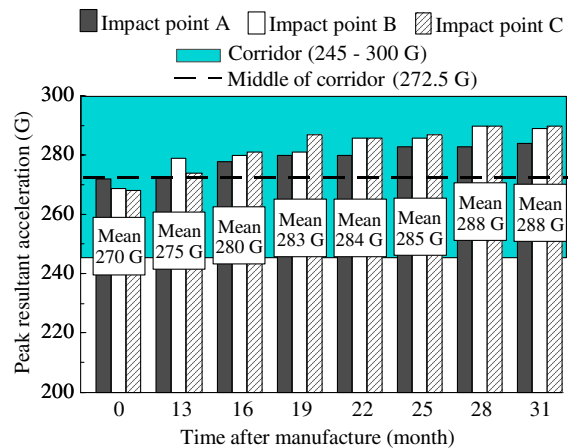


Figure 10. Peak resultant accelerations measured using skin B kept in a room without control of temperature and humidity.

may be drawing very near. The results also indicated that one need not keep skins in a room where the temperature and humidity are well controlled when storing them for a certain period.

## DISCUSSION

In the present study, the durability over time of skin was investigated by the drop certification testing proposed by ISO/IHRA/Japan MLIT for the certification test of pedestrian headform impactor. On the other hand, the draft of the European regulation, EEVC/WG17 [9] employed the other certification test in which the headform impactor is impacted laterally by a ram with a mass of 1 kg (Figure 11). The purpose of this lateral impact certification test is to simultaneously investigate the skin performance and the vibration characteristics. However, a result with high repeatability using this lateral impact certification test method is unlikely, because matching up the ram line of impact through the center of gravity of the headform impactor could be difficult. Since the repeatability of this method has not been verified so far, we did not use it in the present study. If we investigate the durability over time employing this lateral impact certification test, the results would tend to be the same as that obtained in the present study.

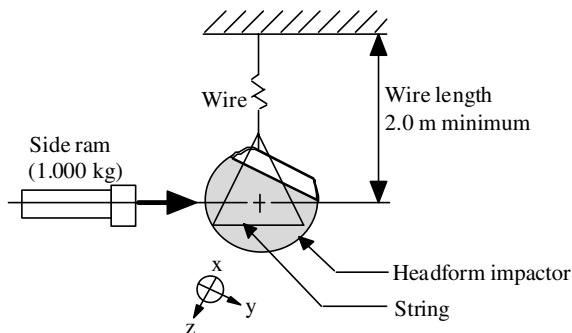


Figure 11. Setup for headform impactor high-velocity certification test.

JAMA and JARI developed child and adult headform impactors complying with the ISO/IHRA/Japan MLIT specifications. The same developed skin can be used with both child and adult headform impactors [6]. Since the mass of a child headform impactor is smaller (3.5 kg) than that for an adult (4.5 kg), its head acceleration at the impactor center of gravity is higher than for the adult headform. Therefore, in the present study, the skin durability over time was investigated employing the JAMA–JARI child headform impactor. If we employ the JAMA–JARI adult headform impactor for the investigation of the skin durability over time, the results would show the same tendency evidenced by the present study.

Regarding the storage period, the skin durability over 31 months was investigated in the present study. The investigation period of 31 months was more than twice the usual storage period, e.g., from a half year to

the maximum one year employed by the Japanese New Car Assessment Program (J–NCAP) pedestrian head protection test which was conducted in JARI. Therefore, the period employed in the present study would obviously suffice to obtain information on skin durability over time.

## CONCLUSIONS

JAMA and JARI have developed pedestrian headform impactors fulfilling the ISO/IHRA/Japan MLIT standards. The present study investigated the durability over time of skin used for JAMA–JARI pedestrian headform impactor measured by the biofidelity certification testing. The results indicated that the peak acceleration impact using the skins immediately after manufacture was 270 G. The peak acceleration of 288 G increased 18 G at 31 months (2 years and 7 months) after manufacture. The increase of 18 G corresponds to 33% of the range of the certification test corridor (55 G). These results indicate that if the acceleration is close to the middle of the drop certification corridor (272.5 G) immediately after purchase by a testing facility, the skin is available for pedestrian impact test use with a storage period of at least 31 months. The results also suggest that if the acceleration is close to the upper limit of the drop certification corridor (300 G), the skin expiration time may be drawing very near. The findings also indicated that temperature and humidity did not significantly affect the skin durability over time.

## ACKNOWLEDGEMENTS

This study project was carried out under contract between the Japan Automobile Research Institute (JARI) and the Japan Automobile Manufacturers' Association (JAMA).

The authors are indebted to the members of the JAMA pedestrian working group, Mr. Masahiro Ito, senior researcher of the Institute for Traffic Accident and Data Analysis (ITARDA), Mr. Akira Sasaki, formerly JARI senior researcher, Mr. Syuji Ono, director of Jasti Technical Center, Mr. Yoshihiro Ozawa, president of Jasti, and to Mr. Kimiaki Niimura, S-Tech Co., Ltd. in Saitama, Prof. Tsutomu Doi, Assistant Professor of Ibaraki Christian University for their valuable comments on the current study, Messrs. Suzuki and Inoue, Jasti researchers, Mr. Masaru Takabayashi, Mr. Hiroyuki Jimbo, Mr. Masakatsu Ikenobe and Mr. Osamu Natori, JARI researchers for their valuable assistance in the biofidelity certification test.

## REFERENCES

- [1] Institute for Traffic Accident Research and Data Analysis of Japan (ITARDA), 'Annual Traffic Accident Report in 2003', Tokyo, 2004 (in Japanese).
- [2] ISO/TC22/SC10/WG2, 'Passenger Cars and Light Truck Vehicles-Pedestrian Protection –Impact Test Method for Child Pedestrian Head', ISO/TC22/SC10/WG2 Working Draft Child Head #3.N622, 2000.
- [3] ISO/TC22/SC10/WG2, 'Passenger Cars and Light Truck Vehicles-Pedestrian Protection –Impact Test Method for Pedestrian Head', ISO/TC22/SC10/WG2 Working Draft Head #7.N623, 2000.
- [4] Mizuno, Y. 'Summary of IHRA Pedestrian Safety WG Activities (2003)–Proposed Test Methods to Evaluate Pedestrian Protection Afforded by Passenger Cars' Proceeding of 18<sup>th</sup> International Technical Conference on Enhanced Safety of Vehicles (CD), 2003.
- [5] Specification of the Headform Impactor, 12<sup>th</sup> International Harmonized Research Activities (IHRA) pedestrian safety working group (PS WG) N230, November 2002.
- [6] Matsui, Y. and Tanahashi, M. 'Development of JAMA-JARI Pedestrian Headform Impactor in Compliance with ISO and IHRA Standards', International Journal of Crashworthiness, 2004 Vol. 9 No. 2, pp.129-139.
- [7] Matsui, Y. Takabayashi, M. and Tanahashi, M. 'Characteristics of 3.5 kg Pedestrian Headform Impactor Prototypes Developed by JAMA–JARI and ACEA–TNO', International Journal of Crashworthiness, 2005 Vol. 10 No. 2, pp.197-210.
- [8] Suminto, J. 'A Wide Frequency Range, Rugged Silicon Micro Accelerometer with Overrange Stops', Sensors Magazine, 1991 Vol. 8 No. 11.
- [9] European Enhanced Vehicle-safety Committee, EEVC Working Group 17 Report – Improved test methods to evaluate pedestrian protection afforded by passenger cars, 1998.

# DEVELOPMENT AND PERFORMANCE OF CONTACT SENSORS FOR ACTIVE PEDESTRIAN PROTECTION SYSTEMS

**Oliver Scherf**

Siemens Restraint Systems GmbH

Germany

Paper Number 05-0021

## ABSTRACT

Over the past few years, the demands on future vehicle generations concerning pedestrian protection improvement have been discussed especially in various European and Japanese automobile committees, consumer protection organizations and by legislation. These discussions led to, amongst other activities, government regulations for Europe and Japan, which prescribe various testing which verifies pedestrian protection. In order to fulfill the prescribed head impact tests, a certain stiffness characteristic of the bonnet is necessary, which can be achieved besides passive means with an active bonnet lifting device. They consist of a sensor system, which detects the pedestrian impact, and an actuator system, which lifts the bonnet.

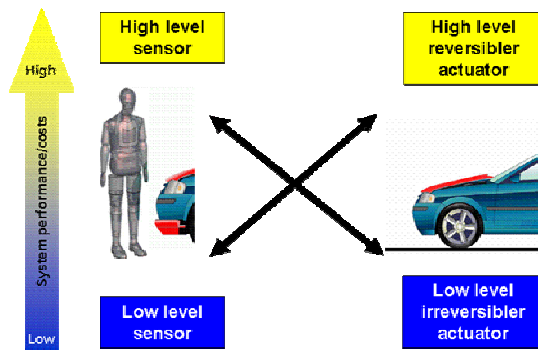
In this article, the main focus will be on the development of a sensor system including the discussion of requirements arising from legislative specifications and OEM market trends. Furthermore, typical test and simulation procedures are presented which provide the input for algorithm development. A central point regarding algorithm performance is the capability of pedestrian detection, especially under consideration of different temperatures, mounting and production tolerances and an inhomogeneous front end stiffness distribution. The differentiation of pedestrian collisions from misuse objects (e.g., stone- and bird-impact, parking dent) is also an important aspect, because a high misuse activation rate has a negative influence on customer satisfaction. This item will be also discussed.

## INTRODUCTION

In order to fulfill the legal requirements from the European directive 2003/102/EC on pedestrian protection which will come into effect 2005 (phase I) and 2010 (phase II), passive as well as active protection measures can be used. Design solutions must be found for the bumper, the front end and in particular the bonnet in order to provide the capability for kinetic energy absorption without exceeding load limits for the pedestrian. This in turn requires an appropriate (low) vehicle structure stiffness in conjunction with a necessary deformation space. A protection concept which has been frequently examined concentrates on the lifting of the bonnet before the head impacts the vehicle in order to provide the necessary energy absorption capability in this area. Apart from the actuators, which are lifting the bonnet, this active protection system also requires sensor technology to recognize and classify the collision object.

A holistic approach is a fundamental requirement of developing an active pedestrian protection system. Among other things this means that suitable actuators need to be developed dependant on the sensor technology's performance. The possibility of the actuators' reversibility must be more or less comfortably characterized according to the detection safety of activation and misuse loading cases. Sensor systems which supply little information about a collision object can necessitate a high level reversible actuator, in order to avoid a garage stop after misuse activation and to ensure customer satisfaction. On the other hand, a sensor with high differentiation capabilities could be combined with a pyrotechnical actuator, because misuse activation probability is low. This relationship is visualized in Fig. 1.





**Figure 1. Relationship between sensor and actuator capabilities.**

A further decisive point is the time required by the sensor system to generate a decision to activate (time to fire, TTF). The shorter the TTF, the lower the requirements of the actuators regarding the positioning time.

Against this background it seems desirable to use predictive (pre crash) sensors for pedestrian detection. Since this however does not seem realistic before 2010 due to the technological challenges which have to be mastered, in short term the sensing of contact via force or deformation in the bumper area will be a considerable solution.

## **CONTACT SENSORS SYSTEMS REQUIREMENTS**

Contact sensor system requirements can be split up into the ability to recognize collision objects and therefore also the differentiation or classification of those, and requirements regarding sensor integration into the vehicle.

### **Differentiation / Classification**

The most important requirement is the ability to classify the object of collision which comes about depending on the necessity of differentiating between the deployment or activation loading case (fire) and a misuse loading case (no-fire).

### **Legal Requirements or Specifications**

An activation loading case based on current regulations must be recognized and the

protection system must be activated. In future, Europe must obey the EC directive 2003/102/EC for pedestrian protection [1] in connection with document 2004/90/EC (technical prescriptions for the implementation of article 3 of directive 2003/102/EC) [2]. Therefore, the lower leg impact should be considered as a basic activation loading case.

### **Field Stability**

An activation loading case in the field and in the approval tests should be detected. Due to part II, chapter I, section 1.1.2 of document 2004/90/EC which states that

"All devices designed to protect vulnerable road users shall be correctly activated before and/or be active during the appropriate test. It shall be the responsibility of the applicant for approval to show that the devices will act as intended in a pedestrian impact"

it seems appropriate to design lower limit impactors, which are able to provide impact characteristics of the smallest relevant pedestrian for verification of active systems. In case these impactors are not available or the sensor algorithm is not proven to activate automatically at higher impact energy in case it does in the lower limit case, full scale crash tests with the dummy of a 6 year old child, the 5 %ile-woman, the 50 %ile- and 95 %ile-man can be conducted. However, the correlation between human and dummy regarding mechanical characteristics in a pedestrian accident is an open issue which needs to be examined further in future.

### **Frontal Crash Detection**

An erroneous activation must be avoided if the safety of the vehicle's occupants becomes endangered. This could be the case for example during a car to car crash or the impacting of an obstacle. A raised bonnet which has not been secured further could possibly penetrate the passenger compartment.

### **Misuse Stability**

Erroneous activation during a vehicle collision for example with stones, snow drift or a traffic beacon (traffic sign) should be avoided in order to ensure customer satisfaction. This point becomes significant particularly with non-reversible actuator systems, when an erroneous activation would require a visit to the garage afterwards. Misuse objects with a high probability of being involved in accidents are listed in Table 1.

**Table 1.**

**Important misuse objects**

<b>Snowdrift, snow hill</b>
<b>Tree, branch on street (after storm)</b>
<b>Big deer (red deer, wild boars,...)</b>
<b>Traffic sign, traffic light</b>
<b>Fence, barrier grid,...</b>
<b>Traffic beacon, pylons, post</b>
<b>Ball</b>
<b>Stone</b>

Physical collision parameters such as collision speed, mass and shape of collision object and front end deformation characteristics (point of contact, intrusion, intrusion speed) can be considered as differentiation criteria. In addition to the choice of differentiation criteria, the relevant thresholds must be determined, in order to distinguish the activation loading cases from the misuse cases. Usually parameters of the collision object (e.g. mass) cannot be determined directly, but rather indirectly via energy, deformation or dynamic characteristics on the front end. Vehicle speed can be processed as additional information from an ABS system via the CAN-Bus.

Activation thresholds for the collision speed can be derived based on statistical investigations for the distribution of injury severity and the frequency of pedestrian and cyclist accidents. Regarding injury severity, it can be seen that at a collision speed of 20 kph to 30 kph, the majority of pedestrians and cyclists (around 80%) remain uninjured or only minimally injured (MAIS 1), whilst approximately 20 % casualties suffer injuries of severity MAIS 2 to 4 [5]. The risk of having lethal injuries in this speed range is however almost zero. An upper threshold for the activation speed range came about due to the fact that already almost 95% pedestrian and cyclist collisions occur under 60 kph. The majority of all pedestrian and cyclist accidents are therefore covered by protection systems, which work in this velocity range [4]. However, precise examination – also with consideration of legal requirements – needs to be carried out in order to establish appropriate upper and lower velocity thresholds for the protection system activation.

## **Vehicle Integration**

Integration into a vehicle places further requirements onto a contact sensor system:

### **Adaptability to Varying Levels of Stiffness on the Front End**

Usually the bumper area of a vehicle is not built homogeneously throughout the width, but rather, shows certain features e.g. openings in the foam for the tow hook and parking sensors or changes in the outer paneling geometry. These variations in constructive design lead to differing stiffness distribution of the bumper over the whole vehicle width. This can lead to different sensor signals being measured at different impact positions with the same collision object. A contact sensor system should be in a position to take these variations into account.

### **Adaptation to Varying Operating Temperatures**

Temperature changes to the front end lead to a change of the mechanical characteristics. This leads for the same collision object to different sensor signals at high or low temperature compared to the signal obtained at room temperature (see section 3.2). These effects must also be taken into account by the sensor system and must not lead to an erroneous activation.

### **Service Life**

The sensor system must work throughout the lifecycle of the vehicle. Requirements arise regarding ageing, environmental conditions, vibration, petty damage etc., according to each automobile manufacturer's specifications.

### **Insensitivity Compared with Installation and Manufacturing Tolerance**

The operativeness of the sensor system may not be impaired due to the variation of component characteristics, e.g. variations of the hardness of the bumper foam and the sensor's position tolerance.

### **Electro-Magnetic Compatibility**

The sensor system's reliability performance must not be impaired by electro-magnetic radiation.

### **Design Neutrality**

The sensor system should be able to be integrated into the vehicle without influencing the exterior. Modifications to components which are not visible and placed on the inside are however allowed but they should be kept to a minimum.

## FIBER OPTIC CONTACT SENSOR (FOS)

Before choosing an appropriate sensor system for active pedestrian protection, the requirements listed in the previous section need to be considered. The fiber optic contact sensor shows a system which correspond with the requirements in a particular way. The signal is not influenced by electro-magnetic waves and minor position deviations. Changes in temperature and a different distribution of stiffness of the front end can be taken into account.

### Setup

The sensor itself is made up of a number of synthetic optical fibers, which are surrounded by light absorbing material, see Fig. 2.

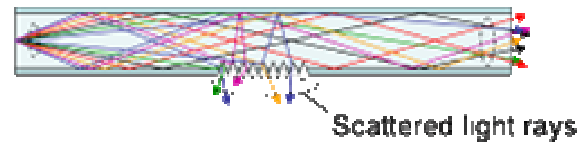


Figure 2. Set up of fiber optical sensor.

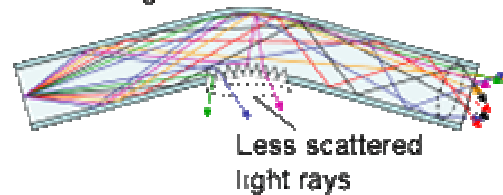
### Operating Principle

The sensor's operating principle is based on the effect of micro bending. Each optical fiber is covered by a reflective coating, in order to minimize the losses during light transfer. By a specific treatment process, the coating is partially removed from the fiber. This results in an amplification or reduction of the light intensity compared to a reference state, depending on the bending direction, see Fig. 3.

### Straight Optical Fiber



### Negative Bending



### Positive Bending

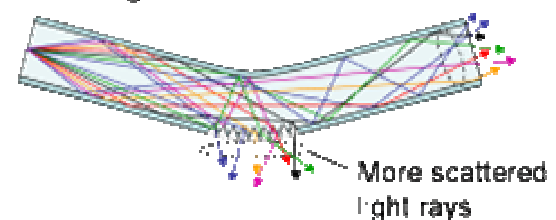


Figure 3. Micro bending principle.

A constant loss of light exists with straight fibers which extends on upward flexion and decreases on downward flexion. The rate of loss is directly related to the direction of the fiber flexion and the height of the curvature. The rate of loss is proportional to the strength of the curvature. The light intensity is converted in an optoelectronic interface into a voltage signal which is directly in proportion to the curvature in the sensitive area of the fiber.

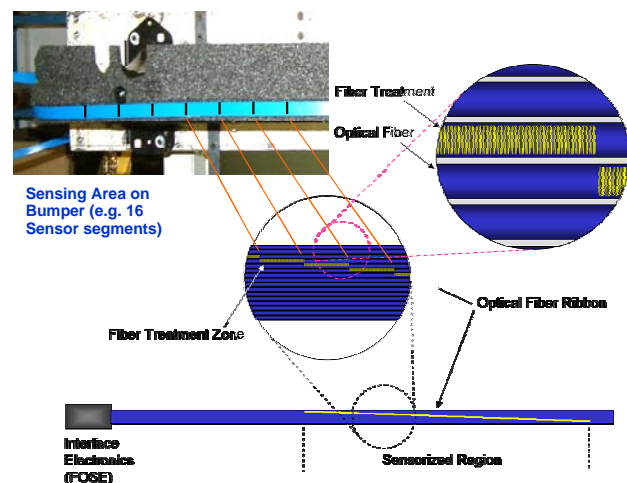


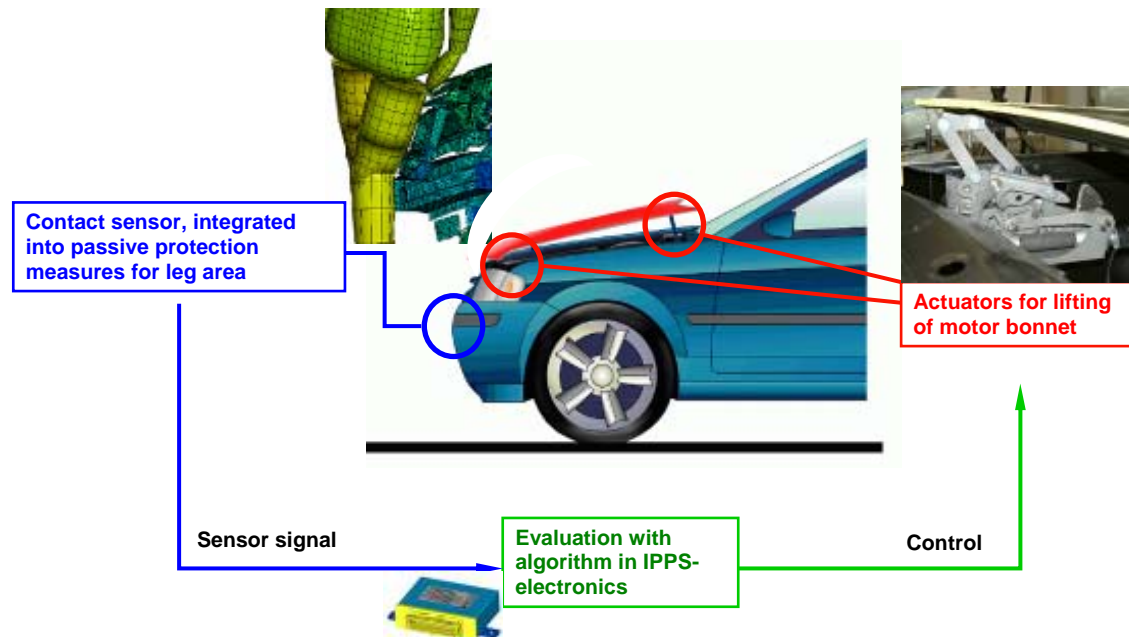
Figure 4. Sensor tape with single segments integrated in bumper foam.

The whole contact sensor is made up of individual sensor segments, see Fig. 4. With simple calibration methods the assigned bend angle for each sensor segment can be determined from the voltage signals. The foam deformation can be calculated via a geometric correlation from the bend angles occurring during operation.

## System Concept and Operating Method

The conceptual set up of the protection system and the operating method are to be described as follows. Fig. 5 shows the principle set up of the system.

Should the vehicle collide with an object, the deformation of the front end leads to bending of the sensor segments, which in turn, as described in the previous section, results in a change in light intensity. The measurement of light intensity change takes place on the reception side of the FOS-loop. These signals are called up constantly on a millisecond cycle. Voltage signals are generated from the light signals via an optoelectronic interface from which the relevant angle can be calculated, by means of calibration data. The processing of the angle data in the algorithm then provides the bumper deformation. The deformation of the front end and the sensor strip is dependant on the collision speed, the mass and the mechanical set up of the collision object. The characteristics of the collision object can be determined from the sensor signal by an appropriate algorithm.



**Figure 5. System set up.**

Data is passed on to the evaluation electronics as the whole bumper is scanned in a millisecond cycle, so that immediate data processing is possible in real time. A fire or no-fire decision can therefore be made within the required time. A typical requirement is that the trigger time – the time of the first contact of the collision object until the fire or no-fire decision – is less than 10ms for higher collision speeds. Higher trigger times can also be accepted in cases of lower speeds due to pedestrian kinematics. But the set up times of the actuators system must always be

considered when determining the trigger times. Due to the condition, both times are linked to one another so that their sum cannot be larger than the time of the first contact of the pedestrian with the vehicle to the head impact on the bonnet.

If the algorithm reaches a trigger decision, the actuators are controlled by the system's electronics and the energy required for triggering or releasing is delivered.

## SYSTEM DEVELOPMENT

During system development, three types of tests can be conducted in order to generate a database for algorithm development: Drop tower tests to gain experience about the basic performance of a sensor system in a specific frontend followed by impactor tests to check system performance e.g. in case of a lower leg impact. By the aid of full scale crash tests, results regarding the system performance can be obtained, which are as close to the real accident scenarios as possible with the currently available testing technology, see also [3].

Each test scenario can also be investigated in numerical simulation, which is especially advantageous in case when extensive parameter studies have to be considered.

Fig. 6 visualizes the development process.

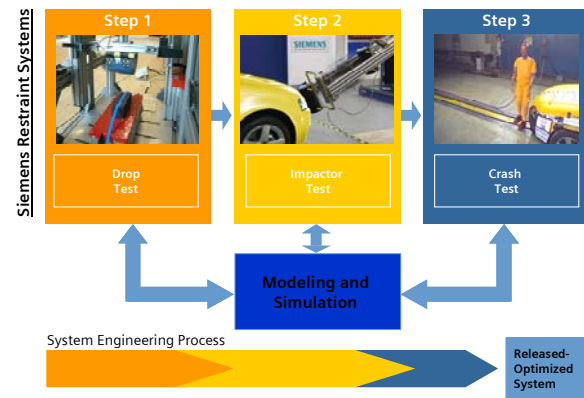


Figure 6. Development process.

## Full Scale Crash Tests

In order to analyze the sensor behavior in real accidents, crash tests can be performed. In Fig. 7 two typical scenarios are shown: The left side shows a pedestrian collision (upper part of Figure) with the associated sensor signal (lower part). On the right side a misuse object (traffic beacon) is presented, again with the associated signal.

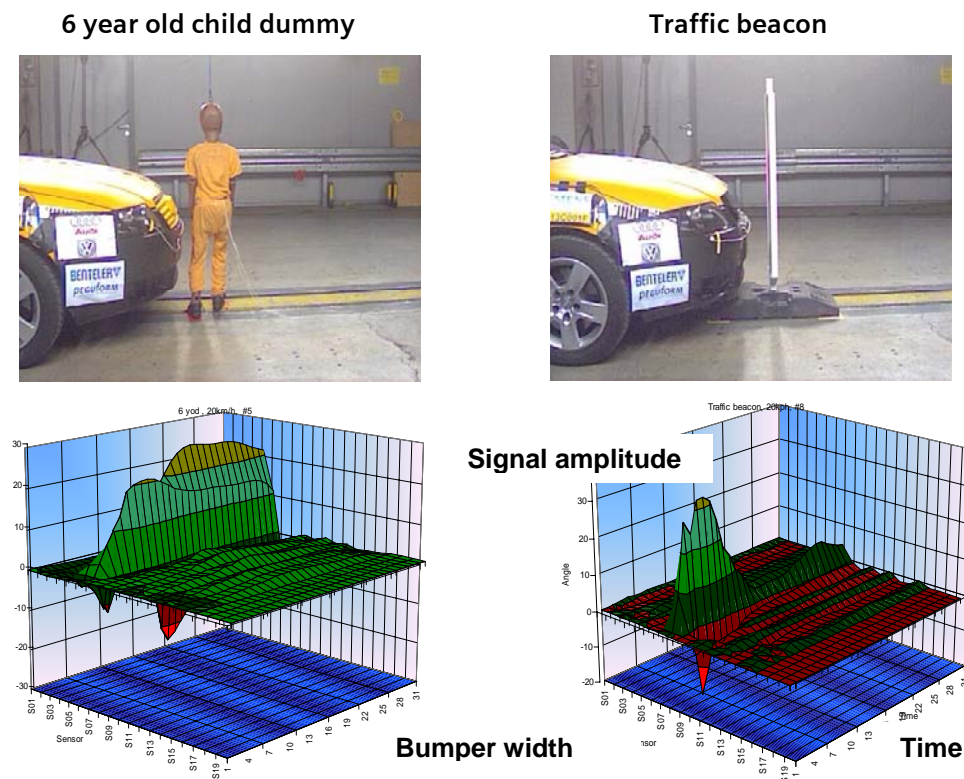


Figure 7. Crash test configurations and associated sensor signals.



The signal diagrams in Fig. 7 show a different shape for the dummy and the misuse object, which can be used to derive criteria for differentiation and classification of collision objects. According to the mass and stiffness distribution of a collision object, a specific object kinematics and deformation of the bumper occurs, which is reflected in the sensor signals.

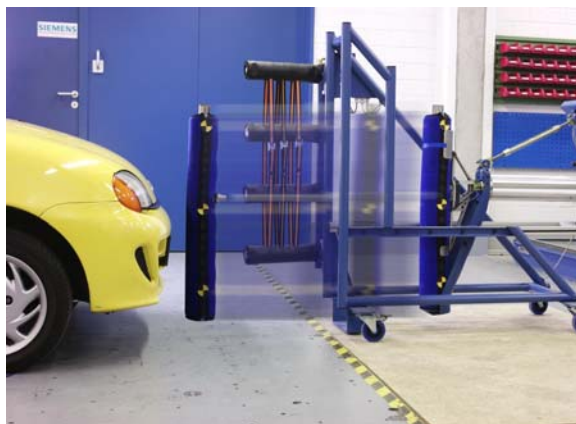
For the dummy, one can observe a continuously increasing signal amplitude up to approximately 10 ms, then a short constant amplitude followed by a second increase and finally a slow decrease phase. The first increase is associated with the effect of the first dummy leg coming into contact with the bumper, followed by the impact of the second one, which results in the second signal increase.

A completely different signal is generated by the traffic beacon. Here, one can observe a short contact duration due to the elasticity of the beacon and the relative low "effective" mass acting onto the frontend.

If one considers the frontend and collision object as a dynamic system, the first natural frequency – which depends on the bumper stiffness and the colliding mass – is different. This is also reflected in the sensor signals in form of the contact duration.

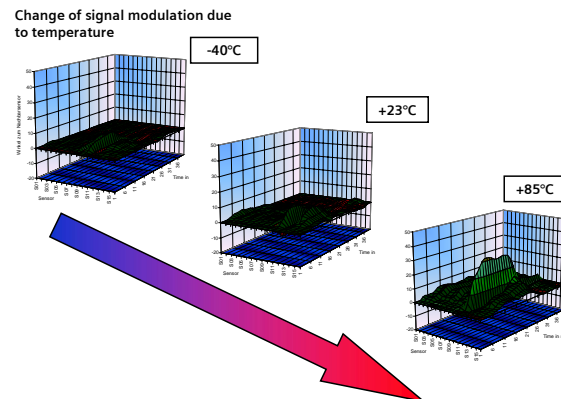
## Impactor Tests

Impactor tests are typically used to gain information about the system behavior in case of lower leg impacts (Fig. 8).



**Figure 8. Impactor test configuration.**

Furthermore, they are used to investigate the influence of different operating temperatures. Results of these tests are shown in Fig. 9, which indicate a clear temperature dependence of the frontend deformation and the signal amplitude. However, this effect can be compensated in the algorithm.

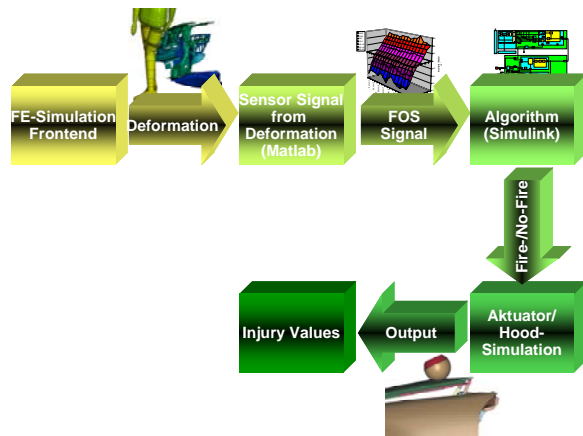


**Figure 9. Temperature dependence of frontend deformation.**

## System Simulation

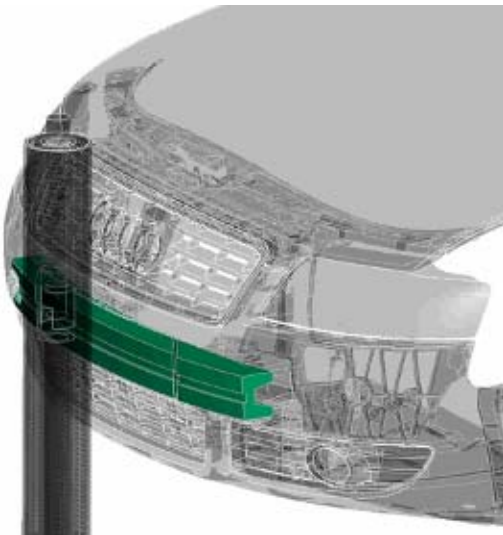
With the aid of numerical simulation, important questions can be clarified in the engineering process. Simulation has a particular advantage compared to testing in the determination of head impact times, due to the availability of validated human models, which represent accident kinematics better than test dummies. Another important advantage is the possibility to carry out extensive parameter studies at low cost, e.g. regarding different dummy postures, point of impact, collision speed, etc.

In order to support pedestrian protection system development by numerical simulation, a process chain was established, which connects different simulation programs, see Fig. 10. FE-codes like PAMCRASH or LS-DYNA are used for mechanical simulations, MATLAB/Simulink for support of algorithm and electronic development and own developed codes for sensor simulation.



**Figure 10. Simulation process chain.**

A standard task of simulation is the configuration of the energy absorption foam insert for passive lower leg protection. For active pedestrian protection systems special attention has to be paid to sensor integration, which necessitates in some cases model updates in order to represent the sensor in an appropriate way. A typical Finite Element Model is shown in Fig. 11.



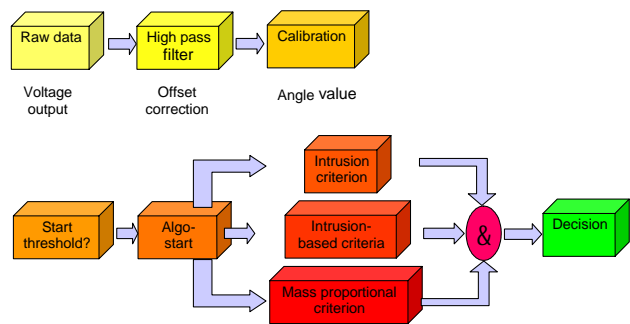
**Figure 11. Simulation model.**

### Algorithm-Development

The significant element of the sensor system is the analysis of the data and its evaluation and assessment in an algorithm which is as robust as

possible. The objective is to establish optimized triggering criteria for the system. At the same time, aspects which have influence on the cost of the system as a whole are considered with respect to manufacturing and cost optimization. Close coordination between sensor development and algorithm development is necessary in order to, for example, minimize the number of individual sensor segments but simultaneously guarantee data or information density which is needed for a robust algorithm.

At the current development stage of the generic algorithms developed at Siemens Restraint Systems, the data is processed as follows: An offset correction is applied to the voltage raw data by means of various filter functions. The correlation between voltage signal and angle is ascertained from the calibration undertaken of the individual sensor segments so that the angle information per segment is available as an input variable size for the algorithm. If the angle value exceeds a starter threshold, the intrusion and further derived rates are calculated, amongst which, criteria which are proportional to the mass of the collision object. The decision about the activation or non-activation of the pedestrian protection system can only be made after the trigger thresholds for the individual criterion have been determined. Fig. 12 shows this process again schematically.



**Figure 12. Algorithm set up.**

The system performance is shown in Table 2. A broad range of misuse objects can be distinguished from activation load cases. Due to different collision velocities which are associated with a different deformation speed of the frontend, different activation times are obtained. However, a smaller collision velocity results also in a larger head impact time, which means that for a given actuator time (which is usually not velocity dependent) the "benefit" of low collision speeds can be given to the sensor system.

The currently discussed requirement of 10 ms TTF at 40 kph collision velocity is met by the FOS system.

**Table 2.**

**Activation times for several load cases**

Collision object	Velocity [kph]	Worst case TTF [ms]	Requirement
6yod	15	16	Fire
6yod	20	13	Fire
6yod	25	11	Fire
50%ile	20	13	Fire
	40	9	Fire
Small leg impactor	20	16	Fire
	40	8	Fire
Lower leg impactor	20	14	Fire
	40	7	Fire
Snow drift	20 - 50	No fire	No fire
Small animal	20 - 55	No fire	No fire
Ball	20 - 80	No fire	No fire
Hammer induced excitation		No fire	No fire
Road testing	0 - 80	No fire	No fire
Curb	60	No fire	No fire

## CONCLUSION

The work carried out shows that a high amount of classification potential exists with the fiber optic sensor system and an algorithm correctly adapted to the vehicle. Misuse load cases can be differentiated between activation load cases. However, the more a misuse object approaches a pedestrian regarding its mass and stiffness distribution, the more difficult the differentiation will naturally be. When a borderline case object falls with its mechanical properties into the category of a pedestrian, a sensor system will no longer be able to differentiate between the misuse object and the pedestrian.

Since there is a high information content in the fiber optical sensor signal, there is far greater classification potential with this kind of system than with contact sensor systems, which are e.g. equipped with a simple switch and a constant threshold.

Further studies show that regarding the transferability of the fiber-optic sensor system and the algorithm on other vehicles, this is possible with relatively small changes since the algorithm parameters needed to be adapted are few.

## REFERENCES

- [1] Directive 2003/102/EC of the European Parliament and of the Council of 17 November 2003 relating to the protection of pedestrians and other vulnerable road users before and in the event of a collision with a motor vehicle and amending Council Directive 70/156/EEC. Official Journal of the European Union, L 321/15
- [2] Commission decision of 23 December 2003 on the technical prescriptions for the implementation of Article 3 of Directive 2003/102/EC of the European Parliament and of the Council relating to the protection of pedestrians and other vulnerable road users before and in the event of a collision with a motor vehicle and amending Directive 70/156/EEC. Official Journal of the European Union, L 31/21
- [3] Matsui, Yasuhiro; Wittek, Adam; Konosu, Atsuhiko. 2002. Comparison of Pedestrian Subsystem Safety Tests Using Impactors and Full-Scale Dummy Tests. SAE Technical Paper Series 2002-01-1021. Warrendale, PA
- [4] Medizinisch Hochschule Hannover, TU-Dresden, BAST, FAT/VAT. GIDAS - German In-Depth Accident Study. Data from 1999 till 2003
- [5] Otte, Dietmar: Unfallforschung. Seminar. Aschaffenburg Safety Update 2003. 7.-May, 8th, 2003, Aschaffenburg, Germany

# DEVELOPMENT AND EVALUATION OF A BIOFIDELIC SHOULDER FOR THE IHRA (JARI) PEDESTRIAN MODEL

Michael S Neale  
Brian J Hardy  
Graham J L Lawrence  
TRL Limited  
United Kingdom

Paper 05-0096

## ABSTRACT

Alterations were made to the shoulders of the Japan Automobile Research Institute (JARI) pedestrian model. The International Harmonised Research Activities Pedestrian Safety Group (IHRA PSG) has chosen the JARI pedestrian model as a basis to develop an improved humanoid pedestrian model. It is anticipated that when the development and validation of this model has been finalised it can be used to refine the current IHRA pedestrian head impact test procedures. In the work described here the shoulders of the JARI pedestrian model were improved to more accurately represent the structure and range of movement observed in real shoulders. Improvements to the model were validated by comparing the original and modified models' predictions against measures from Post Mortem Human Surrogate (PMHS) shoulder impact studies presented in the published literature. In contrast to the original JARI model the predictions from the modified JARI model were comparable to equivalent measures from the PMHS impact studies. Predicted peak shoulder impact forces from the original JARI pedestrian model were up to eight times larger than those measured in the PMHS impact studies or predicted by the modified JARI pedestrian model. Vehicle to pedestrian impacts were then simulated with the original and modified JARI models and predicted head impact responses from the models were compared. Head impact velocities from the modified JARI model were between 0.33 and 1.43 m.s<sup>-1</sup> (2 and 14 %) greater than those predicted by the original JARI pedestrian model. Furthermore, it was found that a vehicle strike to the rear of the pedestrian models rather than to the side, lead to an increase in head impact velocity of up to 4.55 m.s<sup>-1</sup> (39 %). However, before the IHRA PSG make decisions on the JARI model's head impact predictions further reviews of its structure and biofidelic responses are needed.

## INTRODUCTION

The International Harmonised Research Activities Pedestrian Safety Group (IHRA PSG) has developed a sub-system head impact test procedure for assessing the aggressiveness of vehicle fronts in pedestrian head impacts. Many

details of the IHRA head impact test procedure have been provisionally based on the predictions from pedestrian models developed by the Japan Automobile Research Institute (JARI), the National Highway Traffic Safety Administration (NHTSA) in the US and the Road Accident Research Unit (now the Centre for Automotive Safety Research, CASR) in Australia. These three models are lumped-mass models developed and run in the MADYMO code. Under the same impact conditions it was found that the three pedestrian models predicted significantly different head impact conditions. Therefore, the working group decided to develop an improved humanoid pedestrian model. The JARI model was chosen as a basis for the improved model because they were willing to make it available to the working group members. The intention of the working group is to identify and refine all the body parts of the model important to producing biofidelic head impact conditions. When the development and validation of this model is considered satisfactory, then it can be used to refine the current head impact test methods.

It is anticipated that the response of the shoulder during vehicle to pedestrian impacts will be important to the resulting impact conditions for the head, especially if the shoulder strikes the bonnet first prior to the head impact. Previous work has been completed reviewing the shoulder response of the JARI pedestrian model under impact (Neale *et al.* 2003a,b) with a view to developing the model for the purpose of refining the IHRA pedestrian head impact test procedure. In comparison to measured results from PMHS shoulder impact studies presented in the published literature, it was found that the JARI pedestrian model provided a very poor representation of the human shoulder response under impact and was found to be very rigid. Furthermore, the modifications made to the modelled shoulders were not detailed enough to provide an acceptable representation of the biofidelic impact response of the human shoulder. For example, the shoulder to shoulder (acromion to acromion) displacement, predicted by Neale's 2003 modification to the shoulder of the JARI pedestrian model was less than 1 mm, compared with an average of 39 mm as measured in Post Mortem Human Surrogates (PMHS) under equivalent shoulder impact conditions. The shoulder response of a further pedestrian model developed by TNO was also reviewed by Neale in 2003, this version of the TNO model was also found to provide a very rigid shoulder response compared with the measures obtained from the PMHS shoulder impact studies.

However, TRL understand that the TNO shoulder has been improved since.

It is anticipated that a rigid shoulder, as is present in the JARI pedestrian model, could provide increased protection to the head in comparison to a real shoulder. This raises concerns on the accuracy of the model's predicted head impact conditions for the purpose of developing the IHRA head impact test procedures. Consequently, in response to this concern TRL Limited undertook a further study described here, funded by the UK Department for Transport (DfT), to develop a more biofidelic representation of the shoulder for the IHRA (JARI) pedestrian model.

## THE JARI PEDESTRIAN MODEL

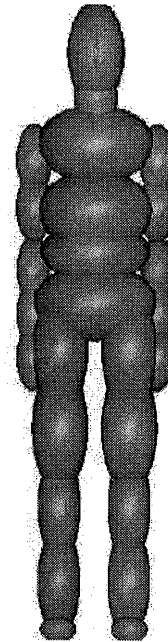
Figure 1 shows the external structure of the JARI pedestrian model. The model represents a 50<sup>th</sup> percentile male pedestrian with a mass of 72.5 kg. It consists of 27 anatomical segments joined by a series of kinematic joints. Table 1 details the connections between the anatomical segments of the model. With the exception of the elbows, the segments of the model are joined by a series of spherical or 'ball-and-socket' joints. The elbows are formed from revolute or 'hinge' joints. All the joints have a defined stiffness characteristic to approximate the stiffness and range of motion of the equivalent anatomical joint. In addition to the regular anatomical joints such as the knees and elbows, further joints have been implemented in the model to simulate the bending response of the long bones in the legs and arms. These have stiffness characteristics approximating the moments needed to bend the bones in these segments of the body. These joints are 8, 10, 13, 15, 18, 20, 23 and 25 in Table 1.

The JARI model was operated in this study with the bending response of the bones in the arms and neck locked (*i.e.* joints 5, 6, 18, 20, 23 and 25 in Table 1), and matched the model setup that had been used for runs of the model completed by the IHRA pedestrian working group (IHRA Pedestrian Safety Working Group, 2002).

## MODIFICATIONS TO THE SHOULDER OF THE JARI PEDESTRIAN MODEL

The arms in the original JARI model are joined to the torso by spherical joints (joints 17 and 22 in Table 1) which are intended to characterise the complete relative range of movement between the torso and the upper part of the arm. In reality the connection between the torso and the upper arm consists of a much more complicated series of anatomical joints, ligaments, muscles and tendons connecting a series of bones in the shoulder. This more complex structure provides a more diverse range of movement in the shoulders compared with the spherical joints that have been used in the

original JARI model. For instance, as shown by Neale *et al.* (2003a,b) published results from shoulder impacts to PMHS reveal a considerable degree of relative movement between the shoulders when impacted (*i.e.* acromion-acromion displacement), but this same response could not be recreated in the original JARI pedestrian model.



**Figure 1. The JARI pedestrian model.**

Figure 2 details the osseous features of the human shoulder. At the anterior medial location of the shoulder the clavicle bone forms the sternoclavicular joint with the sternum, which is located at the centre of the rib cage. The lateral aspect of the clavicle forms the acromioclavicular joint with the acromion, a bony protrusion of the triangular shaped scapula bone, which lies on the posterior of the rib cage. The main body of the scapula bone is secured to the rib cage by a large number of back muscles. This configuration enables the scapula to freely float over the surface of the rib cage allowing a considerable amount of movement in the shoulder. Inferior to the acromioclavicular joint, the humerus (upper arm bone) connects with the scapula to form the humeroscapular joint.

Modifications made to improve the shoulder of the JARI pedestrian model aimed to recreate as close as possible the physical structure and movement of the real shoulder. Figure 3 provides schematics of the improved shoulder developed for the JARI pedestrian model. At the location of the pedestrian model's sternum a spherical joint overlays a planar joint which is rigidly fixed to the torso of the pedestrian model. The planar joint was introduced to consider the anticipated compression and displacement of the rib cage during shoulder



impacts, allowing a degree of medial-lateral and fore-aft movement only at this connection during simulated shoulder impacts. The spherical joint was introduced to represent the movement in the sternoclavicular joint. Axial rotation in this joint has been locked, although the joint is free to flex (rotate) in all other directions.

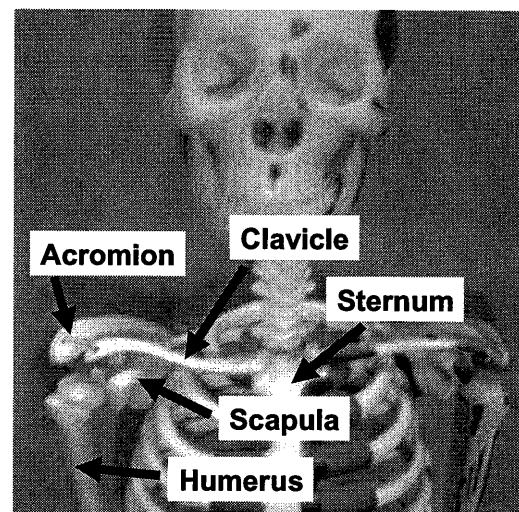
**Table 1**  
**Anatomical segments and joint connections of the JARI pedestrian model**

Joint number	Joint description	Joint type	Joint initial condition
<b>Spine and neck</b>			
1	Pelvis-Lumbar	Spherical	Free
2	Lumbar-Abdomen	Spherical	Free
3	Abdomen-Thorax	Spherical	Free
4	Thorax-Clavicle	Spherical	Free
5	Clavicle-Neck	Spherical	Locked
6	Neck-Head	Spherical	Locked
<b>Right and left legs</b>			
7 & 12	Pelvis-Hip	Spherical	Free
8 & 13	Hip-Femur	Spherical	Free
9 & 14	Femur-Knee	Spherical	Free
10 & 15	Knee-Tibia	Spherical	Free
11 & 16	Tibia-Ankle	Spherical	Free
<b>Right and left arms</b>			
17 & 22	Clavicle-Shoulder	Spherical	Free
18 & 23	Shoulder-Upper arm	Spherical	Locked
19 & 24	Upper arm-Elbow	Revolute	Free
20 & 25	Elbow-Lower arm	Spherical	Locked
21 & 26	Lower arm-Hand	Spherical	Free

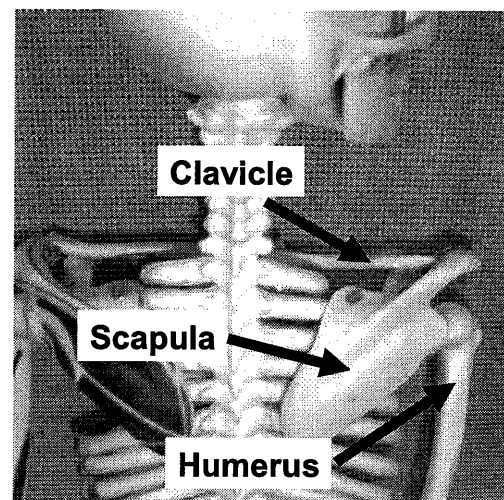
Connected to the spherical joint is a translational joint representing the bending response of the clavicle. The lateral aspect of the translational joint is connected to horizontal and diagonal Kelvin elements which are fixed at their opposite ends to the posterior aspect of the pedestrian model's torso. The connection between the translational joint and the Kelvin elements is intended to be equivalent to the acromioclavicular joint. The intention of the Kelvin elements is to represent the resistance of the scapula bone as it slides over the surface of the rib cage.

Further to the connection between the translational joint and the Kelvin elements a hinge joint has been overlaid to consider the anticipated relative rotation and movement of the scapula

about the acromioclavicular joint. Inferior to the hinge joint a planar joint has been introduced to represent the relative give within the humeroscapular joint under impact. Fore-aft and superior-inferior movement occurs in this joint but no rotation. Overlaying this planar joint a spherical joint has been introduced matching the type and stiffness characteristics of the joints used in the original JARI model to represent the complete shoulder response (*i.e.* joints 17 and 22 in Table 1). This spherical joint in the modified JARI pedestrian model is intended to represent the free range of motion typically observed in the humeroscapular joint.



**Anterior view of the shoulder**

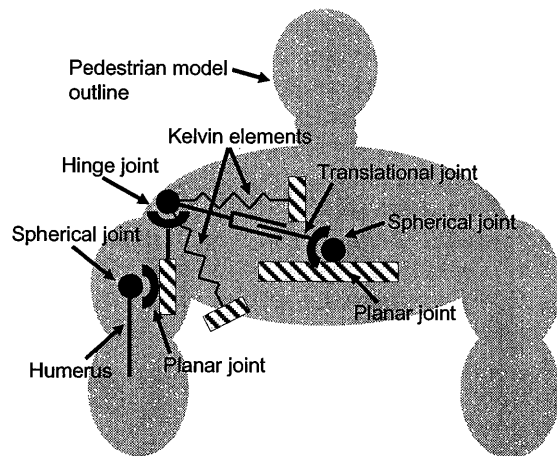


**Posterior view of the shoulder**

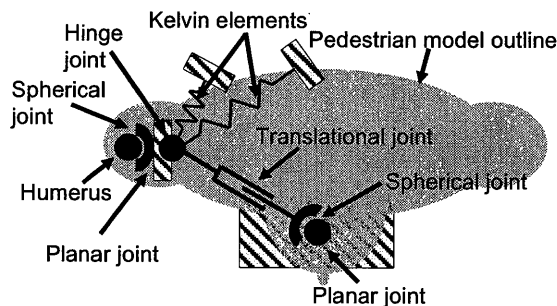
**Figure 2. Details of the human shoulder.**

The location of the spherical joints representing the humeroscapular joints were maintained in the same positions as joints 17 and 22 (see Table 1) in the original JARI model. The position of the remaining joints used in the construction of the improved shoulders for the JARI pedestrian model

were based on measures presented in the published literature (Robbins, 1983).



**Anterior view of shoulder model**



**Plan view of shoulder model**

**Figure 3. Schematic of the modifications made to the shoulder of the JARI pedestrian model.**

#### EVALUATION OF THE MODIFIED JARI MODEL'S SHOULDER RESPONSE

The stiffness characteristics and range of movement in the shoulder structures of the modified JARI pedestrian model were tuned to approximate comparable measures from the Post Mortem Human Surrogate (PMHS) shoulder impacts studies of Compigne *et al.* (2003). In these impact studies four fresh PMHS were used as detailed in Table 2. For the impacts the PMHS were seated on a bench and instrumented with tri-axial accelerometers secured at the following anatomical locations:

- In the mid-sagittal plane at T1 and sternum locations.
- To both the left and right hand sides of the internal and external clavicle extremities and into both acromion.
- On the impacted side only, two were screwed to the medial and inferior angles and two were screwed laterally onto the humerus, approximately 100 and 250 mm below the head of the humerus.

The PMHS were struck by a guided impactor weighing 23.4 kg and fitted with a rigid

150 x 80 mm rectangular impacting plate. A load cell was placed behind the impacting plate in order to record the impact force on the shoulder. The recorded force was corrected by a factor of 1.066 to allow for the mass of the impacting plate placed in front of the load cell.

**Table 2**  
**Details of the PMHS used in the shoulder impact studies of Compigne *et al.* (2003)**

Subject	Age (yrs)	Sex	Weight (kg)	Height (cm)	Shoulder width (mm)	Shoulder flesh thickness (mm)	
						Left	Right
1	77	F	67	161	335	20	24
2	88	M	33	163	355	10	12
3	79	F	52	159	355	12	10
4	82	F	50	155	345	15	15

The right shoulder of each PMHS was subjected to three sub-injurious impacts in which the initial impactor velocity was approximately  $1.5 \text{ m.s}^{-1}$ . For the three repeated shoulder impacts the PMHS were rotated at 0, +15 and -15 degrees with respect to the impact ram, as shown in Figure 4. Following the three sub-injurious impacts to the right shoulder the PMHS were subjected to a 0 degrees injurious impact to the left shoulder. For two of the PMHS the initial velocity of the impactor for the injurious impacts was approximately  $4.2 \text{ m.s}^{-1}$  and for the remaining two PMHS the left shoulders were impacted by an impactor having an initial velocity of approximately  $6.0 \text{ m.s}^{-1}$ .

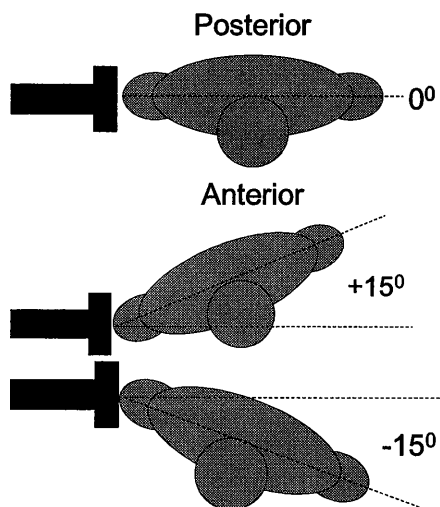
The original and modified versions of the JARI pedestrian model were modified to match the set-up of the various shoulder impact tests as shown in Figure 5. Limited details were available concerning the set-up of the PMHS's for the tests and many of these were estimated in the models. These included details on the exact seating posture of the PMHS and the geometry and structure of the bench that the PMHS were seated on for the impact tests. The simulated contact friction between the pedestrian models and the simulated bench was set at 0.3.

As noted above, repeated shoulder impact simulations were completed with the modified JARI model and the joint characteristics and range of motion in the joints of the modified JARI shoulder were altered in order to tune the response of the model to that of the PMHS test data. During these simulations it was also found necessary to make the following additional alterations to the setup of the modified JARI pedestrian model:

- It was found during simulated shoulder impacts with the modified JARI pedestrian model that the contact definition between the high upper arm ellipsoids and the upper thorax ellipsoid (Figure 5) was obstructing the

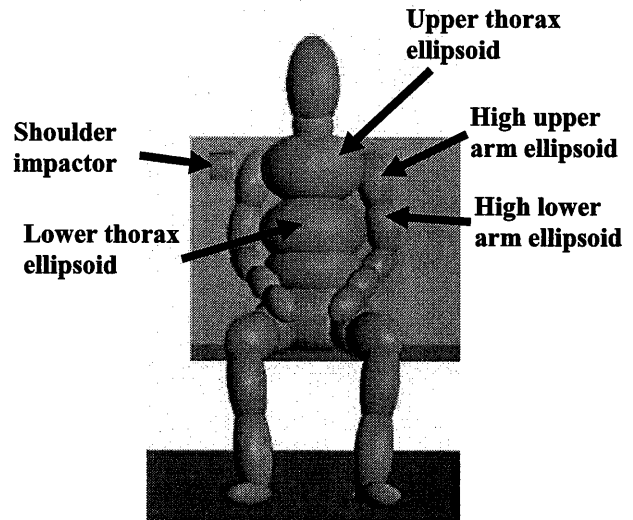
relative shoulder to shoulder displacement. It was rationalised that this contact definition placed an unrealistic constraint on the model as the relative displacement between the shoulders will be mainly controlled by the anatomical connections between the shoulders. As such, the contact definition between the high upper arm ellipsoids and the upper thorax ellipsoid was removed.

- During simulated shoulder impacts with the modified JARI pedestrian model it was found that the contact definition between the high lower arm ellipsoids and the lower thorax ellipsoid (Figure 5) was obstructing the relative shoulder to shoulder displacement. It was rationalised that the offending contact definition was too stiff and did not allow for the fact that the thorax ellipsoids provide a poor representation of the stiffness and profile of the real human thorax. Hence, this contact definition was altered to allow approximately 4 cm of free penetration between the ellipsoids in the contact prior to a contact restoring force being activated.
- The contact stiffness of the high upper arm ellipsoids (Figure 5) in the modified JARI pedestrian model was reduced. This led to a slightly softer contact between the impactor and the right shoulder of the modified JARI pedestrian model in comparison to that generated between the impactor and the right shoulder of the original JARI pedestrian model. This change in the stiffness for the contact definition was partly based on the measured shoulder skin thickness of PMHS made by Compigne *et al.* (2003) as shown in Table 2. The contact stiffness of the high upper arm ellipsoids was also changed from a non-elastic contact to an elastic contact.



**Figure 4.** Setup of the PMHS sub-injurious right shoulder impacts from Compigne *et al.* (2003).

In addition to these modifications the mass of the original and modified JARI pedestrian models was reduced from 72.5 kg to 50.5 kg, equalling the average mass of the PMHS used in the impact tests. This was achieved by scaling the mass of each anatomical component of the modified and original JARI models by 0.69.



**Figure 5.** Set-up of the JARI pedestrian model for the simulated shoulder impacts.

#### **Results - Evaluation of the modified JARI model's shoulder response**

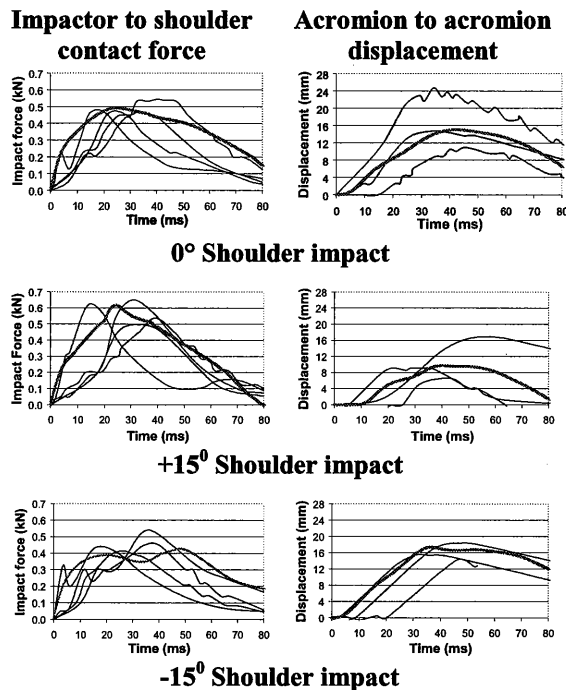
The versions of JARI pedestrian model developed and applied in this study were run under the version 6.1 release of MADYMO. Furthermore, all experimental and simulated predictions were filtered at CFC180. For the evaluation the impact forces and acromion to acromion deflections predicted by the original and modified JARI pedestrian models were compared against equivalent measures made in the PMHS shoulder impact tests of Compigne *et al.* (2003).

#### **Sub-injurious shoulder impact conditions -**

Measured and predicted shoulder impact forces and acromion to acromion displacements measured in the PMHS shoulder impact tests and predicted by the modified JARI pedestrian model are presented in Figure 6. As shown in the figure the predicted results are comparable in both magnitude and duration to those measured, for all directions in which the sub-injurious impacts to the right shoulders of the PMHS were simulated. In contrast to these results Figure 7 includes the predicted shoulder impact force from the original JARI pedestrian model for the 0° shoulder impact. It is noticeable in these results that the peak predicted shoulder impact force from the original JARI pedestrian model are over three times greater than those measured and predicted by the modified JARI pedestrian model. Furthermore, the profile of

the shoulder impact response is very different from that measured and predicted by the modified JARI pedestrian model. In the instance of the shoulder impact force there is an initial peak in predicted shoulder impact force followed by a series of short pulses due to a “chattering” contact between impactor and shoulder. This is a consequence of having a completely inelastic contact definition between the impactor and the shoulder in the original JARI pedestrian model. As described above this has been changed to an elastic contact definition for the modified JARI pedestrian model.

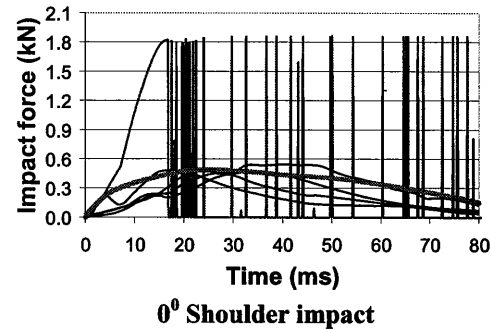
It has been shown by Neale *et al.* (2003a,b) that the shoulders of the original JARI pedestrian model are rigidly connected and do not displace with respect to each other under shoulder impacts, *i.e.* zero acromion to acromion displacement under all impact conditions. This behaviour is considerably different from that measured in the PMHS and predicted by the modified JARI pedestrian model, as shown in Figure 6, where even for the sub-injurious impacts the peak acromion to acromion displacement is between 5 and 25 mm.



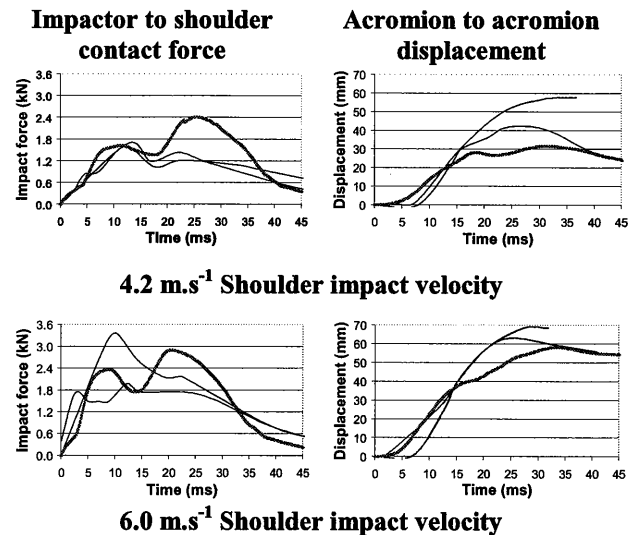
**Figure 6.** Comparison of the modified JARI model's predictions (red) with measured results from the PMHS sub-injurious impact tests of Compigne *et al.* (2003) (black).

**Injurious shoulder impact conditions -** For the injurious shoulder impact conditions the modified JARI model again provides comparable predictions of shoulder impact force and acromion to acromion displacement to those measured, as shown in Figure 8. A noticeable difference in the results is that the modified JARI model predicts a second larger peak in shoulder impact force which

is not observed in the experimental results. It is anticipated that this may be due to the fact that the modified model is currently unable to simulate damage to bones and ligaments of the shoulder. This explanation and behaviour is consistent with the lower peak values of acromion to acromion displacement predicted by the modified JARI model compared with those measured in the PMHS tests.



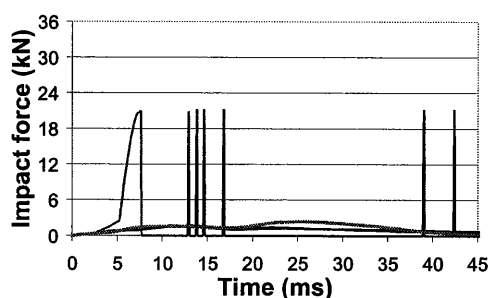
**Figure 7.** Comparison of the original JARI model's predicted shoulder impact force (blue) with that predicted by the modified JARI model (red) and measured in the PMHS sub-injurious impact tests of Compigne *et al.* (2003) (black).



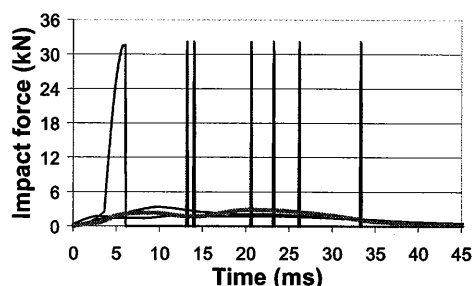
**Figure 8.** Comparison of the modified JARI model's predictions (red) with measured results from the PMHS injurious impact tests of Compigne *et al.* (2003) (black).

Figure 9 overlays the predicted shoulder impact forces from the original JARI pedestrian model with those measured in the PMHS tests and predicted by the modified JARI pedestrian model for the injurious shoulder impacts. The peak predicted shoulder impact forces from the original JARI pedestrian model are over eight times larger than those measured and predicted by the modified JARI pedestrian model and exhibit the same “chattering” response as predicted for the sub-

injurious impact conditions. As previously noted, the original JARI model does not simulate acromion to acromion displacement.



**Impactor velocity = 4.2 m.s<sup>-1</sup>**



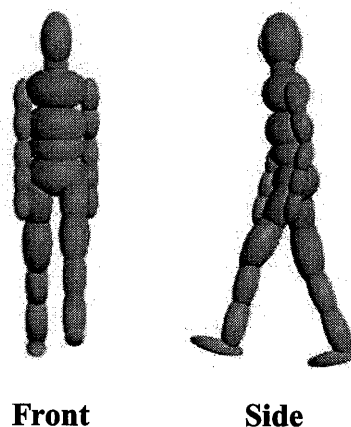
**Impactor velocity = 6.0 m.s<sup>-1</sup>**

**Figure 9. Comparison of the original JARI model's predicted shoulder impact force (blue) with that predicted by the modified JARI model (red) and measured in the PMHS injurious impact tests of Compigne *et al.* (2003) (black).**

#### COMPARISON OF VEHICLE TO PEDESTRIAN HEAD IMPACT RESPONSES

Five simulated pedestrian to vehicle impacts were completed with the original and modified versions of the JARI pedestrian model in order to assess the influence that the changes to the shoulder of the model have had on its predicted head impact response. Details of the setup of the simulations are presented in Table 3. Three vehicle shapes and two initial vehicle speeds were used in the simulations. The pedestrian models for the simulations were set in a natural walking posture as shown Figure 10, which closely matched the WP2 stance set for the pedestrian models in the simulated pedestrian impacts completed by the IHRA and detailed in the IHRA Pedestrian Safety Working Group paper (2002). In all the simulations the pedestrian models were struck on the right hand side by the simulated vehicle, with the exception of model setup 5 in Table 3 in which the pedestrian models were rotated by 90° and were struck from the rear, as shown in Figure 11. These additional runs were completed to consider an impact condition in which the shoulder does not strike the bonnet and would not influence the interaction of the head with the vehicle.

The structure of the simulated vehicle in the model runs matched that used by the IHRA in their model runs, as shown in Figure 11. It is constructed from three cylinders defining the edges of the bumper, bonnet and lower limit of the vehicle front. Planes have been joined between these cylinders to form the skirt, bumper, bonnet and windscreen of the simulated vehicle. These geometric shapes were repositioned and resized to obtain the desired vehicle shapes for the simulated vehicle to pedestrian impacts. As indicated in Table 3 the pedestrian impact with the Mid-sedan at 40 km.h<sup>-1</sup> was repeated with a long and short bonnet to consider impacts in which the head respectively hits the bonnet and windscreen of the vehicle. The stiffness characteristics for the structures of the simulated vehicle were chosen to provide a "safe" vehicle impact with the pedestrian, with the bonnet, bumper and bonnet leading edge of the simulated vehicle having a maximum contact load of 4 kN past 0.02 m of contact penetration, as shown in Figure 12. The simulated friction between the soles of the feet and ground was set at 0.67 and that between the pedestrian dummy and the vehicle front was set at 0.3. For all the impacts the simulated vehicles had a simulated braking acceleration of 0.5 g.



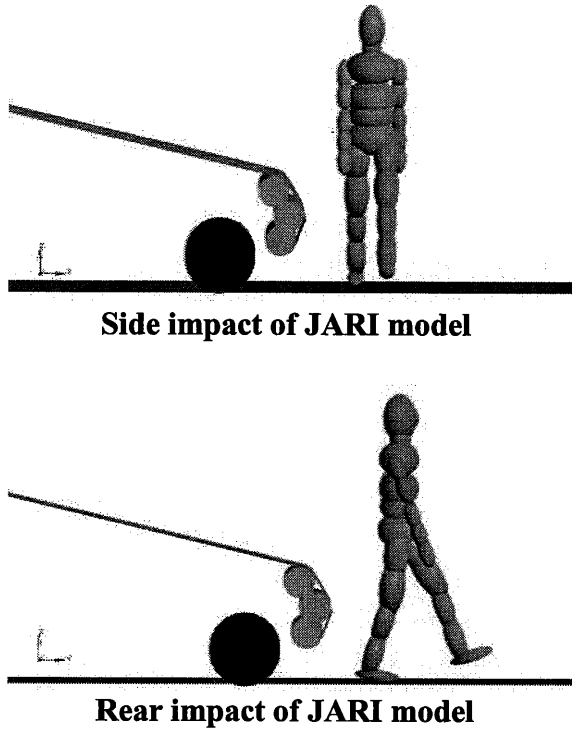
**Figure 10. Posture of the JARI pedestrian models for the simulated vehicle to pedestrian impacts.**

#### Results – Comparison of head impact conditions

Table 4 provides the predicted head impact conditions and head, shoulder and neck loads from the original and modified JARI models' predictions for the simulated vehicle to pedestrian impacts. Also included in the table are predictions from comparable simulated vehicle to pedestrian impacts completed by the IHRA working group with the original JARI pedestrian model (shaded values). However, in the simulations completed by the IHRA the arms of the pedestrian model were folded in front of the torso and the contact stiffness of the principle front end vehicle structures was



200 kN/m, *i.e.* considerably greater than the stiffness of the modelled vehicle used in the present study. Both of these vehicle stiffnesses are shown in Figure 12. The additional results from the IHRA provide added understanding on the variability that can be expected in the predictions from the model depending on how the simulations are set up.



**Figure 11. Orientation of the JARI pedestrian models for the simulated vehicle to pedestrian impacts.**

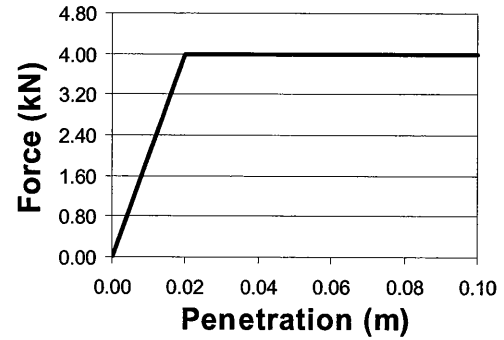
Included in Table 4 are the effective head impact masses from the model runs which were calculated according to the following formula:

$$m = \frac{\int_1^2 F dt}{\Delta v} = \frac{\int_1^2 F dt}{\int_1^2 a dt}$$

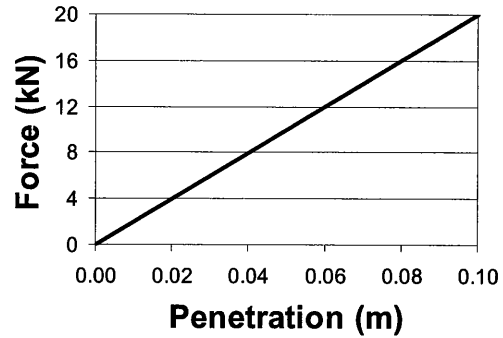
A discussion on the different methods available for calculating effective mass can be found in Annex A.

Direct comparisons of the original and modified JARI model predictions obtained in this present study (*i.e.* all values in Table 4 excluding those that are shaded) provides an indication of the influence that the modifications to the shoulder have had on the model's predictions. For these comparisons it is shown in Table 4 that the modified JARI pedestrian model predicts resultant head impact velocities which are between 0.33 to 1.43 m.s<sup>-1</sup> (2 to 14 %) greater than those predicted by the original JARI pedestrian model. Overall, neither of the models consistently predicts the greatest head impact

angles, although differences in these predictions range between 0.01 and 11.8° (0.01 and 32 %).



(a)



(b)

**Figure 12. Stiffness characteristics of the modelled vehicle – (a) as used in the present study (pedestrian friendly vehicle characteristics) and (b) as used in the JARI model runs completed by the IHRA.**

A comparison of the predicted head impact velocities for setups 2 and 5 shows that rotating the pedestrian model by 90° so that it is struck from the rear leads to an increase in the head impact velocity of 3.45 (28 %) and 4.55 m.s<sup>-1</sup> (39 %) for the modified and original models respectively.

Predicted head impact forces were almost consistently the same at 4.18 kN, which was consistent with the upper contact load limit of 4 kN set for the bonnet in the model runs as shown in Figure 12. Similarly, none of the predicted shoulder impact forces exceeded 4.18 kN. An exception to this trend was the head impact force predictions from model setup 1 which exceed 5 kN as a result of the modified and original JARI model heads striking the simulated windscreen, which had stiffer contact characteristics than the bonnet. In all the simulations completed the impact was sufficient to cause an acromion to acromion displacement greater than 30 mm in the modified JARI pedestrian model.

**Table 3**  
**Setup of the simulated vehicle to pedestrian impacts completed with the original and modified versions of the JARI pedestrian model**

Model setup	Vehicle	Model stance	Vehicle speed (km.h <sup>-1</sup> )	Bonnet length
1	Mid-sedan	Mid-stance	40	Short
2	Mid-sedan	Mid-stance	40	Long
3	Mid-sedan	Mid-stance	30	Long
4	Mid-SUV	Mid-stance	40	Long
5	Mid-sedan	90 <sup>0</sup> Rotated stance	40	Long

**Table 4**  
**Comparison of the modified and original (in brackets) JARI model predictions for simulated vehicle to pedestrian impacts. Shaded values are comparable values obtained by IHRA in their model runs of the original JARI pedestrian models with pedestrian unfriendly vehicle contact forces**

	Model setup (see Table 3)				
	1	2	3	4	5
Resultant head impact velocity (m.s <sup>-1</sup> )	12.05 (11.39) 9.0	10.75 (9.32) 9.0	9.46 (9.01) 10.91	12.08 (10.93)	14.20 (13.87)
Ratio of head impact and vehicle velocity	1.08 (1.02) 0.81	0.97 (0.84) 0.81	1.13 (1.08) 1.31	1.09 (0.93)	1.28 (1.25)
Head impact angle (°)	43.46 (44.91) 60.1	80.82 (69.05) 78.4	84.58 (81.65) 44.0	84.84 (84.83)	29.47 (40.49)
Effective head impact mass (kg)	5.12 (4.34)	4.23 (4.13)	4.21 (4.02)	3.63 (3.60)	6.12 (4.98)
Head impact force (kN)	5.66 (5.20)	4.18 (4.18)	4.18 (4.18)	4.18 (4.18)	4.18 (4.18)
Head to neck force (kN)	3.8 (3.4)	4.4 (2.6)	3.10 (3.06)	3.9 (3.0)	3.9 (4.66)
Acromion to acromion displacement (mm)	48.2 (0.0)	42.0 (0.0)	34.0 (0.0)	50.0 (0.0)	44.1 (0.0)
Shoulder impact force (kN)	3.60 (3.83)	4.18 (4.18)	3.07 (4.18)	3.16 (4.18)	3.78 (4.18)

Differences in the resultant head impact velocities and head impact angles predicted by the modified JARI pedestrian model with those previously obtained by the IHRA (shaded values in Table 4) range between 3.0 m.s<sup>-1</sup> (29 %) and 40.6° (63 %) respectively. In two out of three of the possible comparisons of the results in Table 4 the resultant head impact velocities predicted by the modified JARI pedestrian model are greater than those previously obtained by the IHRA and in

model run 3 the predicted head impact velocity from the JARI pedestrian model is lower than that previously obtained by the IHRA. Unfortunately it is not possible to interpret the reasons for this outcome on account of the fact that in addition to the shoulder structure the posture of the pedestrian model and stiffness of the vehicle structure was different for these two sets of model runs. As such, it is not possible to gauge which of these differences has contributed to this shift in the pattern of the results. However, the comparison of these model predictions does highlight the variations that can be obtained in the predictions from the JARI model compared with those that have previously been obtained by the IHRA and used in the development of the IHRA sub-system head impact test procedures.

## DISCUSSION

The modifications made to the JARI pedestrian model in this work have improved considerably the biofidelic impact response of the model's shoulders. These modifications have also had a considerable influence on the predicted head impact response of the JARI model's head during simulated vehicle to pedestrian impacts. This confirms the anticipated understanding at the onset of the work that the shoulder response is important to the dynamic response of the head during vehicle to pedestrian impacts.

Strictly speaking the biomechanical evaluation does not show that the modified shoulder validates as inputs to the model have been altered (iteratively) in order to get the model's predictions to match PMHS shoulder impact test results. These adjustments were made primarily to the characteristics of the Kelvin elements introduced into the shoulder, while fixed estimates were made for the characteristics of the joints added to the model. This was necessary because the required biomechanical data, which would typically be obtained from sub-system testing of the shoulder structure, was not available and certain anatomical features which would influence the shoulder response were not explicitly modelled. Nevertheless, by matching the key physical structures of the shoulder in the model with those of a real human and obtaining good agreement in five different impact conditions for the same model setup it is considered that the biofidelic response of the improved shoulder has been robustly tested.

The results of this work have significant implications on the IHRA's use of the JARI pedestrian model for developing aspects of the IHRA pedestrian head impact test procedures. It is implied from the model's predictions that if the modified JARI pedestrian model developed in this study were adopted by IHRA then recommended initial head impact velocities for the IHRA sub-system test procedures would be higher than if the

original JARI pedestrian model was used to obtain test parameters for the test procedures. In view of the fact that the modified JARI pedestrian model has been shown to provide accurate predictions of PMHS shoulder impact results there is increased confidence that the modified JARI pedestrian model provides predicted head impact conditions that are more representative than those of the original JARI pedestrian model. However, no firm conclusions can be drawn on what the final ratio of head impact velocity to vehicle speed should be at this stage. This will only emerge once the IHRA working group have completed their task of identifying and refining all the body parts of the model important to producing biofidelic head impact conditions. When the development and validation of this model is considered satisfactory, then it can be used to refine the current head impact test methods. Therefore, it is recommended that the TRL modifications made to the shoulder of the JARI pedestrian model should be adopted by the IHRA Pedestrian Safety Working Group as a first step towards developing their improved biofidelic pedestrian model.

The previous modelling work completed on the JARI pedestrian model (Neale *et al.*, 2003a,b) attempted to improve the model's shoulder response by adopting the same shoulder structure as that used in the pedestrian model developed by CASR in Australia. In addition to this modification, further changes made to the structure of the model in this work included the removal of a secondary contact defined between the legs and arms of the model which was inadvertently introduced by the original authors of the model and the introduction of joints to simulate axial stretching in the spine, the details of which were also taken from the CASR pedestrian model. Despite the fact that the changes made to the shoulders of the model in this previous work did little to improve the biofidelic shoulder response of the model, in several vehicle to pedestrian impacts simulated with the modified and original JARI pedestrian models the modified pedestrian model provided predictions of head impact velocity between 0.33 and 0.86 m.s<sup>-1</sup> (3.4 and 6.5 %) greater than those predicted by the original JARI pedestrian model. The suggestion is that there exist additional representative changes that could be made to the JARI pedestrian model in order to improve the accuracy of its predicted head impact response during vehicle to pedestrian impacts. For instance, it is known that the modelled JARI spine has a far simpler structure and response than that of a real human spine. It is most likely that this simplification of a spine would have a considerable influence on the impact response of the head during vehicle to pedestrian impacts.

It is noticeable from the models' predictions in this present study that the largest influence on the predicted head impact response arose by striking

the model from the rear rather than from the side. It is important to note that the whole body kinematics of the JARI model have not been validated for rear impacts as it has been for lateral vehicle to pedestrian impacts (IHRA pedestrian safety working group, 2002). As such it is necessary to place some caution on the absolute accuracy of the rear vehicle to pedestrian impact predictions and the interpretations that can be made. However, it is anticipated from these predictions that in addition to improving the biofidelic response of the pedestrian model, there are further alterations that could be made to the setup of the accident situation (including pedestrian stance) which could have a greater influence on predicted head impact responses.

The current study used stiffness characteristics for the vehicle that were "safe", with a maximum load per contact of 4.0 kN (see Figure 12). This was done because the IHRA test procedures are likely to be used to type approve cars, in which case the stiffness of those real cars would have to be broadly similar to that used. The contact stiffness is likely to be one of the main factors contributing to the differences noted between the 'original JARI model' runs performed for this study by TRL and previously obtained by the IHRA. It is therefore preferable that models used to obtain test parameters for type approval tests should have an appropriate *i.e.* "safe" vehicle stiffness, so that the headform test is representative of a real head impact into a type-approved vehicle.

## CONCLUSIONS

The aim of this investigation was to improve the shoulder response of the JARI pedestrian model, which has been chosen by the IHRA to develop the IHRA pedestrian sub-system head impact test procedure. The purpose of completing the work has been to improve the shoulder interaction of the pedestrian model during simulated vehicle to pedestrian impacts and so improve the resulting interaction of the head with the simulated bonnet. The modifications made to the shoulder of the pedestrian model have attempted to accurately represent the structure and range of motion of the anatomical shoulder.

Overall, the conclusions of the work are as follows:

- An improved shoulder model has been developed for the JARI pedestrian model.
- In comparison to the original shoulder, the structure of the improved shoulder model provides a much closer structural representation of the real human shoulder anatomy.
- In comparison to the original shoulder model, predictions from the improved shoulder model closely match measured

responses from PMHS shoulder impact test results.

- In general, it is implied from the models' predictions that predicted head impact velocities for simulated vehicle to pedestrian impacts are higher for the JARI model with the improved shoulder model than they are for the original JARI pedestrian model. As such, the recommended IHRA sub-system head impact test velocities would be higher if the structure of the test method were based on the predictions from the JARI model with the improved shoulder response. However, no firm conclusions can be drawn on the correct head impact conditions until all body parts of the model, important to producing biofidelic head impact conditions, have been identified and improved.
- Although it is likely that the shoulder model could be further improved the robust testing of its biofidelic response suggests that it is sufficiently well developed for use by IHRA.
- It is thought likely that the other areas of the pedestrian model such as the spine may need to be improved before its predictions are sufficiently accurate for them to be used by IHRA to specify head impact conditions.

## ACKNOWLEDGEMENTS

TRL Limited is grateful to the UK Department for Transport for funding this work. Further details on this and other associated research work funded by the DfT can be accessed at the DfT website – [www.dft.co.uk](http://www.dft.co.uk). Furthermore, the authors would like to express their thanks to JARI for allowing TRL to work on the development of their pedestrian model.

## REFERENCES

**Compigne S, Caire Y, Quesnel T and Verriest J (2003).** *Lateral and oblique impact loading of the human shoulder 3D acceleration and force-deflection data.* IRCOB Conference. Lisbon, Portugal, September 2003.

**IHRA Pedestrian Safety Working Group (2002).** *International Harmonized Research Activities Pedestrian Safety Working Group. 2002 report.* Document IHRA/PS/215 (1/2). Tokyo, Japan: Japan Automobile Standards Internationalization Center. (Document available at <http://www-ihra.nhtsa.dot.gov/>)

**Neale M S, Hardy B J and Lawrence G J L (2003a).** *Development and review of the IHRA*

*(JARI) and TNO pedestrian models.* Proceedings of the 18th International Technical Conference on the Enhanced Safety of Vehicles (ESV), Nagoya, Japan, 19-22 May 2003.

**Neale M S, Hardy B J and Lawrence G J L (2003b).** *Development and review of the IHRA (JARI) and TNO pedestrian models.* TRL Project Report PR/SE/653/03.

**Robbins D H (1983).** *Anthropometric specification for mid-sized male dummy, Volume 2.* The University of Michigan, Transport Research Institute Report UMTRI-83-53-2. 2901 Baxter Road, Ann Arbor, Michigan 48109: University of Michigan.

## ANNEX A: EFFECTIVE MASS CALCULATION FOR TRL HEADFORM PARAMETER MODEL

There are a number of ways of calculating effective mass when deriving a value for an impactor's mass. There are three decisions to be made:

- Use energy, impulse or average effective mass?
- Which direction to take?
- Which start and stop times to take when integrating?

Document IHRA PS215 (2002) has the formula

$$m = \frac{\int_{t_1}^{t_2} F/a \, dt}{(t_2 - t_1)}$$

This is simply averaging the instantaneous effective mass values over the period  $t_1$  to  $t_2$ . TRL hasn't used this method because it's possible to get values of acceleration ( $a$ ) that are very close to zero. These would at best have too much influence in the final result and could at worst give a result that was significantly high. This risk is much greater when a specific direction is used rather than resultants.

The energy method uses the deformation energy (obtained from integrating force by penetration) and the  $\Delta v$  (which is of course the time integral of

acceleration), and the formula  $m = \frac{2 \int F \, ds}{(\Delta v)^2}$ . TRL has used this method in the past, for upper legform masses.

The impulse method uses impulse (obtained from integrating force by time) and the  $\Delta v$ , and the

$$m = \frac{\int_{t_1}^{t_2} F \, dt}{\Delta v} = \frac{\int_{t_1}^{t_2} F \, dt}{\int_{t_1}^{t_2} a \, dt}$$

formula. This is effectively average force over average acceleration. This is the method used for the results reported.

The effective mass can be different in different directions. Physically, the forces required to cause a given acceleration will depend on the direction.

For instance, at the knee the effective mass would be least in the knee's normal direction of movement (within its normal range), greater for lateral knee bending and highest of all for axial leg movement. The headform parameter model is being used to find the appropriate parameters for a headform impact into a bonnet. Although the headform may hit the bonnet at an angle, the  $\Delta v$  will be nearly normal to the bonnet, with the headform velocity parallel to the bonnet being relatively unchanged. Therefore, TRL considers that the effective mass normal to the bonnet is the appropriate one to take, obtained by taking both bonnet-to-head force and head acceleration normal to the bonnet, ignoring orthogonal components. Using resultant acceleration would include neck interactions that cause head accelerations parallel to the bonnet, which are not appropriate for a headform impactor.

One pair of runs with the normal length bonnet involved head to windscreen impact; in this case the force and acceleration were taken normal to the windscreen.

IHRA PS215 (2002) gave three options for the start and stop times of the integration. The 10% effective mass method is unlikely to work if the forces and accelerations are taken normal to the bonnet, as the effective mass will be more constant over the time history. The dummy model HIC window can be quite different to the actual head to bonnet impact, because of acceleration components parallel to the bonnet, and hence to the eventual headform HIC window. TRL therefore prefers and has used the 10% force method.

IHRA PS215 (2002) doesn't specify what points are taken when the time histories are not uni-modal. Where this occurred the period taken was from the first to the last 10% force value. However, in other cases if there should be a brief spike it might be more appropriate to take only the main part.

# **ANALYSIS OF PEDESTRIAN-VEHICLE CRASHES IN KOREA:**

## **Focused on developing probabilistic pedestrian fatality model**

**Cheol Oh, Youn-soo Kang, Beomil Kim**

Center for Advanced Transportation Technology

The Korea Transport Institute

**Wonkyu Kim**

Hankuk Aviation University, Korea

Paper number: 05-0131

### **ABSTRACT**

Microscopic analysis of pedestrian-vehicle accident data is a backbone of devising various intelligent functionalities of vehicles to mitigate the fatality and injury severity of pedestrian in pedestrian-vehicle crashes. Worldwide significant effort has been directed at developing advanced vehicles for protecting pedestrian by the assistance of analyzing very detailed pedestrian accident data. As a part of the multi-year project titled with 'Development of Advanced Vehicle for Pedestrian Protection', this study analyzes pedestrian-vehicle crash data. Firstly, overview of the characteristics of pedestrian-involved crashes in Korea is presented. Another major focus of the study is to develop a probabilistic pedestrian fatality model. The logistic regression approach, one of the multivariate statistical modeling techniques, is applied in the model development. The developed model is expected to support various safety policies and evaluations of advanced systems of vehicles toward enhancing pedestrian safety. The findings of this study would be an invaluable linkage between pedestrian accident data and the development of various countermeasures for pedestrian protection.

### **INTRODUCTION**

A variety of research efforts including accident

data analyses have been performed to enhance safety on highways significantly. In particular, the most valuable finding from analyzing pedestrian accident data would be to discover effective countermeasures to alleviate both fatality and injury severity of pedestrian. Among various safety-related studies based on accident data analysis, to deal with pedestrian would be considered one of the keen interests. It is mainly because pedestrians are the most vulnerable element in transportation systems, which need to be primarily protected. From this perspective, thorough understanding of causes and effects of pedestrian accidents is a fundamental to prepare for feasible solutions to save human lives.

According to a study dealing with comparing accident statistics [1], it has been identified that Korea has been highly ranked in terms of frequency, fatality, and injury severity among OECD (Organization for Economic Cooperation and Development) countries. Hence, more rigorous and active efforts need to be performed to avoid such dishonor, which motivate this study. This study focuses on analyzing pedestrian-vehicle crashes, which ultimately attempts to find underlying clues to reduce both pedestrian fatality and injury severity. Two view points are taken into consideration in this study. Firstly aggregated pedestrian accident statistics is further analyzed to identify the accident

characteristics. The second view of this study is to develop a probabilistic pedestrian fatality model using data obtained from accident reconstruction. The model would contribute to evaluating advanced safety systems of vehicles and deriving safety policies.

After pedestrian accident data are analyzed statistically to discover the implications on safety policies, how to develop a model of collision speed in a statistical manner is presented. The binary logistic regression modeling approach is employed in this study. Then, the interpretation of the model is given with discussions about findings and future research. Conclusions are described along with the direction of future research.

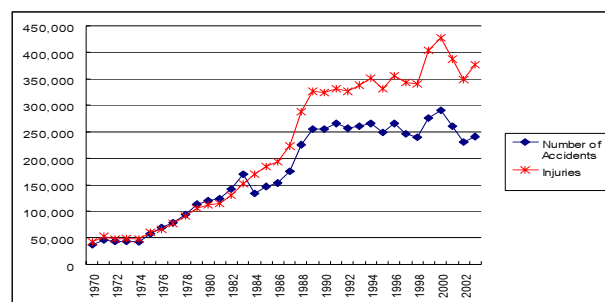
## OVERVIEW OF PEDESTRIAN ACCIDENT IN KOREA

The total number of accidents a year has steadily declined since 1970 in Korea as shown in Figure 1. Furthermore, 1990 can be seen as a turning point of trends in both fatalities and injuries, which shows the trend does not increase rapidly any more. It can be seen that huge national efforts to reduce the accident occurrence have been effective.

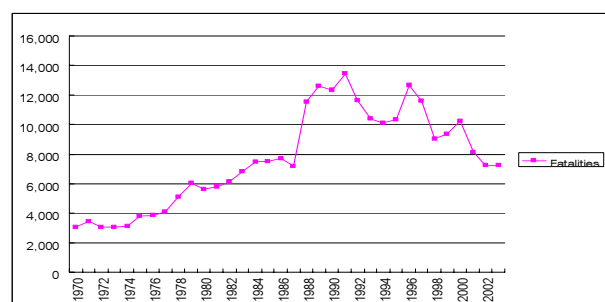
Although the transportation safety environment represented by a couple of accident statistics as the above seems to be improved, we still should pay attention to the international accident statistics. It is stated by the literature [2] that the number of accidents per 10,000 vehicles in Korea is the highest, in comparing with other OECD countries. Figure 2 depicts more details on the comparison.

Another important statistics that should be concerned is the pedestrian-involved accident.

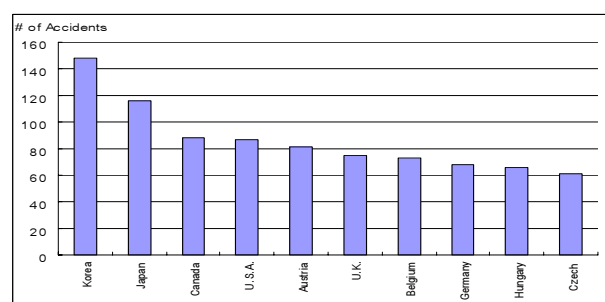
Among 30 OECD countries, Korea has been unfortunately positioned at the first rank, as shown in Figure 3, in comparing the death rate of pedestrian, which is approximately 43.0%. Therefore, it is truly apparent that protecting pedestrian in the transportation system needs to be taken care of with the highest priority by researchers and practitioners.



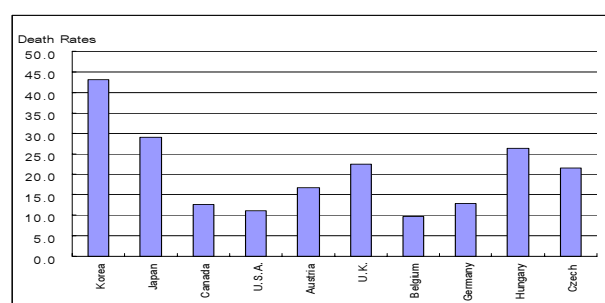
<Figure 1-(a) Trends of accidents and injuries>



<Figure 1-(b) Trend of fatalities>



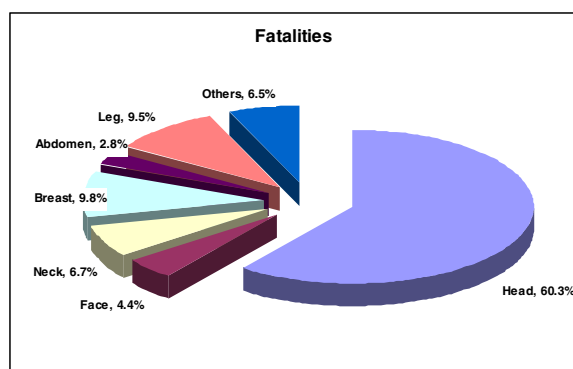
<Figure 2 International comparison of accidents per 10,000 vehicles>



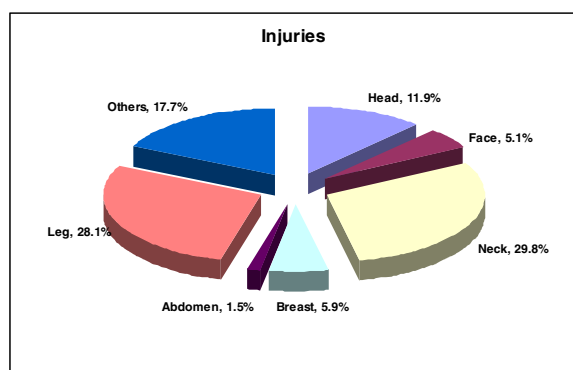
<Figure 3 Death rates of pedestrian for OECD countries>



Identifying injury body regions of pedestrian would be invaluable for further development of countermeasures to protect pedestrian that is the most vulnerable element than any other one in transportation systems. Head has been identified as the most critical injury region resulting in fatalities. In 2003, 1,745 pedestrians passed away mainly due to head injury in pedestrian-vehicle crashes, which corresponds to 60.3% of total pedestrian fatalities. Chest injury was another major body region resulting in pedestrian fatalities. On the other hand, neck and leg region have been recognized as major body region for the pedestrian injury. Neck and leg regions occupy 57.9% of pedestrian injury accidents. Details of injury body regions for fatalities and injuries are presented in Figure 4.



<Figure 4-(a) Injury body regions: Fatalities>



<Figure 4-(b) Injury body regions: Injuries>

Insight into the injury body regions provides us with a precious opportunity of how to cope with

pedestrian accidents. It can be concluded that special cares on both the head part including neck and the leg part needs to be performed. An example of countermeasures toward protecting pedestrian would be to develop an advanced vehicle capable of protecting head and leg of pedestrians.

## DATA PREPARATION FOR MODEL DEVELOPMENT

An accident report form, which was developed for this study, was distributed various agents that are in charge of reporting accidents on June of 2003. The form includes information on pedestrian, vehicle, highway, and environment. A total of 92 pedestrian accident cases have been collected as of now (December, 2004). Acquired accident cases were analyzed by National Institute of Scientific Investigation (NISI) and Center for Accident Analysis of Hanyang University, specialized in accident reconstruction. A major outcome of accident reconstruction was that collision speeds in pedestrian-vehicle crashes were discovered to be further utilized in establishing a model of pedestrian fatality.

As a part of accident reconstruction, estimating collision speed is of keen interest. Useful applications using the model of collision speed are plentiful. One of the nice examples is to be utilized in exploring the analysis of pedestrian trajectories in pedestrian-vehicle crashes, which can be further applied to develop advanced safety systems of vehicles for pedestrian protection. Also, researchers and engineers in the field of pedestrian safety have been recently working on establishing a global technology regulation to protect pedestrians in pedestrian-vehicle crash. Analyses on accident data associated with colliding pedestrians with vehicles are also the backbone of developing the regulation. Recently,

Korea has joined the pedestrian working group for international harmonization activities.

Various studies were performed for estimating more reliable and accurate collision speed. As examples, three methods used widely to estimate collision speed are introduced.

• Schmidt and Nagel (1971)

Schmidt and Nagel [3] found that collision speed is related with the distance from initial collision spot to final location of pedestrian on the ground.

$$V_x = \sqrt{\mu^2 \times h + e - \mu \times h}$$

where

$V_x$  : collision speed (m/s)

$\mu$  : coefficient of friction

$h$  : height of center of pedestrian weight

$d_i$  : distance from initial collision spot to final location of pedestrian

$e$  :  $2 \times \mu \times g \times d_i$

$g$  : gravitational constant of 9.8 m/s<sup>2</sup>

• Stcherbatchef et al. (1975)

It was revealed by Stcherbatchef et al. [4] that the distance from initial collision speed to final location of pedestrian is a function of the collision speed and the deceleration rate of vehicle.

$$d_i = \frac{V_e^2 - V_i^2}{2a} + kV_x$$

where

$k = \lambda \times a$  ,  $\lambda = 0.03$

(empirical value found by experiments)

$a$  : deceleration rate of vehicle (m/s<sup>2</sup>)

$V_i$  : initial vehicle speed (m/s)

$V_e$  : final vehicle speed (m/s)

$t$  : time (sec)

• Collins and Moris (1979)

Collins and Moris [5] reported that the distance from initial collision spot to final location of pedestrian can be estimated by the collision speed and the height of center of pedestrian weight.

$$d_t = \frac{V_x \times \sqrt{h}}{7.97} + \frac{V_x^2}{254 \times \mu} (m)$$

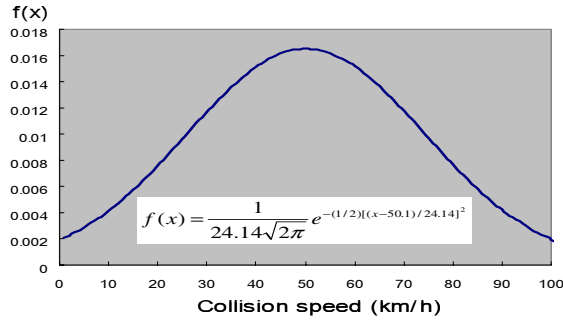
$$x = \frac{-B \pm \sqrt{B^2 - 4 \times A \times C}}{2 \times A}$$

$$A = \frac{1}{254 \times \mu} , B = \frac{\sqrt{-h}}{7.97} , C = -d_i$$

Basic statistics on collision speeds derived from the accident reconstruction are given in Table 1. Additionally the estimated normal distribution of collision speed obtained from accident reconstruction in this study is depicted in Figure 5.

Table 1 Statistics on collision speed

Mean	Std. Error of Mean	Median	Mode	Std. Deviation	Min	Max
<b>50.10 kmp</b>	<b>2.28</b>	<b>45.00</b>	<b>40.00</b>	<b>24.14</b>	<b>4.00</b>	<b>103.00</b>



<Figure 5 Normal distribution of collision speed>

## MODEL DEVELOPMENT: PROBABILISTIC PEDESTRIAN FATALITY MODEL

A statistical model, which is able to measure fatality of pedestrian struck by vehicle in a probabilistic manner, was developed in this study. The developed model relates the fatality of pedestrian in pedestrian-vehicle crashes to collision speed, vehicle characteristics and pedestrian characteristics. The model is expected to be very useful for researchers and practitioners in the field of both transportation safety and automobile. Firstly, the model could assist in estimating safety benefits quantitatively in case that a certain countermeasure associated with collision speed is employed for safety enhancement. An example includes that the effect of change in speed limit, which established from the consideration of collision speed and its effect on fatality, can be more comprehensively quantified. Taking vehicle characteristics into consideration in modeling pedestrian fatality could provide invaluable implications on developing new vehicles for pedestrian protection. Of course, it should be noted that extensive data analyses are required in order to obtain reliable outcomes prior to drawing conclusions.

A logistic regression modeling approach was applied to the pedestrian fatality problem. The

relationship between a dependant variable, which is a non-metric variable in particular, and one or more independent variables is modeled. Unlike discriminant analysis, when the dependant variable has only two groups, logistic regression may be preferred for several reasons [6]. One of the major reasons is that discriminant analysis relies on strictly meeting the assumptions of multivariate normality and equal variance, which logistic regression does not face such an assumption. In a case of binary logistic regression, 1 or 0 is taken as a dependent variable in modeling. The binary logistic regression model predicts the probability that the dependent variable would take 1. Therefore, what the dependant variable takes 1 means that the probability of pedestrian death is 1 in this application.

The form of a logistic regression model in this study is

$$P(F_i = 1 | X_i) = \frac{\exp[f(X_i, \beta)]}{1 + \exp[f(X_i, \beta)]}$$

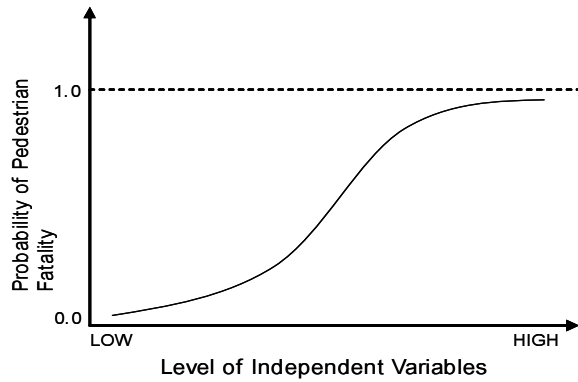
where

$F_i$  : dependant variable representing the pedestrian death ( $F_i = 1$ ) or survival ( $F_i = 0$ ) of the event for pedestrian-vehicle crash  $i$

$X_i$  : vector form of selected independent variables affecting pedestrian fatality

$f(X_i, \beta)$  : a function of  $X_i$  and a parameter vector  $\beta$  to be estimated

Fatality probability values can be any value between 0 (survival) and 1 (death), but the predicted fatality value can not be out of the range of 0 and 1. To define a relationship bounded by 0 and 1, logistic regression uses an assumed relationship between the independent and dependent variables that resembles an S-shaped curve as shown in Figure 6 [6].



**<Figure 6 The logistic relationship between pedestrian fatality and independent variables>**

SPSS statistical analysis package was employed in modeling the pedestrian fatality. A variety of independent variables in the form of accident report

were considered as candidates for representing the pedestrian fatality. Those include collision speed and characteristics of pedestrian, vehicle, highway and environment. Details are presented in Table 2. Based on large efforts on modeling, three independent variables which are collision speed ( $V_x$ ), vehicle type ( $VT$ ), and pedestrian age ( $AGE$ ), were chosen to build up a probabilistic pedestrian fatality model. To investigate the potential of multicollinearity among the variables, the correlation analysis was conducted. As shown in Table 3, any pair of variables did not show high correlation, which correlation coefficients exceed 0.5. Some descriptive statistics of the independent variables are also given in Table 3.

Table 2 Candidates of independent variables

Item	Detailed information
General	Time and location of accident
Pedestrian	Gender, Age, Height, Weight, Drinking, Injury severity, Contact points (1 <sup>st</sup> , 2 <sup>nd</sup> , 3 <sup>rd</sup> )
Vehicle	Vehicle type(1: passenger car, 2: suv, 3: 1box, 4: bus/truck ), Production year
Highway and Environment	Super-elevation, Pavement condition, Accident location (intersection, mid-block, pedestrian crossing), Speed limit, Contact points (1 <sup>st</sup> , 2 <sup>nd</sup> , 3 <sup>rd</sup> ), Weather condition

Table 3 Correlation coefficients and descriptive statistics of the independent variables

Variable/Statistic		$V_x$	$VT$	$AGE$
Correlation Coefficient	$V_x$	1.000	-0.074	-0.233
	$VT$	-	1.000	-0.100
	$AGE$	-	-	1.000
Mean		50.100	40.123	1.384
Standard deviation		24.138	0.892	17.853
Minimum		4.000	1.000	6.000
Maximum		107.000	4.000	75.000
Skewness		0.181	2.295	-0.053
Kurtosis		-0.580	3.959	-0.622

Table 4 summarizes the results of the pedestrian fatality model with the specification of a binary logistic regression. The model pertains to the effect of collision speed, vehicle type, and age on the pedestrian fatality. One of the major findings from the analysis is that we statistically verified collision speed is the most significant variable affecting the pedestrian fatality with the largest Wald statistic and the lowest significance level. The model was able to correctly classify 84.4 percent of the pedestrian-vehicle crashes as pedestrian death or survival, with a classification cutoff threshold of 0.5 membership value.

Table 4 Results of logistic regression

Statistic	$V_x$	$VT$	$AGE$	Constant
Wald statistic	13.700	3.252	2.499	7.880
Standard error	0.025	0.381	0.025	2.094
$\beta$	0.092	0.687	-0.039	-5.878
Significance	0.000	0.071	0.114	0.005

---

- Correct classification rate: 84.4%
- -2 log likelihood: 40.287
- Model chi-square: 37.562
- Nagellerke R-square: 0.631

---

## DISCUSSION OF RESULTS

### Findings

The logistic regression model developed in this paper predicts the probability of pedestrian fatality in pedestrian-vehicle crashes. The variables employed as the independent variables of the model and their coefficients are listed in Table 4. Three independent variables include collision speed, pedestrian age, vehicle type. Collision speed denoted as  $V_x$ , which was recognized as the most significant factor to determine the pedestrian fatality, represents the situation of accident. Age and vehicle type can be viewed as the representatives of pedestrian characteristics and vehicle characteristics, respectively. As shown in Table 4, it can be interpreted by identifying the negative coefficient of  $AGE$  that as pedestrian age increases the probability of fatality decreases. That is, children are exposed to higher fatality in the transportation system. In addition, heavy vehicles have more influence on the fatality than light vehicles.

In a view point, the findings would be natural. However, the contribution is that the model allows us to quantify the pedestrian fatality in a probabilistic manner, which can assist in measuring the safety effects of countermeasures. Further analysis of the probability of pedestrian fatality can be also

converted into monetary value, which leads us to be able to conduct economic appraisals of countermeasures. As an example, the model would support how to estimate the benefits of brake assistant systems (BAS) resulting possibly in reducing collision speeds.

### Future Research

In addition to the considerations in developing the probability model of pedestrian fatality, we still have a variety of research opportunities to improve model development and to derive countermeasures for the pedestrian protection. First of all, a lot of crash data should be collected and further analyzed in order to obtain more statistically reliable and accurate model. Regarding the selection of independent variables, vehicle types can be divided into more substantial variables representing vehicle characteristics. Parameters representing the frontal shape of vehicles can be considered independent variables of the model. Those parameters include bumper lead (BL), bumper center height (BCH), leading edge height (LEH), bonnet length (BL), and bonnet angle (BA) etc. If those parameters can be incorporated into the fatality model, we will be able to see how vehicle frontal shapes affect the pedestrian injury. Establishing fine and huge crash dataset is a matter of course as a prerequisite for future research.

## CONCLUSION

Overview of the characteristics of pedestrian-involved accidents in Korea was presented. The major focus of the study was to develop a probabilistic pedestrian fatality model. The logistic regression approach, one of the multivariate statistical modeling approaches, was applied in the model development. The developed model is expected to support various safety policies and evaluations of advanced systems of vehicles to protect pedestrian. Collision speed, pedestrian age, and vehicle type were used as independent variables of the model. Findings and future research were also discussed. In-depth further study with a lot of crash data will be performed in the future.

## ACKNOWLEDGMENT

This study was conducted as a part of the multi-year project titled with “Development of Advanced Vehicle for Pedestrian Protection” funded by the Ministry of Construction and Transportation (MOCT) under the Korean government.

## REFERENCES

- [1] *Statistical Analysis on Traffic Accidents*, Korea Road Traffic Safety Authority, 2004.
- [2] *A Comparative Study of Accident Statistics for OECD Countries*, Center for Accident Analysis, Korea Road Traffic Safety Authority, 2004.
- [3] Schmidt, D. N, and Nagel, D. A. (1971), ‘Pedestrian Impact Case Study’, *Proceedings of 15<sup>th</sup> Conference Association for Automotive Medicine*.
- [4] Stcherbatcheff, G. et al. (1975), ‘Simulations of Collisions between Pedestrian and Vehicles using Adult and Child Dummies’, *SAE Paper*, NO. 751167.
- [5] Collins, J.C., and Moris. J. L. (1979), ‘*Highway*

*Collision Analysis*’, Thomas Publishing.

- [6] Hair, J.F. et al. (2003), ‘*Multivariate Data Analysis*’, Pearson Education.



## ACTIVE PEDESTRIAN PROTECTION

**Mike McCarthy**

**Ian Simmons**

TRL Ltd

UK

Paper number 05-0164

### ABSTRACT

Vulnerable road users, especially pedestrians, are more susceptible to fatal and serious injury compared with vehicle occupants. Although the frequency of accidents involving pedestrians has reduced in recent years, there are still approximately 800 pedestrians killed and 7,000 seriously injured every year in Great Britain. Furthermore, in the late nineties, more than 6,000 pedestrians were fatally injured annually on EU roads, accounting for approximately 20% of all road fatalities.

The kinematics of pedestrian impacts has been well documented and test procedures have been adopted by EuroNCAP and changes made to EU regulation. Whilst this is aimed at driving improved pedestrian-friendly car design, further benefits could be achieved with the use of pre-crash sensing and active safety systems. Such systems require sensors capable of accurately and reliably detecting the presence of a pedestrian prior to a collision, and activating protective countermeasures effectively in order to reduce the pedestrian injury risk.

Accident data has been collected as part of a project developing a sensing system for cars capable of detecting and reacting to the presence of pedestrians. Systems that use radar, infra-red, laser, or ultrasound sensors to scan the 'target area' for obstacles, must be intrinsically safe, accurate and reliable, yet low cost in mass-production. A sensor array comprising both radar and infra-red devices has been developed as part of a project for the UK Foresight Vehicle programme. Other work has involved systems that have been developed to demonstrate the potential for using external airbags to provide a means of protecting pedestrians during a frontal impact.

This paper examines the pedestrian accident data, and the specification and application for pre-crash sensing. Systems for pedestrian detection and protection have been developed and the research in these areas is described.

## INTRODUCTION

Although the frequency of accidents involving pedestrians has declined over recent years, during 2003 there were 774 pedestrians killed in Great Britain and over 7,159 pedestrians who sustained seriously injury (DfT, 2004). These pedestrian fatalities account for 22% of all road traffic accident fatalities in Great Britain (DfT, 2004). A similar situation exists in the EU, where in 1999, 32,552 road users were killed on EU roads, of which, 6,196 (19%) were pedestrians (OECD, 2001). These figures demonstrate, both in societal and financial terms, the need for improved protection directed at this group of vulnerable road users. This paper describes the requirements for advanced pedestrian protection, which includes a system which detects pedestrians in the vehicle's path, together with a concept protection system designed to minimise injuries to pedestrians involved in an impact with a car.

There are many types of pedestrian protection system that may be considered for vehicles. These include driver warning, brake assist, automatic braking and collision avoidance (primary safety) and external airbags, 'pop-up' bonnets, and advanced energy-absorbing materials (secondary safety). This paper describes some of the findings from work carried out in the UK to develop a detection system that could be combined with an appropriate protection system. The detection system was developed by the Advanced Protection of Vulnerable Road Users project (APVRU) with the aid of funding from the UK Department for Trade and Industry Foresight Vehicle Programme. This followed on from work commissioned by the UK Department for Transport investigating active adaptive secondary safety (AASS, [www.rmd.dft.gov.uk](http://www.rmd.dft.gov.uk)), which showed that pedestrian protection in the form of airbags sited on the bumper and bonnet of a vehicle had the potential to reduce significantly injury potential in 40 km/h (25mile/h) and 48 km/h (30mile/h) impacts. For example, experimental tests conducted as part of the AASS study showed that the Head Injury Criteria (HIC) could be reduced by 93%, chest acceleration by 49%, pelvis acceleration by 12% and lateral knee acceleration by 71% (Holding *et al*, 2001).

If a pedestrian protection system is to confer maximum benefit, the sensor system and algorithms play a vital role in detecting appropriate targets and determining when the system should and should not activate. The system must activate if a collision is imminent in order to reduce the injury risk to the pedestrian. However, the system must not react inadvertently, and must not expose the pedestrian, or interacting road users, to an

increased risk of injury than would otherwise occur without the safety system. Furthermore, the sensors must be capable of distinguishing between pedestrians and inanimate objects, such as roadside furniture. Other issues exist regarding the resetting of any deployable system, the use of which must be fully justified in cost benefit terms.

## PEDESTRIAN INJURIES

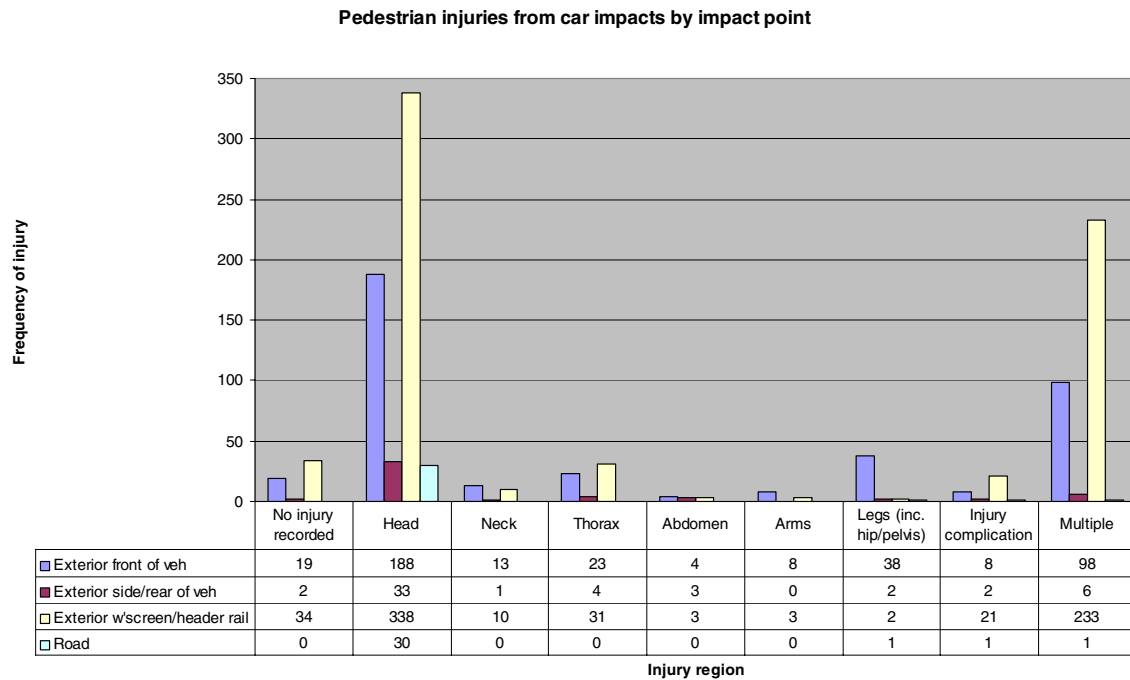
Pedestrian injuries resulting from impacts with cars frequently result from a primary impact to the lower or upper leg, and depending on the speed of the impact, a secondary impact (often causing head injury) on the upper bonnet, windscreen or windscreen surround. Furthermore, there may be a tertiary impact with the ground and also a risk that the pedestrian may be struck by other vehicles. The injury severity resulting from the primary impact may be reduced by using, for example, soft bumpers. Pop up bonnet or airbag systems have the potential to protect against the secondary impact and may also provide a means of retaining the pedestrian on the vehicle bonnet in lower velocity impacts. Research by TRL using external airbags sited on the bumper and bonnet demonstrated the potential for retaining the pedestrian on the vehicle bonnet at the impact speeds tested (Holding *et al* 2001).

The impact velocity is perhaps the most important factor in determining the injury severity of an accident involving a pedestrian. For example, of 543 pedestrians who sustained head injury, Otte (1999) found that the risk of brain injury at 30 km/h was less than 20%, whereas at 40 km/h this risk had risen to 40%. Furthermore, according to the European Transport Safety Council, at impact velocities in excess of 50km/h (31mile/h), the likelihood of pedestrian survival is less than 50%. If however, the impact velocity is 30km/h (19mile/h) or less, approximately 90% of those

struck may survive (Carlsson, 1996). Accident data was investigated because the impact velocity has implications for the number of impacts in which injury mitigation may be successfully conferred. Furthermore, the range of real-life impact velocities for which injuries may be reduced has implications for the time available for the system to detect and react to an imminent impact.

Data from the TRL Fatals database (a Dft funded database analysing fatal police accident files - [www.rmd.dft.gov.uk](http://www.rmd.dft.gov.uk)) was used to gain information estimates of the impact speed. The results of this analysis indicated that 6.4% of fatalities occurred at 32km/h (20mile/h) or less, 41.5% at 48km/h (30mile/h) or less and 70.6% at less than 64km/h (40mile/h). Otte (1999) also noted a strong bias towards low velocities, with approximately 70% of pedestrian impacts occurring at impact velocities up to 40km/h (25mile/h). In higher velocity impacts, Otte (1999) estimated the risk of serious (AIS 2-4) injury to be 65%. He also found that the head was the most seriously injured body region, with 60% of pedestrians involved in car impacts suffering head injuries, and that higher impact velocities were correlated with more severe head injuries. Thus, this indicates that a significant proportion of pedestrians are killed at impact speeds for which an advanced protection system using airbags on the bumper and bonnet has been shown to provide substantial protection (Holding *et al*, 2001).

Figure 1 shows the distribution of pedestrian injuries by impact point from the UK Fatals database. Analysis of this source shows that the body region most frequently injured was the head, 50.8% of cases. Multiple injuries accounted for 29.1% of cases. The next most frequently injured body regions were the thorax, 5.0%, and legs, 3.7%.



**Figure 1. Frequency of pedestrian injuries by impact point (UK Fatals database)**

Identification of the important injury mechanisms of pedestrian injury is essential for the development of an effective protective system. IHRA data, collected from a range of on-the-spot accident research projects, indicates that for injuries AIS $\geq$ 2, the legs are the most frequently injured body region, 35.6%, followed by the head, 29.0%, chest, 12.5%, and neck, 10%. The discrepancy between this data and the UK Fatals database may be explained by the fact that in more severe accidents, the impact velocity is greater and the trajectory of the pedestrian is likely to result in a more severe head strike on the vehicle.

Stats19, the UK database on personal injury road accidents, resulting casualties, and the vehicles involved, data was also analysed for APVRU and showed that the majority of pedestrians hit by cars were crossing the road away from pedestrian crossings. This group accounted for 80.3% of the 1,203 pedestrian casualties. Over 25% of casualties were also recorded as not being seen by the driver of the impacting vehicle due to roadside obstructions to vision.

Holding *et al* (2001) has shown that protective airbags are successful at reducing injury potential in certain impacts up to 48km/h (30mile/h) when sited on the front of the vehicle to protect the legs from the initial contact, and also on the upper bonnet or lower windscreen frame to prevent head contact with the bonnet or windscreen area.

However, further research is required regarding the response of such a system in a wider range of accident configurations and impact speeds to ensure that the injury risk is not increased compared with non fitment.

## SENSOR TECHNOLOGIES

It is apparent that accurate pre-crash sensing is critical to the successful application of advanced protection systems for vulnerable road users. Sensors need to be able to detect and track pedestrians over time and reliably distinguish the vulnerable road user from the environment. They also have a requirement to be unaffected by external influences for example: EMC, solar loading, wind, rain, fog and mud. The type of system chosen must respond sufficiently rapidly and accurately to permit the system to activate correctly to minimise the injuries sustained, hence the range and update rate of the sensors are important.

Research conducted as part of the APVRU project concluded that no single sensor will offer an acceptable solution, and that the problem of pre-crash pedestrian detection is best addressed by using radar for target ranging and passive infrared for distinguishing of pedestrians from the road environment. Radar sensors being developed for ACC (adaptive cruise control) could be used for the early prediction of a collision, before shorter range radars which cover a much greater angle continue

to track targets in closer proximity to the vehicle. An alternative solution would be to use an active transponder. It is suggested that this would be very inexpensive and would not be severely affected by adverse weather. A summary of sensor types reviewed is given in Table 1.

**Table 1.**  
**Summary of sensors used for detecting pedestrians**

System	Range	Cost	Carrier freq	Comments
Microwave radar	30-150m	low	60GHz	not affected by darkness
FMCW radar	2-100m	low	76-77GHz	not affected by darkness
Millimetre-Wave real aperture radar	>100m	low	14 or 56GHz	
Active millimetre wave radar	3-100m	low	76-77GHz	
Passive millimetre wave sensors	<150m	low	24GHz 125MHz	insensitive to fog, snow and rain
Infrared sensors	<25m	low	$\lambda=2-4\mu\text{m}$	resolution problems in hot weather
Active infrared (laser/ LED based)	LED 30m (laser 130m)	med/ high	890GHz	will not work in strong sunlight
Lidar	<60m	med	50ns	insensitive to rain, fog, snow but sensitive to dirt
Passive infrared	up to 25m	med	3kHz	more expensive camera required in hot climates
Ultrasonic	8mm - 20m	very low	22kHz 40kHz 50kHz	some clothing does not reflect signal
Active transponder	<20m	low		
Image based (camera)	up to 50m (poor 45-50m)	med	80ms image	strong shadows, poor lighting
Capacitive	up to 2m	low		sensitive to rain and snow

## REDUCING PEDESTRIAN INJURIES

As part of the Active Adaptive Secondary Safety (AASS) project, active pedestrian protection systems comprising airbags on the front of a Rover 200 and a Land Rover Discovery were evaluated using computer simulation. A ranking analysis using various factors including the simulation results showed that the pedestrian active protection systems gave high potential for injury reduction (compared with occupant systems which were also assessed by AASS). This was due in part to the ability of the airbag systems to reduce head injuries for an adult, from an unacceptably high level to a relatively low one, which may in practice reduce the injury severity potential for accident victims.

Further work sought to substantiate these claims by testing two full-scale vehicles fitted with a variety of foam padding and airbag devices in impacts with adult and child Occupant Protection Assessment Test (OPAT) dummies at two velocities. The first, 40km/h (25mile/h), was chosen because it is the proposed EC legislative test speed, whilst the second, 48km/h (30mile/h), was chosen because it represented a severe impact to an adult or child and imparts 44% more energy than the first, so is likely to produce much greater injuries.

Pedestrian impact protection systems can be passive or active. The first series of tests were designed to establish the passive performance and show that it was similar to the simulation and close to the EEVC Working Group 17 requirements for the bonnet leading edge and bonnet top. This was achieved through the use of open cell foam padding of a specific thickness to replicate a vehicle structure during impact with an OPAT adult pedestrian dummy. A photograph of the test vehicle is shown in Figure 3.

The same foam padding was then used for the OPAT child dummy impact tests, because a current vehicle would behave in a similar manner irrespective of the size of pedestrian impacted. The only region where this was potentially not true, on the Rover 200, was from the bonnet leading edge to part of the way back towards the windscreen. This could be tuned to be softer for a child head impact on a real vehicle. The EuroNCAP protocol demonstrates this, with several different impact sites chosen for adult and child head forms.

When the foam testing had been completed, another series was designed with airbags inflated by pressurised air gas bottles to provide the requisite airflow and pressure to keep the airbags inflated prior to impact. This was thought necessary because the trajectory resulting from contact would be different from that produced by padding and it was critical to obtain the correct

timing before a pyrotechnic airbag test could be contemplated. This was to emulate an active system with pedestrian sensing capability and to investigate the applicability of air bag technology to pedestrian impact protection.

Impact tests were conducted using airbags positioned on the bonnet leading edge and upper bonnet/windscreen area. Testing was carried out at 25 km/h using an adult OPAT dummy. A photograph of the test vehicle is shown in Figure 4.



**Figure 3. Simulated impact protection using foam**



**Figure 4. AASS inflatable external airbag system**

Holding *et al* (2001) reported that for pedestrian impacts at 49km/h (25mile/h), comparing an active adaptive restraint system to the base car performance, the injury reductions recorded for an adult occupant OPAT dummy were:

- HIC<sub>36</sub> reduced by 93%
- Chest g reduced by 76%
- Pelvis g reduced by 24%
- Knee lateral angle reduced by 40%
- Lateral knee force reduced by 4%

### **APVRU - A “PROOF OF CONCEPT” SENSING SYSTEM**

The APVRU project concluded that a prototype sensing system should consist of a combination of radar for identification and ranging of targets and passive infra-red for determination of pedestrians from the environment.

#### **Radar sensor**

Further to the research in the investigation phases of the APVRU project, the radar unit selected was the High Resolution Radar (HRR) developed by M/A-COM. This unit, designed originally for proximity sensing for the American automotive market, is a short range (0.2-20m), radar operating in the 24GHz ISM Band. The unit consists of a microwave front-end, with an integrated Digital Signal Processor (DSP) and a Controller Area Network (CAN) protocol interface. The horizontal 3dB beamwidth is 55° and the vertical beamwidth is 15°. The publicised range accuracy is  $\pm 3\text{cm}$  with an associate resolution of 7cm.

Although capable of Continuous Wave (CW) operation the unit is normally operated in pulse mode and in this mode reports the range and amplitude of the signal reflected back from each of a maximum of ten targets. These are reported, via CAN, using one message for each target on every update cycle (every 20 ms). Targets are assigned identifiers according to their position in a range ordered list, and, if there are less than ten ‘active’ targets (targets that reflect a significant proportion of the transmitted signal), the unit transmits the remaining messages with zero range. The communications load on the CAN bus is therefore constant for each unit.

The radar unit measures 120 mm x 65 mm and is enclosed in a weather proof enclosure with a small push-fit connector, as shown in Figure 5. The ‘printed patch’ transmit and receive antenna are visible of the left and right hand sides of the unit.





**Figure 5. M/A-COM High Resolution Radar**

### Infra-red tracking system

The infrared pedestrian detection and tracking head used for APVRU was an experimental detector platform based around a low element count infrared detector array. This is a novel, low-cost, thermal sensing technology developed by InfraRed Integrated Systems Ltd (IRISYS) with a diverse range of applications in areas such as security, healthcare, retail and transportation.

Infrared radiation is focussed on a 16x16 pyroelectric detector array using a germanium lens giving a 60° field of view, while the array is scanned at just over 30 frames per second. For this application, a long wave pass infrared filter (approximately 6.5 to 15  $\mu\text{m}$ ) was employed so that the device was optimised for the detection and discrimination of humans.

The detector platform includes a DSP which enables all low-level signal processing and target tracking to be handled locally. The tracking system is based around an elliptical contour tracker capable of concurrently tracking multiple thermally distinct moving targets with sub-pixel accuracy. This tracking system provides estimates of the position, shape/size, and velocity of multiple, uniquely identified, targets. Since the IRISYS sensor is only sensitive to changes in incident radiation, whilst the tracker only considered smoothly changing elliptical responses, the system was effective at minimising clutter and noise.

In order to develop a combined sensor system with the HRR unit described above, using a common CAN communications interface, a second infrared head was developed for this project. Since the communications bandwidth required to transmit 256 element array data at 30 frames per second was considered to be an unnecessary burden, the head reported only the position within the image plane and unique identifiers of each target. It must be emphasised that, unlike the data returned from the HRR unit, the tracked thermal target identifiers associate the target estimates from one frame to the

next, allowing trajectory information to be accumulated over time. In order to maintain a fixed load on the CAN bus, and in keeping with the radar sensors, blank (null data) messages are transmitted if there are less than ten thermally distinct moving targets in the field of view. The device is housed in a weather proof enclosure as shown in Figure 5 (note: the external cover for the CCD camera was removed when this photograph was taken).



**Figure 6 IRISYS Passive IR Head**

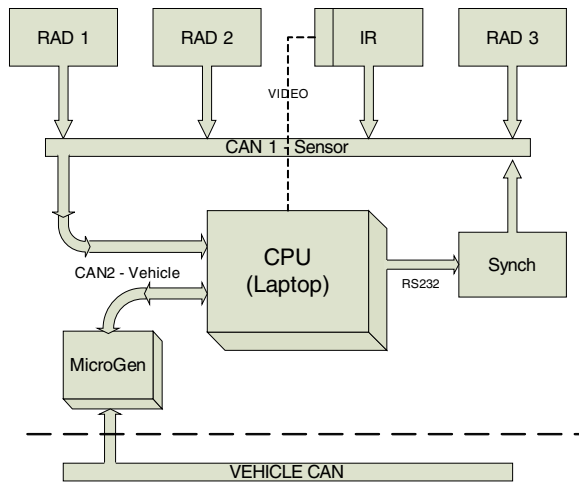
### The prototype sensor array

The final solution used for the APVRU test programme comprised an array of three radar sensors mounted on a roof bar fitted to the test vehicle together with the infra-red array as shown in Figure 7. It should be noted that this arrangement was convenient for development testing and the integration of the sensors within the vehicle was beyond the scope of the project. The three radar sensors were used to provide accurate triangulation of the objects being detected. A schematic block diagram of the system hardware is shown in Figure 8.



**Figure 7. Radar and infra-red sensor array fitted to test vehicle**





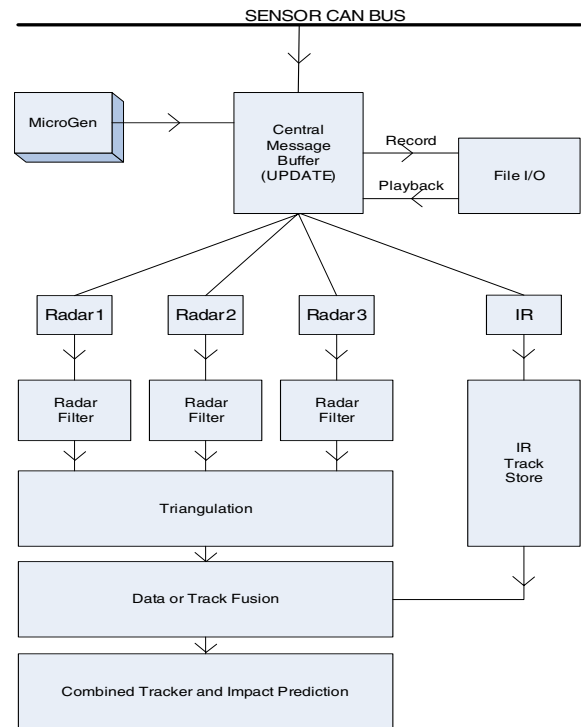
**Figure 8. Schematic block diagram of the APVRU hardware system**

### System software

It is not intended to describe the software used for this work within this paper but a summary of the requirements are listed below:

- Data logging with record and playback functionality.
- Individual radar range filtering (range tracking).
- Computation of ground plane target position measurements from pairs of filtered radar range measurements.
- Combining multiple radar ground plane position measurements with infrared evidence in a multitarget, multisensor, ground plane tracking system.
- Trajectory prediction for determining the likelihood of an impact together with its position and timing.

A schematic block diagram outlining the software is shown in Figure 9. A full description is provided in the APVRU project report (McCarthy *et al*, 2004).



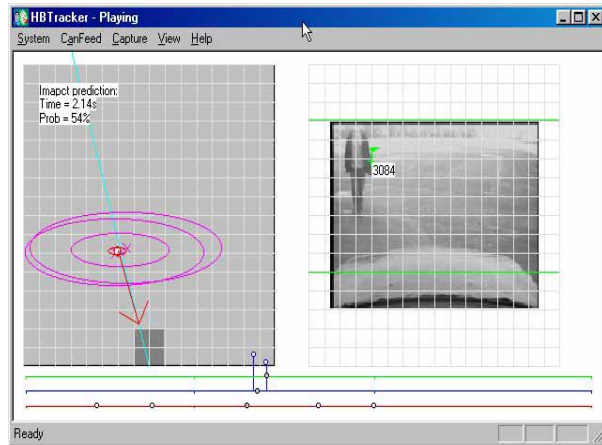
**Figure 9. Schematic block diagram showing the system software**

### APVRU sensor system performance

In order to evaluate the APVRU system, a series of trials of simulated, real-world, accident scenarios, each more progressively challenging were developed. These commenced with a pedestrian walking across in front of the vehicle and then progressed to test angled pedestrian approaches, multiple pedestrians (with different bearings and velocity) and multiple pedestrian movements with roadside clutter in the form of parked and moving vehicles.

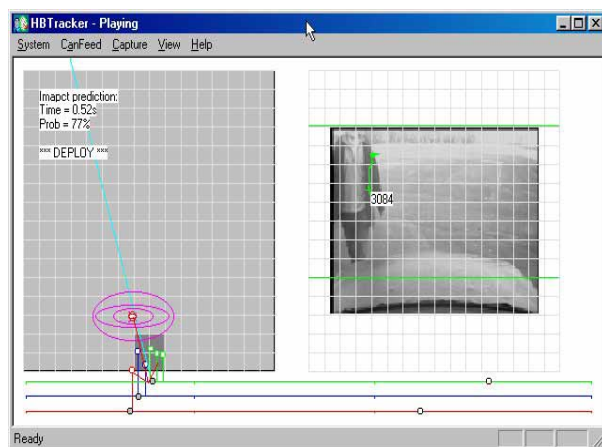
As an example of the APVRU system, Figures 10 and 11 show two captured frames from a scenario in which a pedestrian walked along a collision course towards the left hand side of the vehicle. In these frames the right hand side is video (not used by the system) with the IR view plane superimposed. The left hand part of the image shows the ground plane (with 1m grid lines) showing the tracked position of the target (red circle) and the IR azimuth of the target (cyan line). The arrow shows the target's speed and direction, or velocity vector, in relation to the vehicle. The large magenta ellipses are the confidence regions for the triangulated ground plane measurements (one for each filtered radar response). Even though these measurements appear to be poor, the triangulation of the radar combinations is reporting a strong track with an accurate ground plane position, as indicated by the small red elliptical

confidence region around the target's position. The four grey squares at the bottom of the image represent the bonnet of the car. The data in the top left hand corner of the frame shows calculated data from the APVRU system for the time to collision and the probability of impact.



**Figure 10. Example of APVRU system tracking a pedestrian**

Figure 10 shows that the combined radar and infrared tracking system has successfully locked onto the target and is reporting a high confidence in the ground plane position. The prediction algorithm has estimated a 54% probability of impact. Figure 11 is taken from later in the same sequence, when the pedestrian was 1m from the vehicle. The impact prediction showed a 77% probability with a time to impact of 0.52 seconds. The impact prediction algorithms in this case have indicated that a protective system would be deployed in this situation.



**Figure 11. Example of the APVRU system predicting an impact**

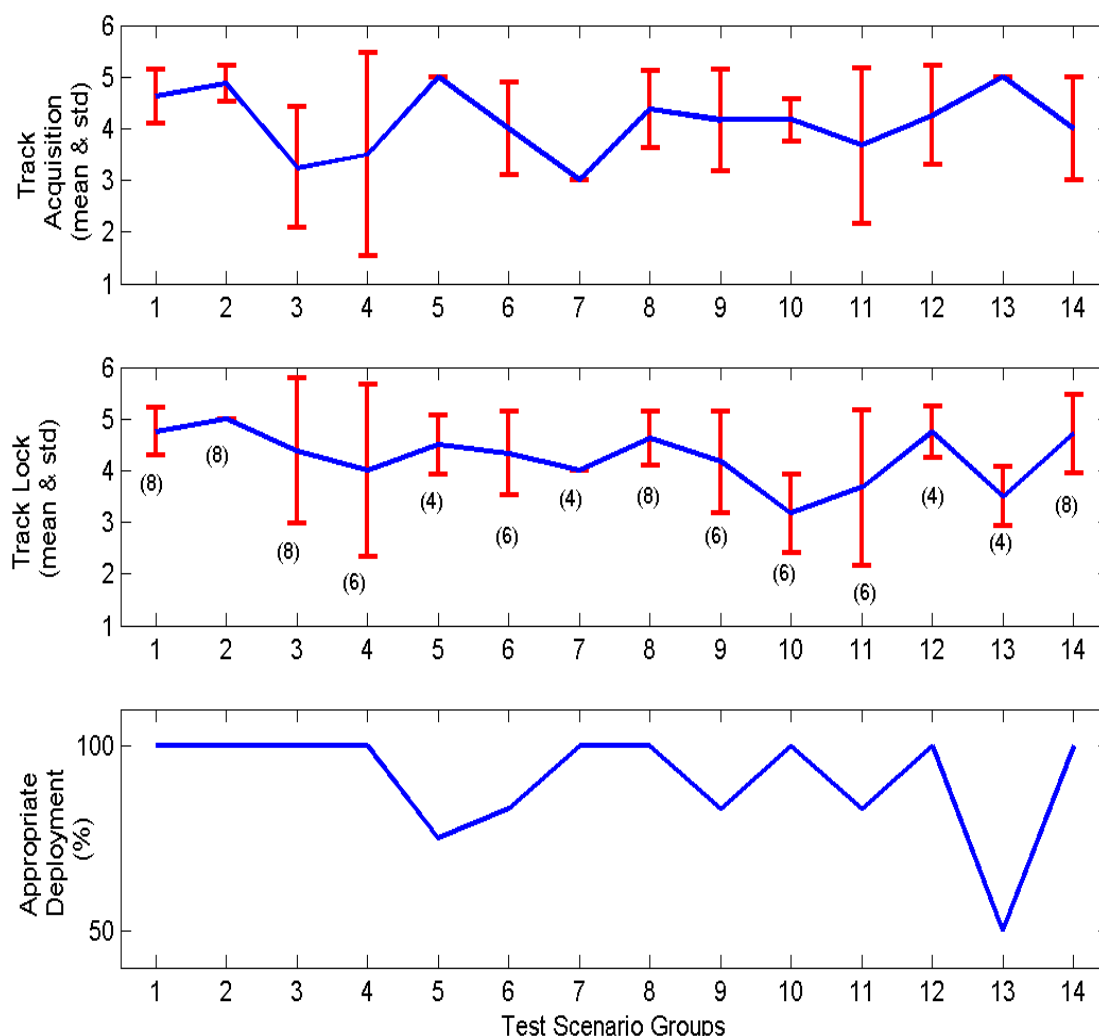
For scenarios which involved multiple pedestrians the results were more varied. Here the scenarios were more complicated and involved instances where the primary target either hit the vehicle or was a near-miss. For targets with velocity vectors parallel to the vehicle, the system performed well. However, when the primary target had a velocity vector at an oblique angle to the vehicle, while the second target had a parallel velocity vector, there was a tendency to trigger a false deployment for near-miss scenarios. This appeared to be due to excessive velocity smoothing in the tracker together with failures to distinguish multiple targets that merged and then separated, within the time available. However, improvements in raw radar data quality, together with more advanced data association mechanisms within the trackers, would be likely to lead to significant performance improvements.

The APVRU system was tested with a number of simulated real-world, accident scenarios. These are detailed below. Groups 1 to 10 were conducted with human volunteers (approximately equivalent to a 95<sup>th</sup> percentile male) walking or running at various trajectories toward the vehicle. Groups 11 to 13 were conducted with a moving vehicle and the final group was conducted with the anthropometric dummy with radar and infrared profiles representative of a 50<sup>th</sup> percentile male developed by the APVRU project.

1. A pedestrian crossing the vehicle left to right or right to left at varying distances.
2. A pedestrian walking along various parallel trajectories toward the vehicle.
3. A pedestrian running along various parallel trajectories.
4. A pedestrian walking along various diagonal trajectories.
5. Two pedestrians walking along various parallel trajectories
6. Two pedestrians walking along various intersecting trajectories toward the vehicle.
7. A pedestrian running past a second pedestrian walking toward the vehicle on parallel trajectories.
8. A pedestrian walking/running at varying speeds across the front of the vehicle and then changing direction toward the vehicle (simulating a pedestrian running into the road).
9. As (8) with a second pedestrian walking parallel toward the vehicle along the pavement.
10. As (8) from behind a parked car.
11. The vehicle driving past a pedestrian standing, at varying distances, at the side of the road.
12. The vehicle driving past two pedestrians walking, at varying distances, at the side of the road.

13. The vehicle driving past pedestrians and vehicles parked at the side of the road.
14. Impact tests with an anthropometric dummy at varying vehicle speeds up to 25kph (15.5mph)

The test speed in the last scenario was due to safety concerns, since both the system operator and driver had to be inside the vehicle during the tests, rather than the performance limits of the system.



**Figure 12. Mean and standard deviation graphs for the system’s track acquisition and tracking lock plus the percentage of appropriate deployments**

Based on a 5-point scale (1 being “poor” and 5 being “good”) the performance of both the system’s ability to acquire a valid track and to maintain a tracking lock for each of the test scenarios was graded by subjective analysis. In each case the inspector also graded the appropriate deployment. The mean and standard deviation of each group was calculated together with the percentage of appropriate deployment and is presented in Figure 12. The numbers in brackets on the central graph indicate the total number of individual tests in each grouping.

These results suggest a good to excellent level of performance, apart from the results for group 13 which showed only a 50% appropriate deployment. This data was taken from only 4 tests and was probably due to lower level of prediction accuracy from tracking multiple pedestrians plus parked and oncoming vehicles. In the majority of tests the system accurately tracked the target’s position on the ground plane, predicted the probability and/or the point of impact, and would have activated a protective system at what appeared to be the appropriate time, including 25 km/h impacts with a test dummy. However, it should be noted that these were simplified test scenarios in a largely

controlled environment and should only be regarded as evidence of 'proof of concept' for the sensor system.

## CONCLUSIONS

The APVRU system has provided the basic foundations of a 'proof of concept' pre-crash vulnerable road user detection system. Such a system may provide the basis of future systems which could decelerate the vehicle to reduce the impact speed and/or deploy an active safety system on the front of the vehicle designed to mitigate the injury to the vulnerable road user.

Data from each of the radars and infrared sensor were successfully synchronised and the data combined in order to track accurately "hot bodied" targets over time. The APVRU system was shown statically to be capable of detecting multiple vulnerable road users in a range of accident scenarios, and was shown, during impact tests, to be capable of detecting a dummy with radar and infrared profiles representative of a human at impact speeds of up to at least 25km/h (15.5mile/h).

However, before such a system is integrated onto a production vehicle, considerable further research and testing is required to ensure system reliability. The APVRU project concluded that it would be beneficial for any final pre-crash system to use radar units integrated with other safety and comfort systems (e.g. Automatic Cruise Control and "stop and go" applications). The vulnerable road user detection radars would need to have a greater maximum and lateral range and an update rate of at least 100Hz (compared with 50Hz for the radars used in the APVRU system).

TRL research has demonstrated the significant injury benefits possible with the use of external airbags to mitigate injury for the primary and secondary impact. However, these test results can only be applied to the specific conditions under which they were tested. Before the possibility of external airbags being fitted to vehicles, the sensor system reliability and airbag deployment must be shown to be effective in responding effectively to the highly complex and variable accident scenarios which are a distinct feature of vulnerable road user accidents. Thus, the first systems employing pre-crash sensor technologies may be linked to driver warning systems and the braking response of the vehicle or an active system which does not confer any increased injury risk other than would occur if the device was not fitted (such as reactive bumper materials or a pop-up bonnet system).

## ACKNOWLEDGEMENTS

The authors wish to acknowledge the support of the UK Department for Transport (DfT) for the AASS project. We also wish to thank the members of the APVRU consortium; Jaguar Cars, IRISYS and the University of Surrey as well as the UK Department for Trade and Industry, DfT and the Engineering and Physical Sciences Research Council (EPSRC) for their support for APVRU Foresight Vehicle Project. Further information regarding the APVRU project can be found at [www.apvru.com](http://www.apvru.com). More information on DfT funded research can be found from [www.rmd.dft.gov.uk](http://www.rmd.dft.gov.uk).

## REFERENCES

- Carlsson G. (1996) Working material based on data from Switzerland. Germany and Austria. NTF, Sweden.
- DfT (2004). Road Casualties Great Britain 2003. Department for Transport (DfT) Transport Statistics branch TSR5, London.
- Holding P.N., Chinn B.P. and Happian-Smith J. (2001). Pedestrian protection - an evaluation of an airbag system through modelling and testing. Proceedings of the 17th ESV Conference, Amsterdam, June 2001.
- McCarthy M.G, Moxey E., Johnson N., and McLundie W. (2004). The Advanced Protection of Vulnerable Road Users (APVRU): Final Report. PR/SE/970/04. TRL Limited, Crowthorne, UK.
- Organisation for Economic Co-operation and Development (2001). International Road Traffic and Accident Database (IRTAD), Summary Report. Federal Highway Research Institute (BASt), Bergisch, Germany.
- Otte, D (1999). Severity and mechanism of head Impacts in car to pedestrian accidents. Proceedings of the 1999 IRCOBI Conference on the Biomechanics of Head Impact, Barcelona, Spain.

# COMPONENT LEG TESTING OF VEHICLE FRONT STRUCTURES

**Ann Mallory**

Transportation Research Center Inc.

**Jason A. Stammen**

National Highway Traffic Safety Administration  
United States of America

**France Legault**

Transport Canada  
Canada

Paper Number 05-0194

## ABSTRACT

Current and proposed pedestrian test procedures in Europe and Japan evaluate lower extremity injury risk by using a projectile legform to impact the bumper of a stationary vehicle. Although there are no pedestrian regulations in North America, bumper design is affected in both the United States and Canada by regulations limiting damage in low-speed impact testing. The main objectives of this study were to (1) evaluate differences in instrumentation capability and kinematic response of two pedestrian legforms (FlexPLI 2004, TRL), and (2) determine if and to what extent vehicles designed to conform to North American bumper regulations are more aggressive toward pedestrians than similar vehicles designed to conform to European bumper impact requirements. The results indicated that none of the North American bumpers were able to achieve the level of pedestrian lower leg protection required by future European Union regulations. It was also found that both legforms have limitations in testing the North American bumpers. The bumpers damaged the FlexPLI legform in repeated tests and exceeded the measurement limits of the TRL legform.

## INTRODUCTION

On average, 374 pedestrians and 55 cyclists are fatally injured in Canada every year, making up 14.9% of fatalities among all road users (5-year average 1999-2003) [1]. In the United States, 4,749 pedestrians and 622 cyclists were killed in 2003, comprising 12.6% of all motor vehicle-related fatalities [2]. Combined international statistics from the United States, Europe and Japan indicate that approximately 30% of moderate to catastrophic pedestrian injuries involve the lower extremities, with the front bumper identified as injury source for the majority of those injuries [3]. Transport Canada is investigating whether its bumper regulation is detrimental to the safety of pedestrians. Because bumper designs for the Canadian market are largely

similar or identical to those sold in the United States, this research has potential implications for all vehicles in the North American fleet.

The Canadian Motor Vehicle Safety Standard (CMVSS) 215 for bumpers is based on a series of 8 km/h longitudinal impacts and 4 km/h corner impacts after which the safety systems of the vehicle have to function as intended [4]. The United States CFR 49 Part 581 standard and the United Nations Economic Commission for Europe Regulation No. 42 (ECE R42) have lower impact speeds, with longitudinal impacts conducted at only 4 km/h. Both regulations apply only to passenger cars. The U.S. criteria are for no cosmetic or safety system damage, whereas the European requirements are for no damage to safety systems only. Thus, Canada's higher test speed and the broader U.S. damage limitations make the bumper damage criteria in both countries different from the European requirements. Research and testing was deemed necessary to determine if bumpers designed to meet the North American bumper regulations are more aggressive toward pedestrian lower extremities than their European counterparts designed to meet UN ECE Regulation No. 42.

The European New Car Assessment Program (EuroNCAP) includes pedestrian testing to assess aggressiveness of vehicle frontal areas [5]. The procedure calls for a free-flight bumper impact at 40 km/h with a legform developed by the Transport Research Laboratory (TRL Limited, Berkshire, UK). This legform is a simplified device that approximates human anthropometry while using frangible steel knee ligament surrogates designed to deform plastically during impact [6]. The legform's instrumentation allows it to measure tibia acceleration, shear displacement, and bending angle at the knee.

European Union regulations specify tests relating to the protection of pedestrians and other vulnerable



road users in Directive 2003/102/EC [7]. The procedure includes tests for legform to bumper evaluation, as well as for head impact testing and leg to bonnet edge testing. The lower legform to bumper test performed at 40-km/h limits maximum dynamic knee bending angle to 21 degrees, maximum dynamic knee shearing displacement to 6 mm and acceleration at the upper tibia to 200 g. Although the TRL legform is not explicitly named in the directive, the required injury measures correspond exactly to the values that the TRL legform is equipped to measure.

The FlexPLI 2004 has been more recently developed by the Japanese Automobile Research Institute (JARI). This legform has been described to have improved biofidelity over the TRL legform as well as increased instrumentation capabilities [8]. This device is more complex than the TRL legform, with 14 hollow cylindrical steel segments along its length that surround two surrogate bone cores representing the femur and the tibia. These cores are made of glass reinforced plastic (GRP) and are equipped with strain gauges mounted at defined locations. The FlexPLI is also equipped with four cabled surrogate ligaments at anthropometrically accurate locations within the knee structure. It is designed to be completely non-frangible, and it is able to measure bending moments in the upper and lower segments as well as knee ligament displacements and individual segment accelerations.

The objective of this study was to use the TRL and FlexPLI legforms to assess the pedestrian aggressiveness of a sample of North American model bumper systems and then compare those systems to their European counterparts.

## METHODS

Pedestrian lower extremity testing was performed by impacting the front bumpers of five different passenger car models with projectile legforms. All bumpers in the test series were tested using a TRL legform impactor. Selected bumpers were also tested using the FlexPLI 2004.

Legforms were launched in this test series by a carriage mounted to a hydraulic linear ram. During acceleration, the legforms were suspended from a pin at the top of the carriage and supported horizontally by padded fixtures mounted on the carriage adjacent to the upper leg and the lower leg (Figure 1).



**Figure 1. Test setup.**

Legform acceleration to free-flight speed was achieved over a distance of approximately 24 cm for the TRL legform and 28 cm for the FlexPLI legform. Legform height at the time of impact with the bumper was such that the bottom of the legform was within  $\pm 10$  mm of ground reference level, which is defined as the horizontal plane that passes through the lowest points of contact for the tires of the vehicle in normal ride attitude. As defined in the EuroNCAP procedure, the legform was vertical in the sagittal and coronal planes and aligned about the z-axis so that the lateral side of the legform contacted the bumper.

Target impact speed was  $11.1 \pm 0.2$  m/s ( $40 \pm 0.7$  km/h) for all testing with the TRL legform. Target impact speed for the FlexPLI legform was initially the same as for the TRL legform but reduced in subsequent tests to  $8.3 \pm 0.2$  m/s ( $30 \pm 0.7$  km/h). Velocity was measured by integrating upper tibia acceleration data.

The TRL legform was equipped with angular displacement transducers in the lower femur and upper tibia components that allowed calculation of shear displacement and bending angle in the knee [6]. Tibia acceleration was measured by a 500 g uniaxial accelerometer mounted on the non-impact side of the upper tibia. The FlexPLI's instrumentation consisted of 3 pairs of strain gages mounted on the thigh bone core, 4 pairs of strain gages mounted on the lower leg bone core, and three linear potentiometers across the knee joint. The strain gages were used to measure bending moments along the length of the femur and tibia, while the knee potentiometers measured stretch of the ACL, PCL, and MCL ligaments. In addition to this standard instrumentation, a uniaxial accelerometer was mounted on the non-impact side of the FlexPLI's upper tibia. All data was sampled at 20 kHz, pre-filtered at 3 kHz, then filtered using CFC 180 (300 Hz). Lateral and overhead high-speed video documented the tests at 1000 frames per second.



The five vehicles tested were the following North American models:

- 2000 Volvo S40
- 2001 Ford Focus
- 1999 Volkswagen Beetle
- 2001 Honda Civic
- 2002 Mazda Miata

All vehicles were purchased in the United States and selected because the corresponding European models of each one had been previously evaluated in EuroNCAP pedestrian testing. These vehicles have similar bumper systems in Canada and in the U.S.

In total, 28 impact tests (23 with TRL, 5 with FlexPLI) were conducted in this study (Table 1).

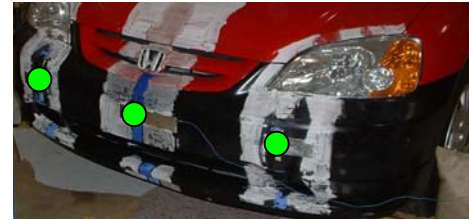
**Table 1.**  
**Test matrix (impacts at full speed unless noted otherwise)**

Vehicles	TRL		FlexPLI	
	Center	Lateral	Center	Lateral
Volkswagen Beetle	2	3	--	--
Mazda Miata	2	3	--	1 <sup>A</sup>
Ford Focus	2	3	--	--
Volvo S40	2	2	1 <sup>A</sup>	2 <sup>A</sup>
Honda Civic	2	2	--	1

<sup>A</sup> Tests were done at 30 km/h

Bumper impacts were targeted at the areas near the left and right side bumper supports and centrally at the bumper midline. Figure 2 illustrates the impact points on each vehicle bumper. The locations of the off-center (hereafter referred to as “lateral”) impacts on each vehicle were symmetrical about the vehicle centerline. No impact points were within 65 mm of the bumper corner, as defined in the EuroNCAP procedure. Tire pressure was set according to manufacturer’s instructions. The emergency brake was engaged. No additional ballast was added to the vehicle weight. Tests were performed at all three locations before replacing the entire bumper system.

Honda Civic



Ford Focus



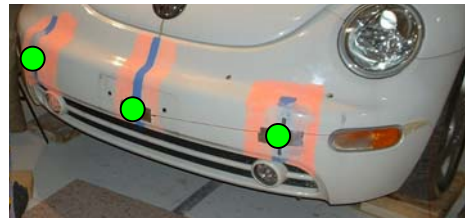
Mazda Miata



Volvo S40



VW Beetle



**Figure 2. Impact points on each bumper system.**

External inspection of the bumper systems for damage was done immediately following each test, and internal inspection was performed after bumper replacement. Post-test inspection of each legform was carried out according to manufacturer’s instructions.

## RESULTS

### TRL Legform Impacts

Kinematics during the first 20 milliseconds after impact are shown in Figure 3. These video frames show the moment of initial contact between the lateral side of the legform and the bumper, followed by the legform's position 10, 15, and 20 milliseconds

after impact. Initial interaction between the bumper and the legform is visible at 10 milliseconds when the legform tends to follow the contour of taller bumpers that are more rounded (such as the Ford Focus and Mazda Miata) while narrower or more angular bumpers (such as the Volkswagen Beetle or Volvo S40) tend to produce a more pronounced bend at the knee.

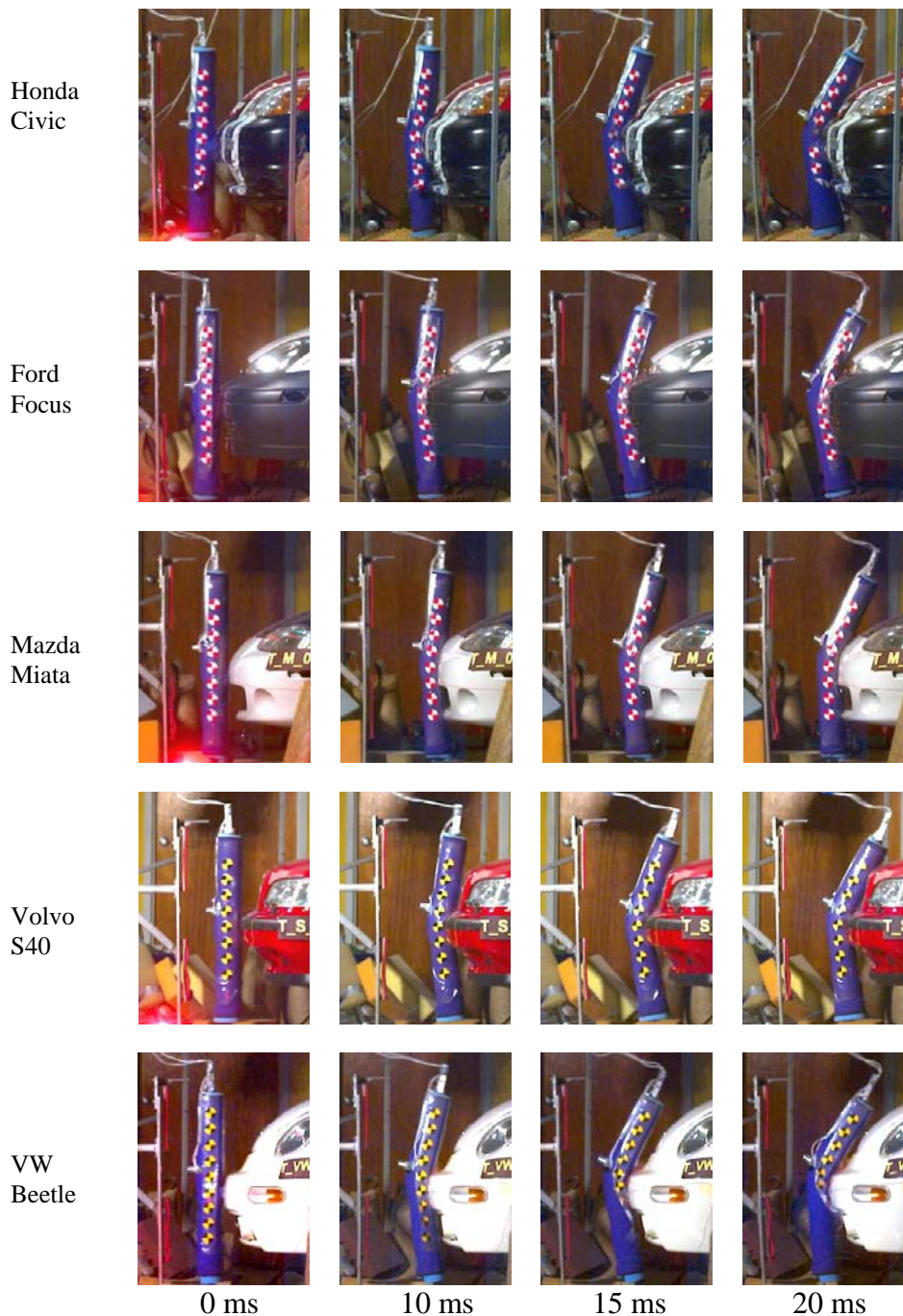


Figure 3. Kinematics of TRL legform for five vehicles.

At 15 milliseconds, the effect of lower bumper shape on lower leg motion is visible. By this time, the tibia component of the legform has reached its maximum forward angle against the inward slanted lower bumpers of the Ford Focus and the Honda Civic. The more vertical front face of the Mazda Miata bumper has limited the bending of the knee even more than the Ford Focus or Honda Civic bumpers. The legforms impacted into the Volvo S40 and Volkswagen Beetle bumpers have not yet impacted the lower bumper structures at 15 milliseconds and are still free to wrap under the bumper and increase knee bending angle. The frame at 20 milliseconds represents the approximate time of maximum bending for each legform as the femur component reaches the grille or hood area. The vehicles with more upright grille or hood structures appeared to limit forward femur movement the most, effectively limiting knee bending.

Post-test inspection of the TRL legform revealed no major structural damage after any of the tests. Instrumentation damage that required repair between tests was limited to a torn femur potentiometer wire and a displaced tibial potentiometer shaft that was press fit back in place. Neither affected the usable portion of data. Deformed frangible knee ligaments were replaced after each test.

In most tests, the vehicle and bumper systems showed either no damage or damage limited to fine scuffing, scratching, or cracking of the paint related to contact with the legform or instrumentation. No deformation was found to the internal bumper structures or energy absorbing elements.

Impact speed measured in the TRL legform tests was  $10.9 \pm 0.2$  m/s, which was slightly slower than the nominal target range of  $11.1 \pm 0.2$  m/s. Orientation of the legform at impact was as specified according to review of lateral and overhead high-speed video.

For each test, upper tibia acceleration, knee shear displacement, and knee bending angle were measured. In all tests, peak values of these measures were recorded in the first 30 milliseconds after bumper contact. Time histories for acceleration, shear displacement, and bending angle are shown for typical impacts with each vehicle in Figures 4 through 6.

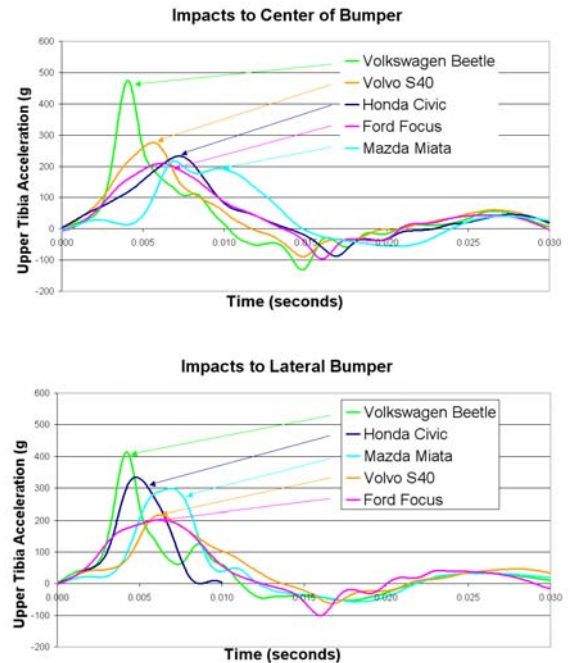


Figure 4. Upper tibia acceleration.

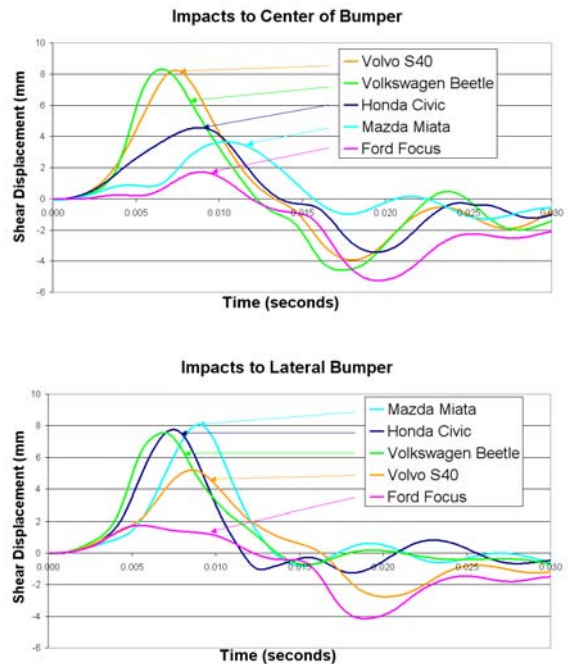
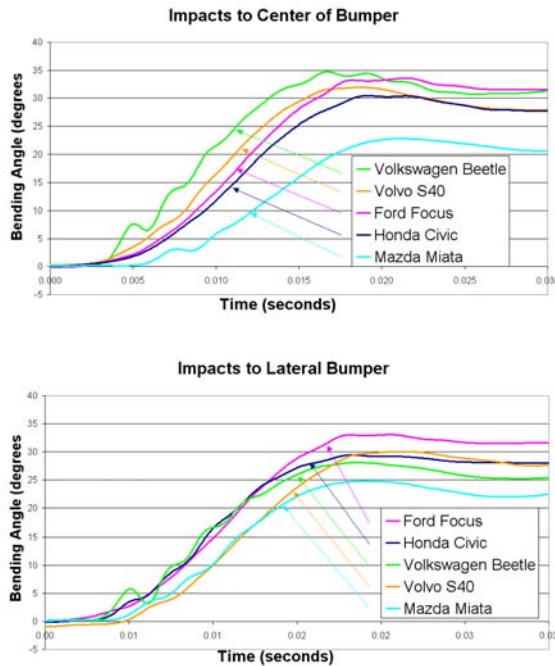


Figure 5. Knee shear displacement.





**Figure 6. Knee bending angle.**

Although the bending angle measurements shown in Figure 6 indicate peak bending angles in excess of 30 degrees, the limit of bending angle accuracy for the TRL legform is considered to be 30 degrees because of contact between the tibial and femoral components at this angle [9]. Subsequent to that contact at a knee bending angle of approximately 30 degrees, resistance to bending is expected to increase. Although measurements above 30 degrees are expected to correspond to progressively worse actual bending angles, the exact value of any peaks above 30 degrees is uncertain.

Two center-bumper impacts and two or three lateral-bumper impacts were performed for each vehicle. No significant variation was found between left-sided and right-sided impacts or between impacts performed on an untested bumper versus impacts into a bumper tested previously in a different location. Repeatability analysis of injury measures for testing on vehicles for which three lateral impacts were performed showed coefficients of variation ranging from 2% to 15%. Because of this range of test result variation, comparisons between bumpers were made using averaged values of peak injury measurements for all center impacts to each vehicle (Table 2) and for all lateral impacts for each vehicle (Table 3).

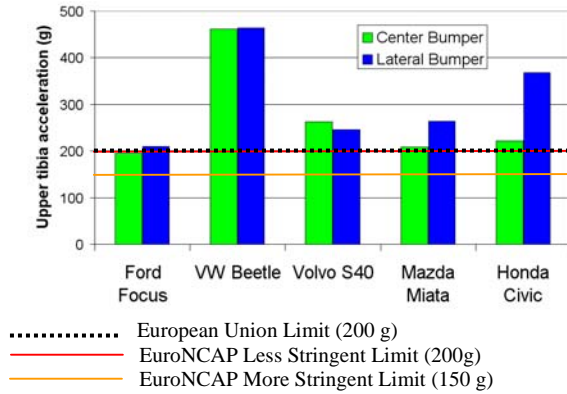
**Table 2.**  
**Average peak injury measures for all center-bumper impacts.**

Vehicle	Average Peak Acceleration (g)	Average Peak Bending Angle (degrees)	Average Peak Shear Displ. (mm)
Ford Focus	195.0	33.4	-4.9
Honda Civic	221.4	31.0	4.7
Mazda Miata	208.8	24.7	3.4
VW Beetle	461.9	34.7	8.3
Volvo S40	262.9	31.1	8.2

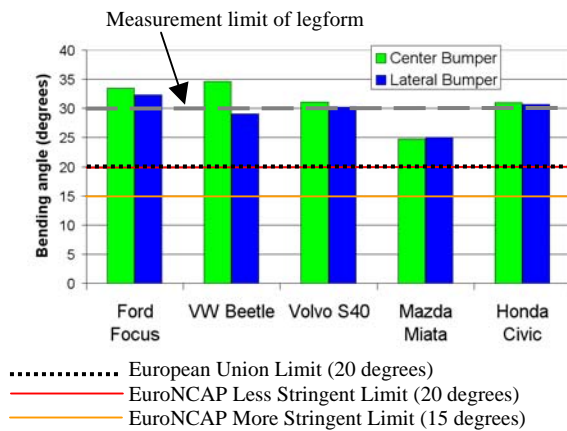
**Table 3.**  
**Average peak injury measures for all lateral-bumper impacts.**

Vehicle	Average Peak Acceleration (g)	Average Peak Bending Angle (degrees)	Average Peak Shear Displ. (mm)
Ford Focus	209.3	32.3	-3.8
Honda Civic	368.5	30.7	7.7
Mazda Miata	264.3	25.1	7.4
VW Beetle	464.2	29.1	8.2
Volvo S40	246.0	30.2	6.2

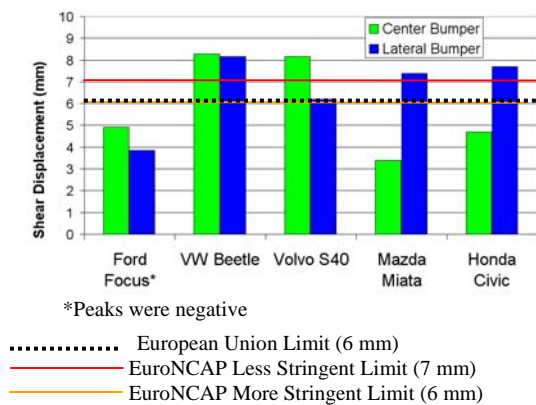
Figures 7 through 9 compare the averaged peak values for each vehicle and impact location to European Union requirements [7] and to the more stringent and less stringent performance limits used to rate vehicles in the EuroNCAP point system. In the EuroNCAP system, injury measurements meeting the more stringent limit receive 2 points, measurements between the two limits receive an interpolated point value, and measurements exceeding the less stringent limit earn 0 points [5]. The total point value awarded for an individual test is equal to the lowest of the calculated acceleration, bending and shear point values. The point values for three lower extremity tests are added to the point values earned in head impact and upper leg press tests to calculate the vehicle's overall pedestrian star rating.



**Figure 7. Peak upper tibia acceleration**



**Figure 8. Peak knee bending angle averaged for all impacts at each location.**



**Figure 9. Peak knee shear displacement averaged for all impacts at each location.**

Since no impacts in the current series produced a bending angle lower than the less stringent limit of 20 degrees, the bending angle point value for all tests would be zero. Therefore, all impacts in this series would result in overall EuroNCAP lower extremity point values of 0. In order to compare the

performance of the tested vehicles in the current study to each other, rather than to vehicles previously tested under EuroNCAP procedures, a modified version of the EuroNCAP point system was used. Under the modified point system, point values were interpolated between 2 and 1 for injury measurements between the EuroNCAP less stringent and more stringent limits, and interpolated between 1 and 0 for injury measurements that exceeded the EuroNCAP less stringent limit but were less than double that limit. For example, an injury measurement that exceeded the less stringent limit by 50% earns 0.5 points while an injury measure that was two times that limit would earn 0 points. Modified point values calculated for the averaged results at each vehicle location are listed in Table 4.

Table 4 shows that by the modified EuroNCAP point system the Mazda Miata bumper (0.76 center and 0.68 lateral) was least aggressive toward pedestrian legforms. It was followed in order of increasing aggressivity by the Volvo S40 (0.49 lateral and 0.45 center), the Honda Civic center bumper (0.45), the Ford Focus (0.38 lateral bumper and 0.33 center bumper), the Honda Civic lateral bumper (0.16), and the Volkswagen Beetle (0.0 lateral and center).

**Table 4.**  
**Modified point values earned for each injury measurement, averaged for each vehicle/location (final overall modified score in *italic bold*)**

Vehicle	Location	Upper Tibia Accel.	Bending Angle	Shear Displ.
Ford Focus	Lateral	0.95	<i><b>0.38</b></i>	2
	Center	1.90	<i><b>0.33</b></i>	2
Honda Civic	Lateral	<i><b>0.16</b></i>	0.46	0.9
	Center	0.89	<i><b>0.45</b></i>	2
Mazda Miata	Lateral	<i><b>0.68</b></i>	0.75	0.95
	Center	0.96	<i><b>0.76</b></i>	2
VW Beetle	Lateral	<i><b>0</b></i>	0.55	0.83
	Center	<i><b>0</b></i>	0.27	0.82
Volvo S40	Lateral	0.77	<i><b>0.49</b></i>	1.12
	Center	0.69	<i><b>0.45</b></i>	0.83

Of the three EuroNCAP injury criteria, shear displacement was the easiest for the vehicles to meet. The Ford Focus (both lateral and center), Honda Civic (center), and Mazda Miata (center) all met the more stringent shear displacement requirement of 6 mm and no other impact

locations resulted in a modified score lower than 0.82.

Bending angle was the most difficult limit to meet, with no impact location achieving a modified score above 0.75. The widest range of modified scores was in tibia acceleration, from a score of 0 by the Volkswagen Beetle in both the center and lateral locations to 1.90 by the Ford Focus at the center location.

The impacts at each vehicle location were also evaluated against limits defined in the European Union directive 2003/102/EC. The maximum acceleration limit of 200 g was exceeded for all impact locations except the center bumper of the Ford Focus, which produced upper tibial acceleration of 195 g. The 21-degree bending angle limit was exceeded for center and lateral impact locations for all vehicles tested. The Ford Focus was the only vehicle tested to remain under the maximum shear displacement angle of 6 mm for both center and lateral impacts, while the Mazda Miata and Honda Civic were able to stay below that limit for the center bumper location only. The Volkswagen Beetle and Volvo S40 shear values were over the limit at both locations.

### **FlexPLI Legform Impacts**

Five bumper impacts were performed with the FlexPLI legform: one impact to the Honda Civic at full speed (nominally 40 km/h or 11.1 m/s as in the TRL tests), one to the Mazda Miata at a reduced nominal target speed of 8.3 m/s (30 km/h) and three to the Volvo S40, also at a target speed of 8.3 m/s. The legform sustained damage in the Honda Civic test, necessitating the reduction in speed. It was also damaged in the Mazda Miata test and the third Volvo S40 test at the lower speed.

Kinematics of the FlexPLI are shown for tests into the lateral bumper of the Honda Civic, Mazda Miata, and Volvo S40 in Figure 10. The frames at 10 to 20 milliseconds show the knee end of the femur, and to a lesser extent the tibia, bending away from the bumper after contact in the knee area. The resulting convex curvature of the thigh and leg away from the bumper is

followed by concave curvature toward the vehicle by 20 to 30 milliseconds after contact. As the knee flexes around the front of the vehicle, the upper and lower leg segments also bend, essentially wrapping under the bumper and around the hood leading edge. The lower leg bending appears greater for the Honda Civic and Volvo S40 bumpers where their recessed lower structures allow the lower leg to wrap under the bumper. The more flat-faced Mazda Miata bumper restricts tibial bending below the bumper structures. The upper leg bending appears most limited by the Volvo S40 bumper, which has a more upright grille area than the other vehicles.

Post-test inspection of the FlexPLI legform showed major damage following three tests. After the impact into the right lateral bumper of the Honda Civic at 40 km/h, routine inspection of the tibial bone core showed an anterior-posterior crack through the tibial bone core. Dismantling of the lower leg structures revealed that the linear crack started at the top of the tibia, but did not extend down to the bottom of the bone.

A replacement FlexPLI legform underwent two subsequent tests into the lateral and center bumper of a Volvo S40 at a reduced speed of 30 km/h without sustaining damage. A third impact into the lateral bumper of the Volvo S40 produced a small crack in the distal femoral bone core. A final impact into the lateral bumper of the Mazda Miata, also at reduced speed, resulted in an additional fracture of the tibial bone core.

Time histories of the moments measured at each level in the thigh and lower leg are shown for the first impact into the Volvo S40's lateral bumper impact location at reduced speed (Figures 11 and 12). Positive moment in the leg and thigh corresponds to moment that produces concave lateral bending, as when the femur wraps around the hood leading edge or the tibia wraps under the bumper. Negative moment corresponds to moment that produces convex lateral bending, as when the knee is initially pushed medially.

Honda Civic  
(Right side full speed)



Mazda Miata  
(Left side reduced speed)



Volvo S40  
(Left side reduced speed)



0 ms

10 ms

20 ms

30 ms

Figure 10. Kinematics of FlexPLI legform for three vehicles.

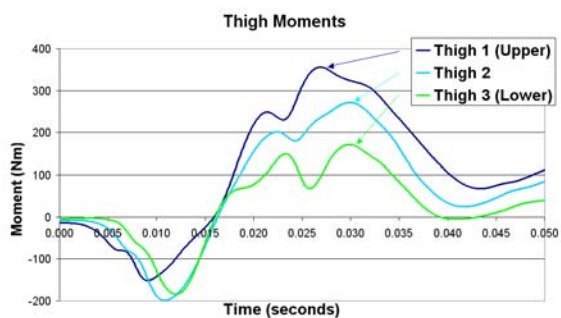


Figure 11. Thigh bending moments for right lateral impact into Volvo S40 bumper at reduced speed.

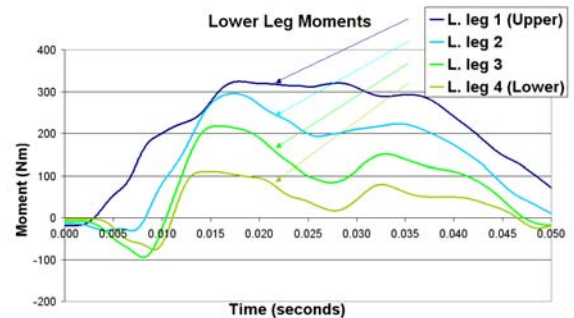
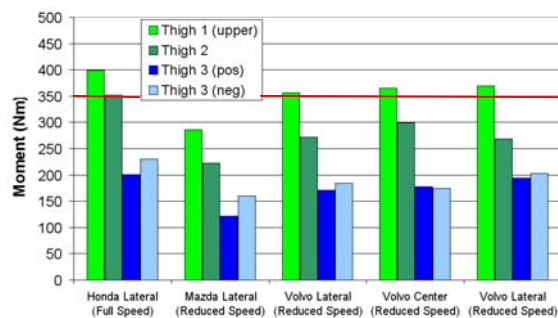


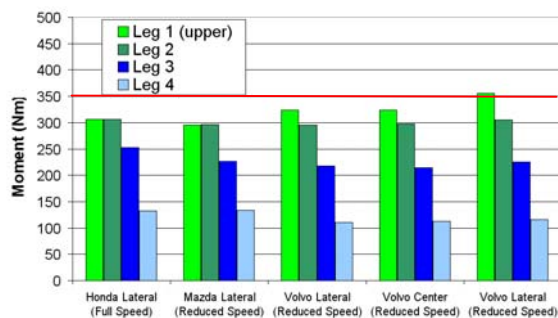
Figure 12. Lower leg moments for right lateral impact into Volvo S40 bumper at reduced speed.



Figures 13 and 14 compare the peak magnitude of moments measured in all tests performed with the FlexPLI. In all tests run with the FlexPLI, the peak positive moments were greater in magnitude than the peak negative moments in the leg and for the upper two moment sensors in the thigh. In the lowest moment sensor in the thigh, positioned closest to the knee, negative moment was greater in magnitude than positive moment. Peak bending moment in the thigh tended to be greatest for sensors further from the knee, while peak bending moment in the lower leg tended to be greatest for sensors closer to the knee. Values are compared to preliminary proposed injury limits for the FlexPLI legform [10]. The full-speed Honda Civic test and the reduced speed Volvo S40 tests all exceeded the moment limit at the upper thigh sensor, while the Mazda Miata was within moment injury limits in the thigh. In the lower leg, the only measurement to exceed the injury limit was the bending moment adjacent to the knee in the final Volvo S40 test.



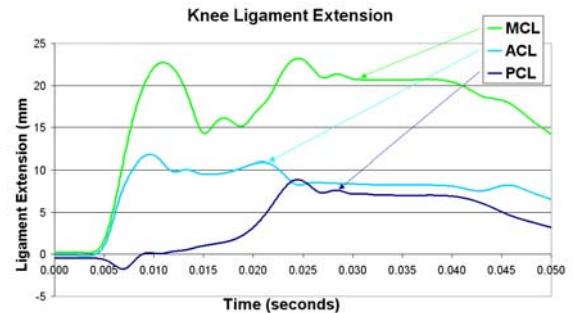
**Figure 13. Thigh moments for all impacts with FlexPLI legform (proposed injury limit of 350 Nm).**



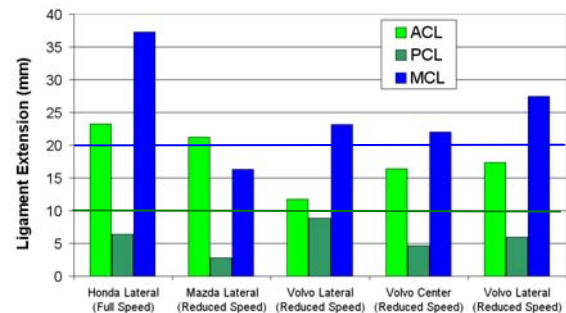
**Figure 14. Lower leg moments for all impacts with FlexPLI legform (proposed injury limit of 350 Nm).**

Displacements of the potentiometers representing knee ligament extension are shown for the example impact with the Volvo S40 bumper in Figure 15 and compared for all tests in Figure 16.

The full-speed Honda Civic test exceeded the proposed injury limits for two of the three ligaments. Among the reduced speed tests, the Mazda Miata exceeded limits for the ACL, and the Volvo S40 exceeded the ACL and MCL limits on all tests.

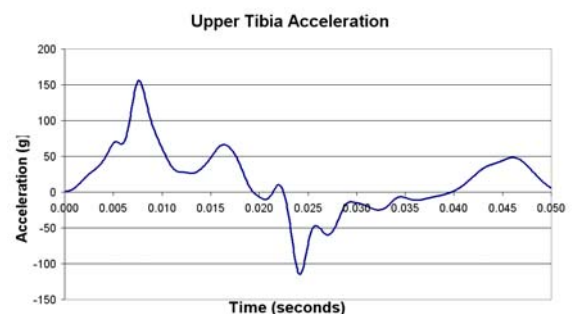


**Figure 15. Ligament extension for right lateral impact into Volvo S40 bumper at reduced speed.**

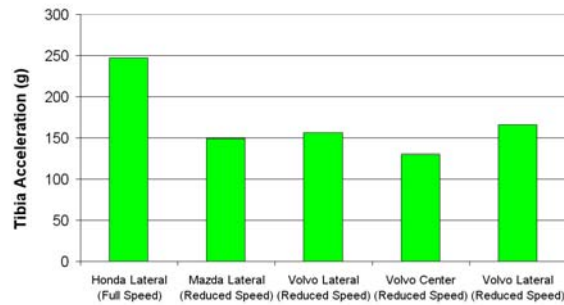


**Figure 16. Ligament extensions for all impacts with FlexPLI legform (proposed injury limits of 20 mm for MCL and 10 mm for ACL and PCL).**

Upper tibial acceleration is shown for the example impact with the Volvo S40 bumper in Figure 17, and compared for all tests in Figure 18. No injury limits have been proposed for acceleration of the FlexPLI legform.



**Figure 17. Upper tibia acceleration for right lateral impact into Volvo S40 bumper at reduced speed.**



**Figure 18. Upper tibia acceleration for all impacts with FlexPLI legform (no injury limit proposed).**

## DISCUSSION

### Evaluation of TRL and FlexPLI Legforms

Figures 3 and 10 show the marked difference between how the TRL and FlexPLI legforms interact with the vehicles. The single-jointed TRL bent only at the knee while the FlexPLI's flexible femur and tibial elements allowed it to wrap around the front of the vehicle. This difference in how the legforms conform to the vehicle shape is likely to affect not only the magnitude of bending angle at the knee but all injury measures. Variations in the shape of the bumper, grille, and hood leading-edge structures may have a different effect on injury measures recorded by one legform than they do on the other legform.

The knee shear displacement and knee bending angle calculated using rotary potentiometers by the TRL legform relate directly to physiologic measurements for which known biofidelity corridors exist [11, 12]. These quantities, along with upper tibial acceleration, are the only measurements made by the TRL legform. The simplicity of the instrumentation system contributes to its reliability and the lightness of its wiring umbilical helps to maintain the leg's orientation during free flight.

The instrumentation in the FlexPLI 2004 includes moment measurements along the flexible femur and tibia components as well as injury measurements at the knee joint. This additional information may allow better understanding of how specific structures on the upper or lower vehicle front interact with a pedestrian lower extremity and also offer insight into injury potential of the long-bones rather than just the knee. Although the additional instrumentation in the FlexPLI increases the potential for damage to wiring and loss of data, the pairs of strain gauges mounted to the bone cores allow redundant data to be collected at each level, reducing

the risk of lost data as a result of wiring damage. Unfortunately, this built-in redundancy further increases the number of wires in the legform's umbilical and makes it difficult to maintain perfect orientation during free-flight. An onboard data acquisition system may be a useful feature for any free-flight legform.

Both legforms tested in this study were designed outside of North America and had limitations for testing vehicles from the North American market. The FlexPLI legform fractured when used with North American vehicles at 40 km/h or even at a reduced speed of 30 km/h. The bone core elements fractured in three of five tests. The core fractured even before reaching the proposed injury limit for bending moment in two of those three tests that produced fracture.

Although the TRL legform withstood the testing without structural damage, its bending limits were exceeded, restricting measurement of peak values. Peak values of all injury measures were likely affected since this mechanical bending limitation affected the motion of the legform rather than simply its ability to measure the motion.

### Comparison of North American and European Bumpers

Comparison of North American and European versions of the specific vehicles tested is possible because the North American vehicles selected for this study corresponded to European vehicles previously tested under EuroNCAP procedures. Although there were minor differences in the launch procedure for the current study from the EuroNCAP procedure, the tests are essentially comparable. The slightly slower than targeted impact speed in the current study makes the comparison conservative in that the current tests were slightly less demanding than the comparison EuroNCAP tests.

The bumpers tested in EuroNCAP procedures were subject to European bumper damage regulations while those tested in the current study were subject to North American bumper standards. However, EuroNCAP results for the European versions of the vehicles tested showed that lower leg pedestrian test performance was not consistently better for the European versions of these same five vehicles. In fact, only the European Honda Civic and Volvo S40 scored any EuroNCAP points in the legform to bumper tests. Table 5 contains peak measurements made for EuroNCAP data for vehicles in the same model year range as the vehicles in this test study

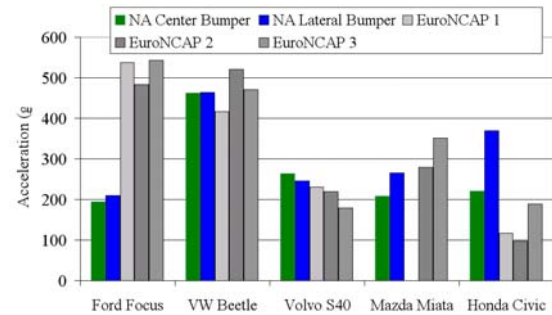
[13]. These peaks are compared to the corresponding peak measurements in the currently reported tests on the North American models in Figures 19 to 21.

**Table 5.**  
**Peak Measurements in EuroNCAP testing of European models of test vehicles.**

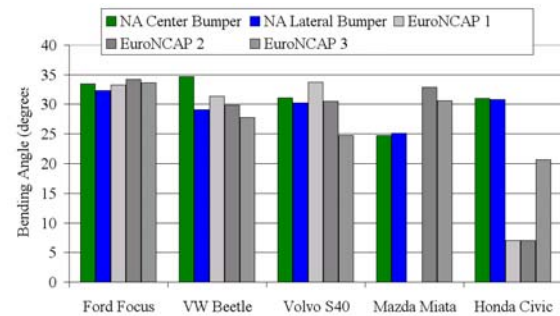
	Test No.	Upper Tibia Accel	Bend Angle	Shear Displ.	Euro NCAP Points
1999 Ford Focus	1	536.7	33.3	6.6	0
	2	483.7	34.2	8.0	0
	3	542.7	33.6	5.8	0
2001 Honda Civic	1	116.4	7.1	1.9	2
	2	97.7	7.0	2.3	2
	3	189.6	20.7	2.1	1.01
2002 Mazda MX-5 / Miata	1*				0
	2	278.1	32.9	4.3	0
	3	351.1	30.6	6.8	0
1999 VW Beetle	1	416.0	31.4	7.0	0
	2	520.0	29.8	7.4	0
	3	470.0	27.7	7.0	0
1997 Volvo S40	1	231.0	33.7	7.4	0
	2	220.0	30.5	7.5	1
	3	180.0	32.8	7.0	0

\* No Mazda impact was performed at site 1 because identical to site 3.

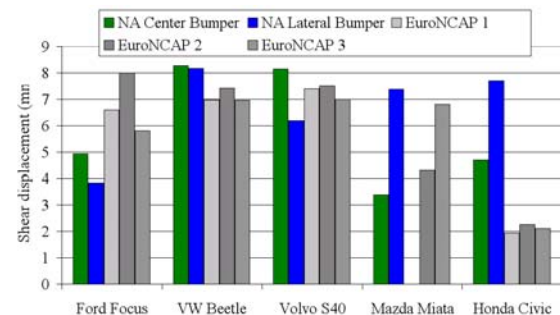
The North American Ford Focus performed better than its European counterpart in terms of shear displacement and tibia acceleration, while the European and North American Ford Focus both exceeded the 30-degree bending angle limit of the TRL legform. The North American Mazda Miata's performance was better than the European model in both bending angle and upper tibial acceleration. Peak measurements made on the North American Volkswagen Beetle and Volvo S40 were comparable to those made in tests of their European models. The European version of the Honda Civic performed dramatically better in lower leg testing than the North American model. In fact, Honda peak injury measurements were lower in every test than in any of the other North American vehicles tested in this study.



**Figure 19. Peak average upper tibia acceleration for North American models compared to European models.**



**Figure 20. Peak average knee bending angle for North American models compared to European models.**



**Figure 21. Peak average knee shear displacement for North American models compared to European models.**

The similar performance of the Volkswagen and Volvo vehicles compared to European versions suggests that there may not have been significant differences in the international versions of their front bumper systems. The better performance of the North American Ford Focus and Mazda Miata over their European counterparts and the European Honda Civic over its North American counterpart suggests that bumper design differences exist between the international versions of these vehicles.

The European models of the Volvo S40, Volkswagen Beetle, Ford Focus, and Mazda Miata did not appear to offer better pedestrian leg protection than the North American models of those vehicles in spite of the fact that the European vehicles were required to meet different bumper damage requirements than the North American versions. In contrast, the European 2001 Honda Civic showed much improved pedestrian leg protection over the North American Honda Civic in the same year range. Given that the European vehicles tested were not yet required to meet the upcoming European Union pedestrian safety requirements, the better performance of the European 2001 Honda Civic may reflect a trend toward improvement to meet the upcoming pedestrian requirements.

### **Damageability and Bumper Performance**

The relationship between bumper performance in pedestrian lower extremity impacts and bumper damageability was also considered. Damageability testing has been reported for 3 vehicles that are in the same model and year range as the vehicles tested in the current study [14]. Low-speed flat barrier, angled barrier and pole impact tests were performed at  $7.96 \pm 0.24$  km/h [15] on vehicles including the 2000-2005 Ford Focus, 2001-2005 Honda Civic, and the 1998-2005 Volkswagen Beetle. By the IIHS qualitative rating scale, in which the vehicles that sustain the least damage in testing score highest, the Volkswagen Beetle scored Good, the Honda Civic Acceptable, and the Ford Focus Marginal. It was reported that the North American Volkswagen Beetle model tested had indeed been one of the best cars ever tested for bumper performance in the low-speed damage tests and that it performed better in damage tests than the European version of the Volkswagen Beetle [16].

In contrast, the North American Volkswagen Beetle was the worst performer in the current series of pedestrian lower extremity tests, using the modified EuroNCAP point calculation. Next worse of the three vehicles was the Honda Civic lateral bumper tests, both Ford Focus tests, then the Honda Civic center bumper tests. The contrary results of bumper damage tests and pedestrian lower extremity tests illustrate the incompatibility between bumper damage reduction and pedestrian lower extremity safety.

The fact that the more damage-resistant bumpers tended to perform worse in these pedestrian safety tests suggests that structural stiffness of bumper components influences the severity of pedestrian

lower extremity injury. However, there were other design elements that appeared from video to have an effect on leg deformation, and therefore loading. These included the depth and angle of the bumper face and the shape of the grille and hood leading edge. Bumpers with a tall, flat face like the Mazda Miata's reduced bending at the knee and below by limiting wrapping of the tibia under the bumper. Similarly, vehicles like the Volvo S40 with upright hood structures above the bumper reduced bending of the knee and upper leg by reducing wraparound onto the hood in this free-flight test.

### **CONCLUSIONS**

The single-jointed TRL legform and the flexible femur and tibia of the FlexPLI legform lead to marked differences in how the two legforms interact with vehicle front structures. Variations in bumper design may have different effects on the injury measures recorded by the two legforms.

Both legforms had limitations in testing North American vehicles in this test series. The FlexPLI 2004 fractured in three tests and the TRL legform was unable to produce reliable peak measurements when bending exceeded thirty degrees.

The North American bumpers tested in this series would not have met European limits set for pedestrian leg loading and repeatedly fractured or exceeded the measurement capabilities of the legforms developed for use in international pedestrian testing. Although four of the five European vehicles tested under comparable conditions also performed inadequately in similar tests, the European version of one vehicle tested showed dramatically improved pedestrian leg protection over its North American counterpart. Although these tests do not establish that the North American bumper standards are the reason for the aggressiveness of North American bumpers, IIHS testing suggests that bumpers that are more robust (i.e., those that score better in their bumper damage tests) may be more aggressive toward pedestrians.

Although this study suggests that less damageable bumpers may be more aggressive toward pedestrians, it does not establish that vehicles meeting North American bumper standards cannot achieve improved pedestrian leg safety. Further work should be done to determine if vehicle front design could be improved to better protect pedestrians while still conforming to current bumper regulations. This work may include both bumper and pedestrian testing of more recent models of the

vehicles tested in this study to see how much each of them has changed with new pedestrian regulations on the horizon.

## ACKNOWLEDGEMENTS

The authors are grateful to Honda R&D Americas and the Japan Automobile Research Institute (JARI) for loaning the pedestrian legforms used in this study. Mr. David Hyder is acknowledged for his assistance in running the tests.

## REFERENCES

- [1] Transport Canada. 2004. "Canadian Motor Vehicle Traffic Collision Statistics: 2003." Report No. TP 3322.
- [2] NHTSA. 2004. "Traffic Safety Facts 2003: A Compilation of Motor Vehicle Crash Data from the Fatality Analysis Reporting System and the General Estimates System." DOT HS 809 775.
- [3] Mizuno Y. Ishikawa H. 2001. "Summary of IHRA Pedestrian Safety WG Activities – Proposed Test Methods to Evaluate Pedestrian Protection Afforded by Passenger Cars". 17<sup>th</sup> International Conference on the Enhanced Safety of Vehicles, Amsterdam, June 2001, Paper Number 280.
- [4] Canada Motor Vehicle Safety Standard (CMVSS) 215. "Bumpers". Chapter M-10 Revised Statutes of Canada, 1985 and SOR/91-692.
- [5] EuroNCAP. 2004. "European New Car Assessment Programme (EuroNCAP) Assessment Protocol and Biomechanical Limits." [www.euroncap.com](http://www.euroncap.com), accessed January 2005.
- [6] TRL Limited. 2003. "TRL Pedestrian Legform Impactor User Manual." Version 2.3a.
- [7] European Union. 2003. "Directive 2003/102/EC of the European Parliament and of the Council of 17 November 2003 relating to the protection of pedestrians and other vulnerable road users before and in the event of a collision with a motor vehicle and amending Council Directive 70/156/EEC", Official Journal of the European Union L 321/15, <http://europa.eu.int>.
- [8] Konosu A. and Tanahashi M. 2003. "Development of a Biofidelic Flexible Pedestrian Legform Impactor." Stapp Car Crash Journal, Vol. 47, pp. 459-472.
- [9] Lawrence G. 2005. Personal communication.
- [10] Konosu A. 2004. Personal communication.
- [11] Ivarsson J., Lessley D., Kerrigan J., Bhalla K., Bose D., Crandall J., and Kent R. 2004. "Dynamic Response Corridors and Injury Thresholds of the Pedestrian Lower Extremities," Proc. International IRCOBI Conference on the Biomechanics of Impacts, pp. 179-191.
- [12] Wittek A., Konosu A., Matsui Y., Ishikawa H., Shams T., and McDonald J. 2001. "A new legform impactor for evaluation of car aggressiveness in car-pedestrian accidents," Proc. 17th International Technical Conference on the Enhanced Safety of Vehicle, Paper No. 184.
- [13] Dotraux F. 2005. Personal communication.
- [14] Insurance Institute for Highway Safety. 2004. "Bumper Ratings: Small Cars." [www.hwysafety.org/vehicle\\_ratings/low\\_speed\\_smcars.htm](http://www.hwysafety.org/vehicle_ratings/low_speed_smcars.htm), accessed January 2005.
- [15] Insurance Institute for Highway Safety. 2002a. "Low-Speed Crash Test Protocol." Version V.
- [16] Insurance Institute for Highway Safety. 2002b. "Same cars? Not Exactly." Status Report, Volume 37, Number 3, March 1-4.

# DEVELOPMENT OF A FINITE ELEMENT MODEL FOR FLEX-PLI

**Yuji Kikuchi**

Honda R&D Co., Ltd.

Japan

**Yukou Takahashi**

Honda R&D Americas, Inc.

**Fumie Mori**

PSG

Paper Number 05-0287

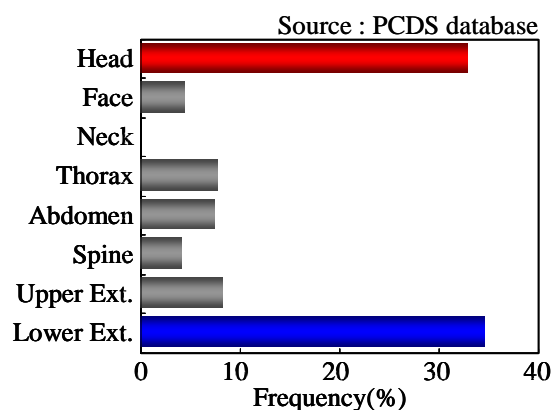
## ABSTRACT

A finite Element (FE) model of the next-generation flexible pedestrian leg-form impactor (Flex-PLI) developed by the Japan Automobile Manufacturers Association (JAMA) and Japan Automobile Research Institute (JARI) was developed in this study. The Flex-PLI is intended to be used in evaluating safety of car front structures against the lower limbs of pedestrians. A 3D geometry of each part was reproduced in PAM-CRASH<sup>TM</sup> based on drawings of the Flex-PLI. For material characterization, the stress-strain characteristics were determined from the results of the material tests on each individual component, with the strain rate dependency of the material taken into account. The results of the dynamic 3-point bending test for the thigh and leg and the dynamic 4-point bending test for the knee joint performed by JARI were used to validate the model. The validation results showed that the computer simulation results for the force-deflection response of the thigh and leg as well as the moment-angle response of the knee joint agreed well with the test results. Impact tests against vehicles at 40 km/h were reproduced using the model, and the results were compared with the test results. The results of the comparison showed that the kinematics of the Flex-PLI could be reproduced by the computer simulation. It was also found that the bending moment of the thigh and leg as well as the elongation

of the ligament cables of the knee joint could be accurately reproduced.

## INTRODUCTION

According to pedestrian accident data, pedestrians account for approximately 30% of fatalities in traffic accidents in Japan. For this reason, pedestrian protection along with occupant protection is considered as an important issue in the improvement of vehicle safety [1]. Distribution of AIS 2+ injuries from the Pedestrian Crash Data Study (PCDS) database in the U.S. shows that the frequency of injuries to the head and lower limb dominates as shown in Figure 1. Because injuries to the head are often fatal, head injuries are considered as the most serious injuries. Lower limb injuries are also important because of their long-term consequences and high social costs.



**Figure 1. Distribution of AIS2+ pedestrian injuries by body region**



In order to reduce these injuries in pedestrian accidents, the European Enhanced Vehicle-safety Committee (EEVC) Working Group 17 has proposed a vehicle test procedure employing a head-form impactor, upper leg-form impactor, and leg-form impactor. For the leg-form impact test, a leg-form impactor developed by the Transportation Research Laboratory (TRL) known as TRL-PLI has normally been used [2]. However, it has been pointed out that it is necessary to improve the biofidelity of the TRL-PLI and the validity of the injury criteria [3]-[5]. Accordingly, a flexible-pedestrian leg-form impactor (Flex-PLI) has been developed jointly by JAMA and JARI as a next-generation impactor that has greater biofidelity. The thigh, knee joint and leg of the Flex-PLI have been built of flexible structure in order to obtain more realistic kinematics of the human lower limb. The published test results using Post Mortem Human Subjects (PMHS) were used to validate the dynamic response of the limb [6]-[8].

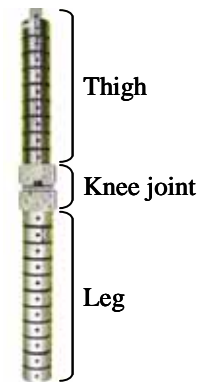
In this study, an FE model for the Flex-PLI was developed for use in vehicle development for improved safety of vehicle front structures against pedestrian lower limbs.

## MODEL DESCRIPTION

As shown in Figure 2, the Flex-PLI consists of three segments, the thigh, knee joint, and leg. The thigh and leg were made flexible in order to reproduce deflection of the human bones. The knee joint of the Flex-PLI has a simplified structure that represents geometry of bones and ligaments. However, the knee joint is capable of reproducing bending and shear in human knee joint due to lateral impact from a vehicle to the lower limb of a pedestrian.

The 3D geometry of each component of the Flex-PLI was precisely reproduced in PAM-CRASH™ based

on the drawings of the Flex-PLI [9]. Since the fairly rigid steel and aluminum parts were modeled as rigid bodies, it was necessary to determine mass and moment of inertia of those parts for the rigid body definitions. Those numbers were determined by importing the 3D geometry of the parts into PAM-GENERIS™ and giving appropriate density for the parts [10]-[12].



**Figure 2. Flex-PLI**

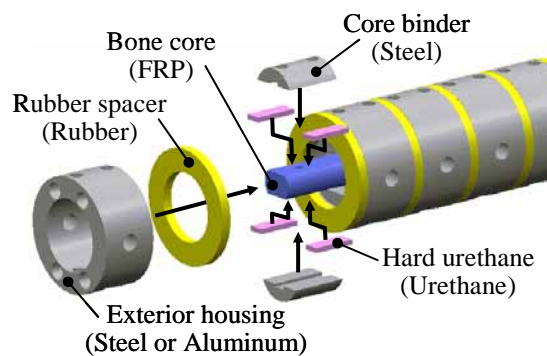
### Thigh and Leg

Figure 3 shows the bony structure of the thigh and leg. The bony structure is assembled by surrounding the bone core with the core spacer and core binder, fixing these parts together with adhesive, inserting them into the exterior housing, then bolting them from outside of the exterior housing, as shown in the cross-sectional diagram (Figure 4). By tightening the bolt, the core binder is pushed against the core spacer compressing it, after which the exterior housing is fixed to the bone core. The exterior housings are piled up axially with the rubber spacers in between. The thigh and leg are with nine and eleven exterior housing blocks, respectively. Figure 5 shows the FE model for the thigh and leg. Since the resin bone core, core spacer and rubber spacer are subjected to large deformation, those parts were modeled as deformable solid elements. The fairly rigid steel and aluminum parts such as the exterior housing and core binder were modeled as rigid bodies. The cross section of

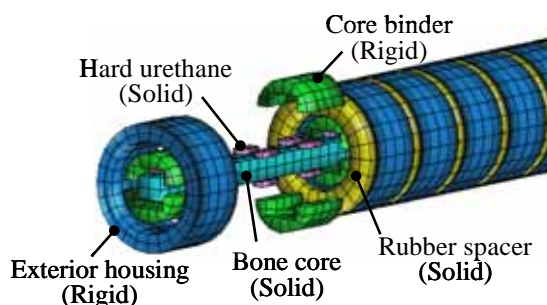


the bone core is shown in Figure 6. Since the length of one side of the bone core is not long enough to provide practical level of time integration step in PAM-CRASH<sup>TM</sup> (estimated time step was  $0.575 \mu\text{sec}$ ), it was decided to simplify the cross section with a rectangular shape in such a way that the areal moment of inertia is conserved as shown in Figure 7. This resulted in the time step of  $1.04 \mu\text{sec}$  and significantly reduced CPU time.

The constraints used in the model for each part were determined based on the actual Flex-PLI assembly procedure. Because the core spacer and core binder are glued to the bone core and core spacer, respectively, there is no degree freedom on the interface. Consequently, Sliding Interface Type 10

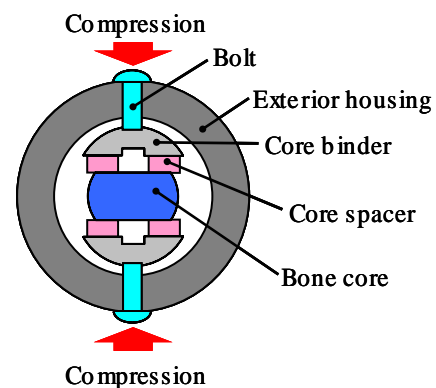


**Figure 3. Structure of thigh and leg**

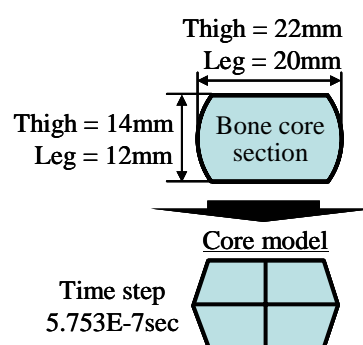


**Figure 5. Thigh and leg model**

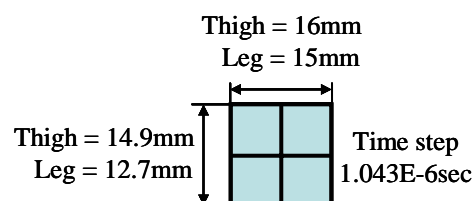
(Tide Contact) was used on the contact surface between the bone core and the core spacer as well as the contact face between the core spacer and core binder. A joint element with all degrees of freedom fixed was used to connect the core binder to the external housing. Since the rubber spacer is glued to one side of the exterior housing, Sliding Interface Type 10 was applied to define the interface between those parts. On the other side of the rubber spacer, which is not glued to the exterior housing, Sliding Interface Type 33 was used to define the contact with the exterior housing. This modeling reproduced the deformation of the rubber spacer by selecting appropriate contact models that accurately represent the actual interface conditions.



**Figure 4. Section of thigh and leg**



**Figure 6. Bone core section and model section**

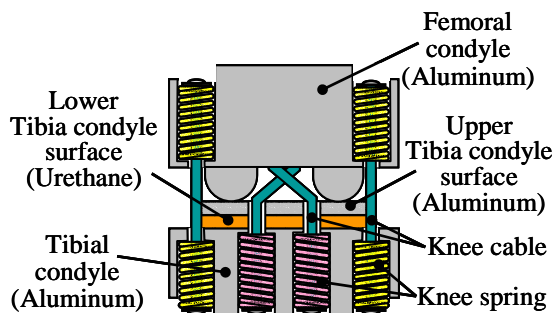


**Figure 7. Section of bone core model**

## **Knee Joint**

Figure 8 shows the structure of the knee joint for the Flex-PLI. The upper and lower tibia condyle surface are glued to the lower tibia condyle surface and the tibial condyle, respectively. Knee springs that determine the tensile properties of the knee ligaments are installed in the femoral and tibial condyle. Knee cables simulating the knee ligaments pass through the inside of the knee springs, connecting the femoral condyle to the tibial condyle to configure the knee joint.

The FE model for the knee joint is shown in Figure 9. Rigid aluminum components such as the femoral condyle, upper tibia condyle surface, and tibial condyle were modeled as rigid bodies while the lower tibia condyle surface, which is made of hard urethane, was modeled using solid elements. All nodes were shared on the two interfaces between the upper and lower tibia condyle surface and the tibial condyle. Each pair of the knee springs and knee cable representing four major ligaments in a human knee

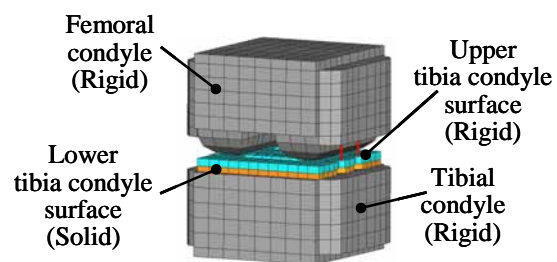


**Figure 8. Structure of knee joint**

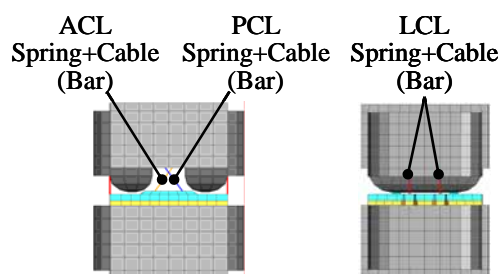
(Anterior Cruciate Ligament; ACL, Posterior Cruciate Ligament; PCL, Medial Collateral Ligament; MCL, Lateral Collateral Ligament; LCL) was lumped together and modeled using one single bar element as shown in Figure 10. The material properties of the springs were modeled using Material Type 205 in PAM-CRASH™.

## **Flesh**

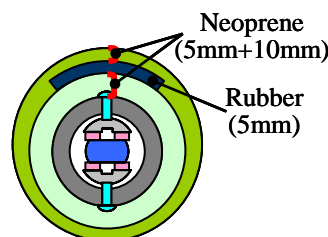
As shown in Figure 11, Neoprene sheets with the thickness of 10 mm and 5 mm are wrapped around the thigh, knee joint and leg as the flesh of the Flex-PLI. In addition, on the side of the impactor that is supposed to be impacted by a vehicle, a rubber sheet with the thickness of 5 mm was inserted between the two Neoprene layers. Those sheets were modeled using solid elements with exactly the same thickness as shown in Figure 12. For defining contact of the flesh to the thigh, leg, and knee joint, Sliding Interface Type 33 was used in order to accurately reproduce motion of the flesh relative to the thigh, leg, and knee joint.



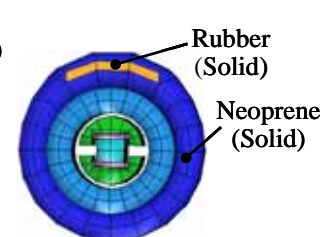
**Figure 9. Knee joint model**



**Figure 10. Knee spring and ligament model**



**Figure 11. Structure of flesh**



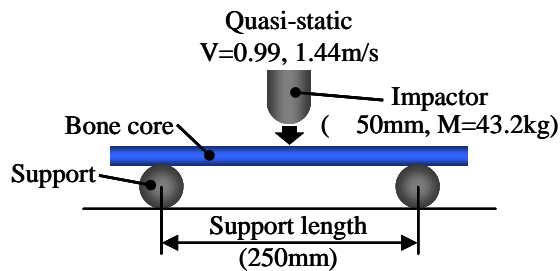
**Figure 12. Section of flesh model**

## VALIDATION OF MATERIAL PROPERTIES

In order to ensure accuracy of the model, the stress-strain characteristics of the material models for the resin parts were determined by running some material tests using those parts. The target for the model validation was that the computer simulation results fall within  $\pm 10\%$  of the average experimental results.

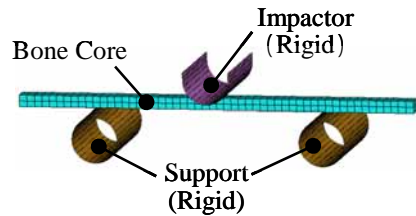
### Bone Core

The bone core model was validated against the results of the quasi-static and dynamic 3-point bending tests performed by Konosu et al. [6]. Figure 13 shows the test set-up used by Konosu et al. The bone core was simply supported using circular cylinders with 50 mm diameter placed underneath its both ends. The span length was set at 250 mm. An impactor with 43.2kg weight and 50 mm diameter tip

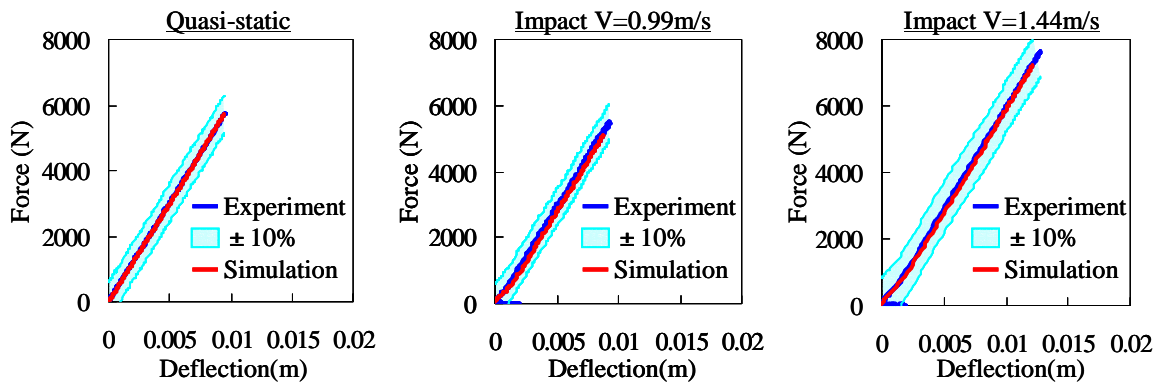


**Figure 13. 3 point bending test setup for bone core**

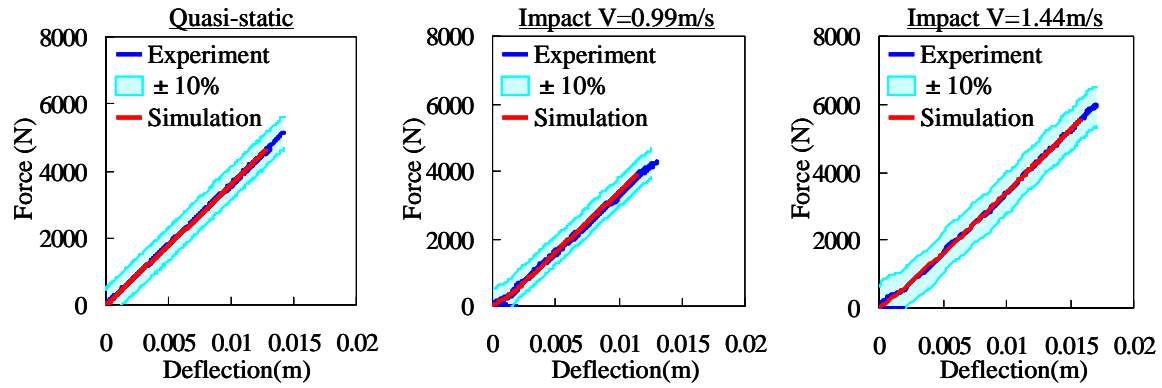
applied load at mid-span in quasi-static condition (0.1mm/s) as well as at impact speeds of 0.99 m/s and 1.44 m/s to obtain force-deflection response. Since the rate dependency was not observed in the measured force-deflection response, Material Type 16 in PAM-CRASH™ was used to apply linear elastic material model. Figure 14 shows a set-up of the model that simulates the 3-point bending test conducted by Konosu et al. The results of the comparison between experiment and computer simulation are shown in Figure 15 and 16 for the thigh and leg bone core, respectively. The computer simulation results fell within  $\pm 10\%$  of the results of the test results in all loading rates, indicating good agreement. The results also suggest that the model with a simplified cross section can yield good results as long as the areal moment of inertia is maintained.



**Figure 14. Model setup for bone core validation**



**Figure 15. Comparison between load-deflection response and simulation result of thigh bone core in 3 pint bending**



**Figure 16. Comparison between load-deflection response and simulation result of leg bone core in 3 pint bending**

### Other Resin Components

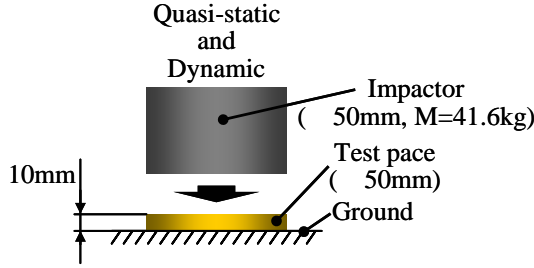
The mechanical characteristics of the resin components such as the core spacer and rubber spacer of the thigh and leg, the lower tibia condyle surface in the knee joint, and the flesh were measured in this study. As shown in Figure 17, compression tests with the impactor of 41.6 kg weight and 50 mm diameter tip were run against a test specimen made of each material, and the dynamic force-deflection responses were measured. Similarly, quasi-static compression tests were also performed in order to obtain quasi-static force-deflection responses that were used to determine stress-strain relationship for the materials.

The degree of strain rate dependency can be evaluated by comparing the quasi-static and dynamic force-deflection responses of each material. Since the test results showed that the materials tested were rate dependent, strain rate dependent material models were used. As shown in Figure 18, computer simulation models that simulate the material tests were built in order to determine material model parameters. Force-deflection responses from the quasi-static compression tests were converted into stress-strain relationships. The stress was obtained from the compressive force divided by the initial cross sectional area of the test specimen, and the strain was calculated from the displacement of the

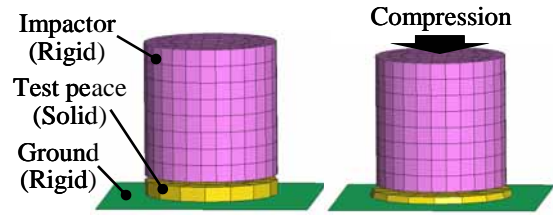
impactor divided by the initial thickness of the test specimen. Material Model Type 21 (Solid element) in PAM-CRASH<sup>TM</sup> was used to characterize the materials. As for the strain rate dependency, Cowper-Symonds strain rate model was used and the strain rate parameters for this model were determined in such a way that the computer simulation results best match the test results. Figure 19 shows the results of a comparison between experiment and computer simulation in quasi-static compression for each material. The results showed that the stress-strain relationships estimated from the force-deflection responses were valid. Once quasi-static stress-strain relationships were established, strain rate parameters were determined so that the computer simulation results for dynamic compression of the materials agree well with the test results. As shown in Figure 20, the simulation results were within  $\pm 10\%$  of the test results, thus indicating that the strain rate parameters used in the models accurately characterize the strain rate dependency of the actual materials.

### **VALIDATION OF THIGH AND LEG MODEL**

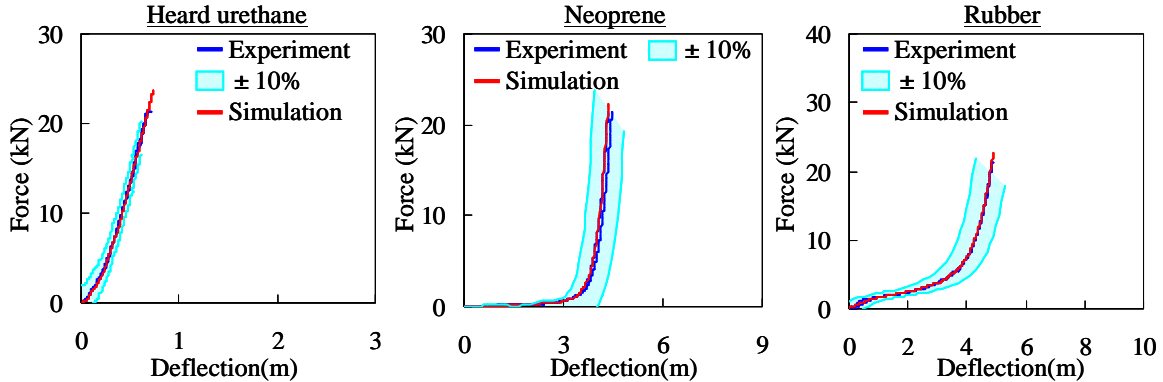
Since the results of the material model validation of the bone core and each resin part confirmed accuracy of the material models, the dynamic response of the



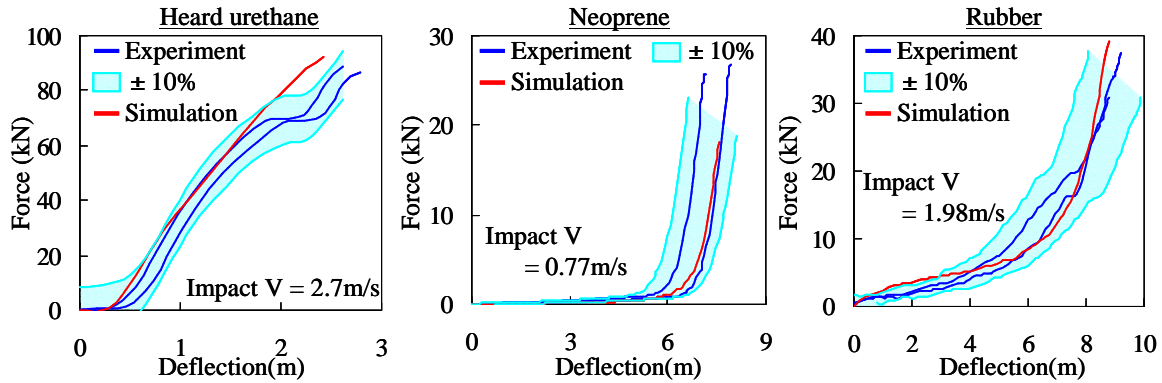
**Figure 17. Compression test setup for resin materials**



**Figure 18. Compression test model setup for resin materials**



**Figure 19. Comparison between load-deflection response and simulation result of resin materials in quasi-static compression test**



**Figure 20. Comparison between load-deflection response and simulation result of resin materials in dynamic compression test**

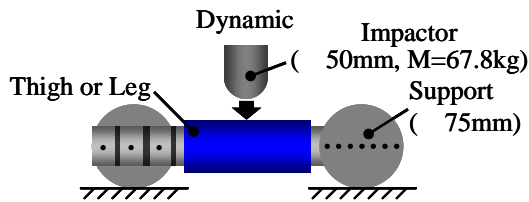
thigh and leg model was validated as the next step. In the model validation, the results of the 3-point bending tests for the thigh and leg performed by Konosu et al. [7][8] were used. As shown in Figure 21, both ends of the thigh or leg were simply supported. An impactor that weighed 67.8 kg was impacted against the mid-shaft of the thigh or leg in lateromedial direction at an impact speed of 1.0 m/s, and the force-deflection response was measured. The computer simulation model shown in Figure 22 was

created using the thigh and leg model to simulate the experiment, and the test results were compared with the computer simulation results. Figure 23 shows the results of the comparison between the test and computer simulation for the force-deflection response. The figure shows that the computer simulation results are within  $\pm 10\%$  of the test results, thus confirming that the model can accurately reproduce the dynamic response of the thigh and leg. As can be seen from the cross-section of the

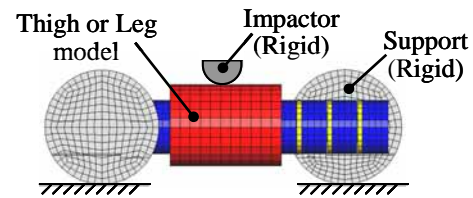
deformed thigh model in Figure 24, the rubber spacer and core spacer of each part are compressed, the internal bone core deflects smoothly without large local deformation, the exterior housing and core binder follow the bone core, and the overall deflection of the bone structure is reproduced. By determining constraints for the model of each part in such a way that the constraint precisely represents the actual assembly procedure, it was possible to simulate the response of the thigh and leg as a result of accurate reproduction of load paths inside the exterior housings.

## VALIDATION OF KNEE JOINT MODEL

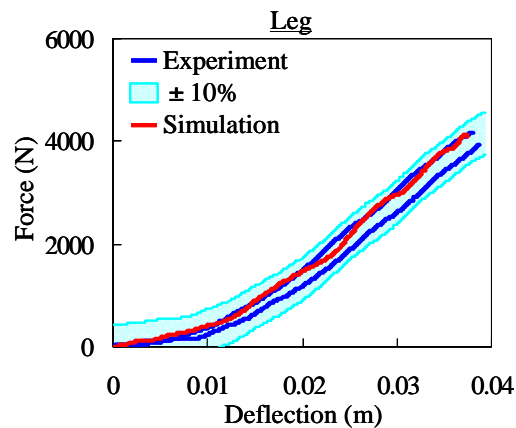
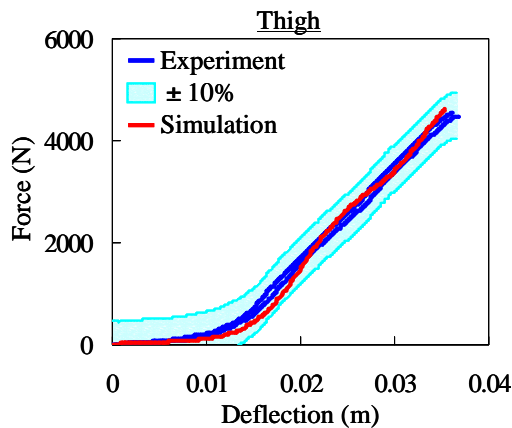
To validate the knee joint model, the results of the 4-point bending test of the knee joint performed by Konosu et al. [7] were used. The set-up used by Konosu et al. is shown in Figure 25. A load cell and a shaft were installed on both sides of the knee joint, and both ends of the knee test specimen assembly were rigidly attached to a support roller to provide simply supported condition. A fork with two prongs weighing 74.5 kg applied load onto the knee joint test specimen assembly at a speed of 1.4 m/s in such a



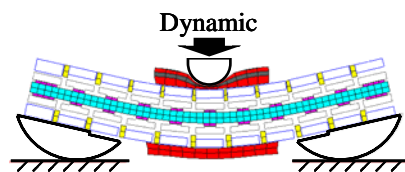
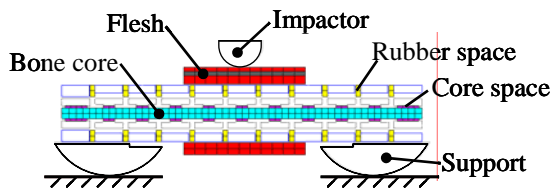
**Figure 21. Dynamic 3 point bending test setup for thigh and leg**



**Figure 22. Dynamic 3 point bending model setup for thigh and leg**



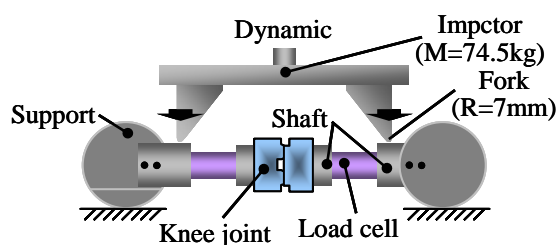
**Figure 23. Comparison of load-deflection response of thigh and leg between experiment and simulation**



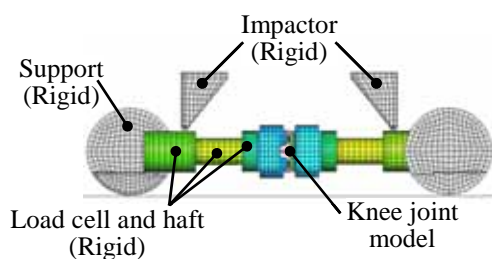
**Figure 24. Kinematics of the thigh model for 3 point lateral bending test simulation**

way that the knee bends in valgus. The moment-angle response of the knee joint was then measured. The definition of the knee moment was the average moment from the load cells installed on the inferior and superior side of the knee joint. A computer simulation model that simulates the experiment was created as shown in Figure 26 in order to validate the dynamic response of the knee joint. Figure 27 shows the comparison between experiment and computer simulation. The bending moment in the initial phase generated by the inertial effect was higher for computer simulation. However, the bending moment in the subsequent phase, which is primarily from the knee bending response, agreed well between the test and computer simulation, confirming that the dynamic response of the knee joint can be reproduced by the model.

Based on the above shown validation results, high accuracy of the model was confirmed in component level.



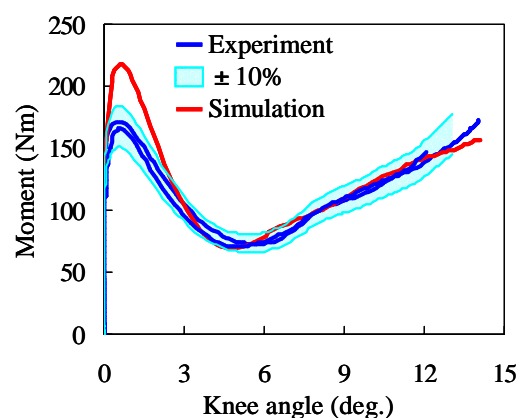
**Figure 25. Dynamic 4 point test setup for knee joint**



**Figure 26. Dynamic 4 point model setup for knee joint**

## MODEL VALIDATION AGAINST VEHICLE IMPACT TEST

Vehicle impact tests using the Flex-PLI were performed and the results were used to validate the model in assembly level. A passenger car and an SUV were used in the vehicle impact tests to investigate the differences in the impact response of the Flex-PLI due to the difference in car front shape. As shown in Figure 28, the vehicle tests were performed at 40 km/h, and the Flex-PLI was propelled into the laterally center part of the vehicle. In terms of instrumentation, three and four strain gauges were affixed to the bone core of the thigh and leg, respectively, as shown in Figure 29. The bending moment at each position on the thigh and leg (Thigh 1-3, Leg 1-4) was calculated from the strain measured. The moment calculation was based on the separate quasi-static mid-shaft 3-point bending test where the correlation factor between the strain of each strain gauge and the moment calculated from the reaction force from one support multiplied by the distance between the strain gauge and the support was determined. In addition, the knee joint of the Flex-PLI features potentiometers to measure the displacement of both ends of the ligament cable



**Figure 27. Comparison of moment-knee angle response of knee joint between experiment and simulation**



relative to the tibial and femoral condyle. In order to compare the results of those measurements with the computer simulation results, Section Fore in PAM-CRASH<sup>TM</sup> was set at each position of the strain gauges to provide bending moment at each cross-section. In the model, each set of the knee cable and knee springs was modeled as a single bar element and force-elongation property that corresponds to the stiffness of the combination of the two knee springs was applied to it, the displacement of the ends of the knee springs was automatically obtained by looking at the elongation of the bar element. Thus, the elongation of the bar element from the computer simulation was directly compared with the displacement of the ends of the knee spring in the experiment. Figure 30 compares the kinematics of the Flex-PLI between the computer simulation and experiment for both the passenger car and the SUV. As seen from the test results for the passenger car, the thigh and leg were significantly deformed around the knee joint, then the thigh leans onto the hood, and the leg is bounced off the bumper. The computer simulation model reproduces the same behavior as that obtained experimentally. In the case of the SUV, since the hood edge is high relative to that of the passenger car, the hood and the grille of the SUV can restrain the thigh. This results in smaller deflection of the thigh compared to that of a passenger car. However, the leg enters the space beneath the bumper, resulting in greater deflection in the lower end of the leg. The computer simulation model also shows deflection of the thigh and leg similar to that of the experimental results. It was therefore confirmed that the characteristic kinematics resulting from the difference in the front shape of the passenger car and SUV can be reproduced.

Figure 31 shows a comparison between the results of the experiment and computer simulation for the

maximum values of the bending moment of the thigh and leg. While the simulation result for Thigh-1 in the case of the passenger car is higher than the test results, the simulation results for other parts are within  $\pm 10\%$  of the test results, indicating good agreement. Because Thigh-1 is struck by the hood edge, deforms about the hood edge, and consequently generate bending moment, the hood edge of the vehicle model is most likely more rigid relative to that of an actual vehicle considering the fact that the FE model for the passenger car used in this study was for a slightly different model from the car used in the tests. Therefore, better agreement between the test results and computer simulation results for Thigh-1 should be able to be obtained by improving the model for the parts in the vicinity of the hood edge. However, since the objective of this study was to validate the Flex-PLI model, improved accuracy of the vehicle model was considered as an issue for future study. In the case of SUV, the trend of the simulation results for the bending moment of both the thigh and leg agreed with that of the test results, and the simulation results were within  $\pm 10\%$  of the test results. This indicates good quantitative agreement between the test results and computer simulation results. Figure 32 shows a comparison of the maximum elongation of the bar element that represents the knee cable and knee springs (for the experiment, this is equivalent to the displacement of the ends of the knee springs) between the experiment and computer simulation. The simulation results for the elongation of the knee cables were within  $\pm 10\%$  of the test results for both the passenger car and SUV, indicating good accuracy.

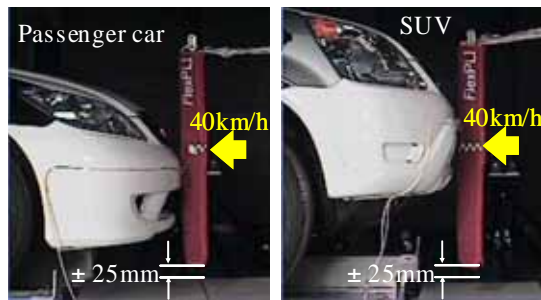


Figure 28. Vehicles impact test setup

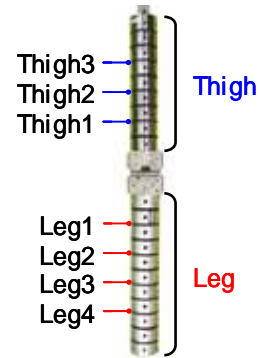


Figure 29. Strain gauges attachment position for thigh and leg

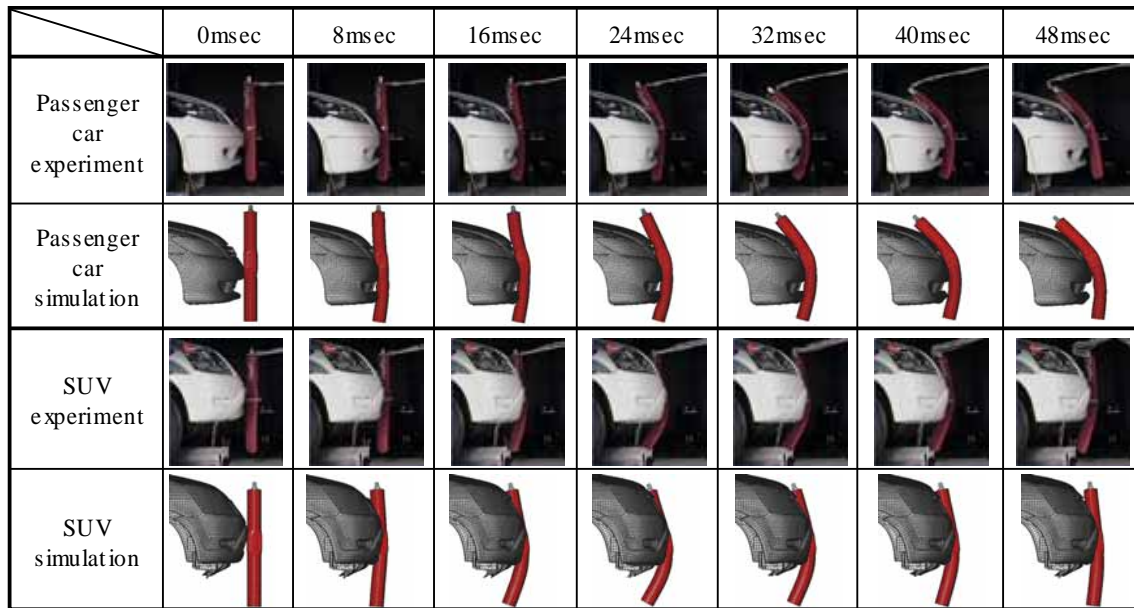


Figure 30. Comparison of the Flex-PLI motion between experiment and simulation for vehicle impact test

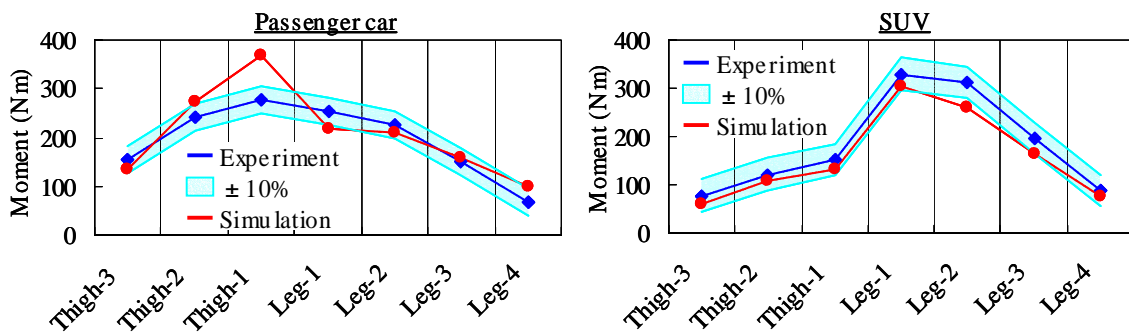


Figure 31. Comparison of peak bending moment for thigh and leg between experiment and simulation

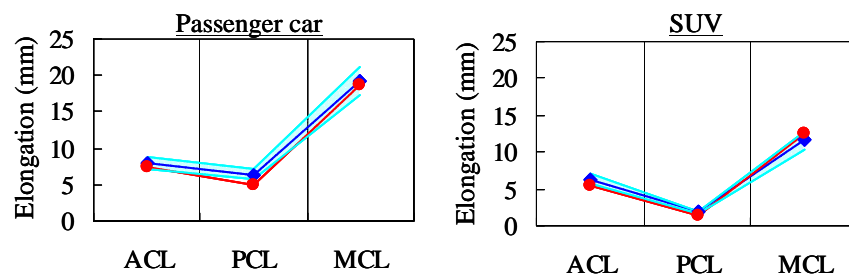


Figure 32. Comparison of knee spring expand between experiment and simulation

## CONCLUSION

In order to reduce the CPU time for the bone core model in the bony structure of the thigh and leg, a model was made by calculating the areal moment of inertia from the cross-section of the bone core, and by replacing the cross section with more simple one yet conserving the areal moment of inertia. As a result, it was possible to reduce the CPU time without compromising the accuracy of the model. In addition, the force-deflection property obtained from the 3-point bending tests for the bone core were compared with the simulation results, and the comparison showed that there was good agreement between the results even with the simplified cross-section of the bone core.

Regarding the resin material characterization for each part, quasi-static and dynamic compression tests were carried out to determine the material property. Because the strain rate dependency of the material for each resin material was observed from these results, the strain rate dependency was incorporated in the material model. Consequently, the results of the quasi-static and dynamic compression tests agreed well with the simulation results, confirming that the force-deflection response of the resin material could be reproduced.

An FE model that accurately reproduced the geometry of the parts based on the Flex-PLI drawing was validated in 3-point lateral bending of the thigh and leg and 4-point lateral bending of the knee joint. It was found that the simulation results for both the thigh, leg and knee joint fell within  $\pm 10\%$  of the test results. This indicates good accuracy of the model as well as validity of the modeling technique.

In the validation of the Flex-PLI assembly model, vehicle impact tests were performed. The kinematics obtained from the tests with the passenger car and the

SUV, which have different front shape, was compared with that of the model. As a result, it was confirmed that the model reproduced the characteristic kinematics of the Flex-PLI due to the difference in the vehicle front shape. Also, the maximum bending moment of the thigh and leg as well as the maximum elongation of the knee cables were compared between the experiment and computer simulation. The results showed that there was quantitative agreement between the experiment and computer simulation. However, in the reproduction of the vehicle impact test, a highly accurate vehicle model is required. Thus, more accurate modeling for the parts in the front of the vehicle as well as improvement in the accuracy of the material model for those parts are issues for future study.

## ACKNOWLEDGMENTS

The authors would like to express their sincere thanks to Mr. Atsuhiko Konosu of the Japan Automobile Research Institute, who developed the Flex-PLI, for his valuable guidance in assembling the Flex-PLI, and for his kind cooperation with the tests carried out during the development of the Flex-PLI model.

## REFERENCES

- [1] 1995. "International road traffic and accident database."
- [2] European enhanced vehicle-safety committee. 1998. "EEVC working group 17 report, Improved test methods to evaluate pedestrian protection afforded by passenger cars."

- [3] Matsui Y. and Sasaki A. etc. 1999. "Impact response and biofidelity of pedestrian legform impactor." IRCOBI.
- [4] Konosu A. and Ishikawa H. etc. 2001. "Reconsideration of injury criteria for pedestrian subsystem legform test - Problem of rigid legform impactor - " 17<sup>th</sup> ESV conference, Paper number 263.
- [5] Takahashi Y. and Kikuchi Y. 2001. "Biofidelity of test devices and validity criteria for evaluating knee injuries to pedestrians." 17<sup>th</sup> ESV conference, Paper number 373.
- [6] Konosu A. and Tanahashi M. 2003. "Development of a biofidelic flexible pedestrian legform impactor." Stapp, Paper number 03S-09.
- [7] Konosu A. and Tanahashi M. 2004. "Development of a biofidelic legform impactor – application in a car-pedestrian subsystem test." SAE, Paper number 04B-22.
- [8] Konosu A. and Tanahashi M. 2005. "Development of a biofidelic flexible pedestrian leg-form impactor (Flex-PLI 2004) and evaluation of its biofidelity at the component level and at the assembly level." SAE, Paper number 05B-161.
- [9] Japan automobile manufacturers association, inc. 2004. "Flex-PLI 2004 plan."
- [10] 2002. "Pam system international, PAM-CRASH<sup>TM</sup> PAM-SAFE<sup>TM</sup> version 2002 notes manual."
- [11] 2002. "Pam system international, PAM-CRASH<sup>TM</sup> PAM-SAFE<sup>TM</sup> version 2002 reference manual."
- [12] 2002. "Pam system international, PAM-GENERIS<sup>TM</sup> for PAM-CRASH<sup>TM</sup> & PAM-SAFE<sup>TM</sup> version 2001.1 reference manual."

## STRUCTURAL HOOD AND HINGE CONCEPTS FOR PEDESTRIAN PROTECTION

**Christoph Kerkeling**

**Joachim Schäfer**

**Dr. Grace-Mary Thompson**

GM Europe – Adam OPEL AG

Germany

Paper Number: 05-0304

### ABSTRACT

Future legislation for pedestrian protection in Europe and Japan considers standardized test methods and test requirements relevant for a type approval. The first phase of legal introduction starts in 2005 and a more stringent second phase will follow in 2010.

This paper consists of three main chapters. The chapter “Requirements” starts with a summary of the pedestrian protection-related requirements for head impact and its conflicting requirements for the vehicle handling and driving.

The second chapter “Hood Concepts” discusses how the hood design could become compatible with the pedestrian protection requirements. Concepts for the hood design fulfilling both, the European as well as the Japanese requirements are described. The impact of the hood design parameters on the head impact performance are shown and different concept solutions are presented.

The third chapter “Hood Hinge Concepts” examines the hinge performance for pedestrian protection in detail. The mounting points of the hood, such as hinges, latches and bumper stops, are the most critical points for head impact. Different hinge concepts and their impact on the head impact performance are shown. The influence of the hinge parameters on the acceleration curves and the HPC values is discussed and conclusions for the hinge design as well as for the vehicle structure are drawn.

### INTRODUCTION

Accident statistics (IRTAD, 2002) [1] show that in Europe about 41.000 fatalities occur in traffic participation. 6.100 (15%) of these are pedestrians and another 3.900 (10%) are cyclists.

For pedestrians the most frequent injuries occur in the head, upper and lower extremities. 62% of all fatalities are caused by head injuries. These head injuries occur when the pedestrian contacts the vehicle or the ground.

To reduce the frequency of pedestrian fatalities and injuries, measures from the automotive industry as well as environmental changes are required.

The European Enhanced Vehicle Safety Committee (EEVC WG 10 and WG 17) has developed test procedures to assess the level of pedestrian protection for vehicle fronts. Based on the EEVC WG 17 report, legal requirements have been derived. The European directive (2003/102/EC) [2] consists of head impact, upper leg impact and lower leg impact. The requirements will be enforced in two phases. The Japanese directive (TRIAS63) [3] consists of head impact only. Globally harmonized requirements are currently discussed by an IHRA working group.

The risk of head injuries is investigated by free-flying head form impacts against the vehicle front. The impact area is defined by reference lines determined at the vehicle front:

- WAD 1000 = wrap around distance 1000mm
- BLE = bonnet leading edge
- BSRL = bonnet side reference line
- BRRL = bonnet rear reference line

The impact area consists of the vehicle hood and its surrounding components such as grille, headlamps, fender, cowl and windscreen. Major changes to these components as well as to its mountings and the structure underneath are required to fulfill the requirements for pedestrian protection.

Concepts for the hood and its mountings have been investigated at OPEL ITDC in advance. Based on these investigations, design guidelines have been established to enable the development of future vehicles fulfilling these requirements.

The new OPEL ZAFIRA II [4] is GM's first car that has been designed to meet the targets for pedestrian protection. Its pedestrian protection concepts are based on the measures presented in this paper.

## REQUIREMENTS

### 1. Legal Requirements

For EU Phase 1 as well as for Japan, the limit for HPC is separated into two different areas:

- bonnet top zone A:  $HPC \leq 1000$
- bonnet top zone B:  $HPC \leq 2000$

In addition, the bonnet top zone A must not exceed one third of the complete bonnet top zone. It is up to the manufacturer to define the locations of bonnet top zone A and B.

#### Europe Phase 1

Just one head form (ISO child head) is applied and will impact the vehicle with an angle of  $50^\circ$  to the ground reference line at a speed of 35 km/h.

**ISO  
Child Head**  
 $v = 35 \text{ km/h}$   
 $m = 3,5 \text{ kg}$   
 $E = 165 \text{ J}$

Limits  
 1/3:  $HPC \leq 2000$   
 2/3:  $HPC \leq 1000$

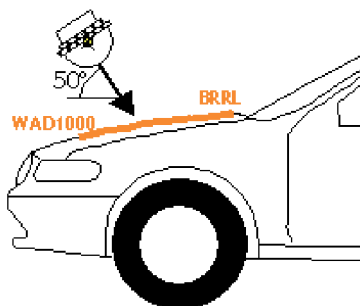


Figure 1: Head Impact EU Phase 1

#### Japan

Two head forms are applied: the ISO child head and the ISO adult head. The intersection for both head forms is located at a wrap around distance of 1700mm (WAD 1700). In comparison to EU Phase 1, the impact speed has been reduced to 32 km/h. The impact angle will be varied depending on the vehicle type (Sedan, SUV, Van).

**ISO  
Child Head**  
 $v = 32 \text{ km/h}$   
 $m = 3,5 \text{ kg}$   
 $E = 138 \text{ J}$

**ISO  
Adult Head**  
 $v = 32 \text{ km/h}$   
 $m = 4,5 \text{ kg}$   
 $E = 178 \text{ J}$

Limits  
 1/3:  $HPC \leq 2000$   
 2/3:  $HPC \leq 1000$

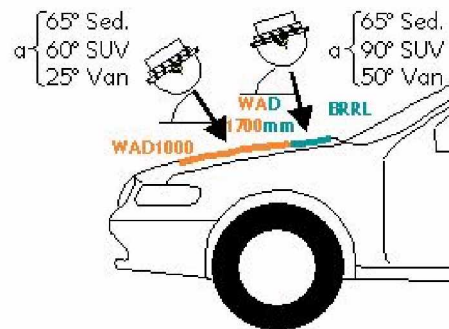


Figure 2: Head Impact Japan

#### Europe Phase 2

In the second phase, two head forms will be considered in Europe as well. Both head forms differ from those used in EU Phase 1 and Japan. The impact angle for the child head form is set at  $50^\circ$  to the ground reference line whereas the impact angle for the adult head form is set at  $65^\circ$ . Both head forms should contact the bonnet top zones at an impact speed of 40 km/h.

**EEVC  
Child Head**  
 $v = 40 \text{ km/h}$   
 $m = 2,5 \text{ kg}$   
 $E = 154 \text{ J}$

**EEVC  
Adult Head**  
 $v = 40 \text{ km/h}$   
 $m = 4,8 \text{ kg}$   
 $E = 296 \text{ J}$

Limit  
 $HPC \leq 1000$

Limit  
 $HPC \leq 1000$

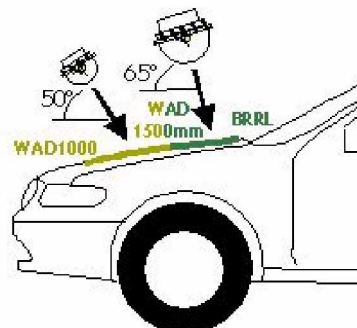


Figure 3: Head Impact EU Phase 2

Currently, the EU Commission is studying the technical feasibility of phase 2 content and alternative vehicle safety measures.

## 2. EuroNCAP Requirements

European consumer (EuroNCAP) [5] tests differ from the legal tests. The head forms used are identical to the head forms used by EU Phase 2. The intersection line is also located at a wrap around distance of 1500mm (WAD 1500). The rear limit of the bonnet top zone is not defined by the BRRL (bonnet rear reference line) but by the wrap around distance 2100mm (WAD 2100).

EEVC Child Head	EEVC Adult Head
v = 40 km/h	v = 40 km/h
m = 2,5 kg	m = 4,8 kg
E = 154 J	E = 296 J

Limit	Limit
HPC ≤ 1000	HPC ≤ 1000
HPC < 1350	HPC < 1350
HPC ≥ 1350	HPC ≥ 1350

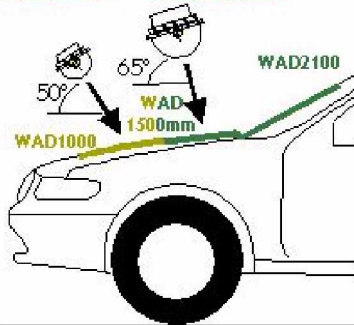


Figure 4: Head Impact EuroNCAP

## 3. Head Impact Performance Criterion

The head form impactors are equipped with a three dimensional accelerometer. From the measured resulting acceleration the HPC (Head Performance Criterion) is calculated as

$$HPC := \max \left\{ \left[ \frac{1}{t_2 - t_1} \int_{t_1}^{t_2} a(t) dt \right]^{2,5} (t_2 - t_1) \right\}$$

The maximal time frame is limited to 15 milliseconds.

For the manufacturer, the optimum head impact is achieved when the HPC target is fulfilled and the impact on the vehicle architecture is as low as possible.

Minimized impact on the vehicle architecture means to provide the necessary energy absorption by the lowest possible deformation space. According to the HPC calculation algorithm the optimal acceleration pulse shows an initial high peak followed by a lower constant level [6].

To achieve the HPC target at a minimum intrusion, the following acceleration characteristic is recommended.

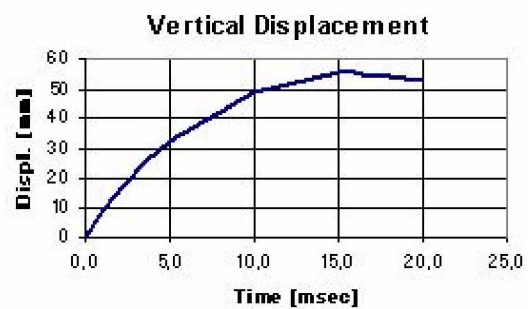
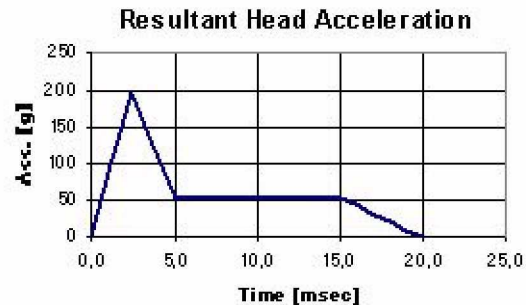


Figure 5: Optimal Acceleration Characteristic (2.5kg head form)

It needs to be noted that real technical designs deviate considerably from this theoretical reference and will require more deformation space.

The above graphs have been generated with a simplified Excel tool [7], which calculates the HPC value and head form intrusion based on the input of the key features for the acceleration.

To keep the HPC below the OPEL in-house target of 800, the initial acceleration peak should not exceed 200g. The later acceleration should remain at a continuous level between 50g and 60g:

- To be outside the HPC time frame
- To reduce the occurring intrusion.



To achieve the above listed targets, two main principles are necessary:

- Provision of sufficient deformation space
- Provision of a low stiffness of the impacted vehicle body parts

The deformation space is a physically necessary enabler, whereas the stiffness is a parameter that needs to be balanced and optimized for each vehicle. Details about the structural measures will be explained in other chapters.

The acceleration of the first few milliseconds is defined by the initial active mass. Therefore the materials, the gages and the number components struck are of major influence. The later acceleration is defined by the stiffness of the structure. The component sizes, their mountings and their design are of increasing influence at this stage.

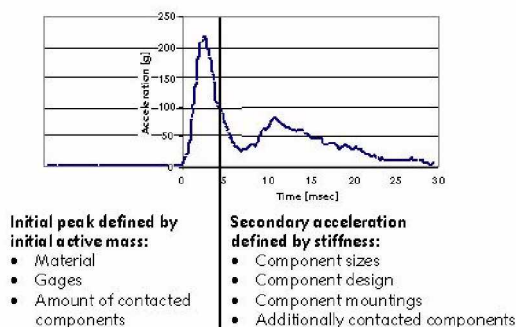


Figure 6: Influence of Mass and Stiffness on the Acceleration

#### 4. Conflicting Vehicle Requirements

With regards to the upcoming targets for pedestrian protection, it is the aim of the vehicle manufacturers to develop future vehicles complying with both sets of targets: the performance targets for the vehicle driving and handling, as well as the new pedestrian protection requirements.

The most important load cases that have to be balanced with the pedestrian protection requirements are listed below:

- Boundaries for vehicle dimension
- Vehicle durability under driving conditions
- Endurance of movable hang-on parts
- Misuse of components and parts
- Performance under handling conditions
- Visual impression
- Acoustical impression

- Tactile impression
- Performance under crash conditions
- Insurance classification

Since the pedestrian impact areas are defined by the outer geometry of the vehicle, the pedestrian protection measures are very styling-dependent. The preferred concepts are those that leave as much design freedom as possible.

### HOOD CONCEPTS

#### 1. Overall Hood Structure

The optimal acceleration characteristic as described in the previous chapter is a theoretical reference value only. In reality, the characteristic varies with the impact location. The following list summarizes the main parameters influencing the acceleration:

- Active mass
- Stiffness
- Clearance to package components
- Impact location (hood center, hood edge)
- Interaction of parts

The active mass varies during the impact. More and more mass has to be accelerated, while the head causes the impacted structure to deform. A deformation front starting at the first point of contact runs in a circular wave to the outer. The active mass increases with the duration of the impact.

The active mass for a head impact at the hood edge will be less than for an impact in the hood center, as long as no other components (fender, hinges, headlamp, etc.) are contacted.

The stiffness of the hood depends on the material, the gages, the gluing and the design of outer panel, inner panel and reinforcements. Other components will add to the overall stiffness when located within the deformation zone.

A certain amount of clearance is necessary to achieve the head impact targets. To simplify the vehicle development process with regards to pedestrian protection OPEL has defined the clearance required for each head form to enable the HPC targets. These design guidelines are considered as general enablers. Sporadic deviations from the defined design guidelines could be accepted but requires an adoption of contacted components (collapsible design and/or reduced mass).

Based on the defined clearances, the required head impact deformation space will be generated below the styling surface. Package components that penetrate the generated deformation space are

considered as critical and need to be relocated or tuned to fulfill the HPC targets.

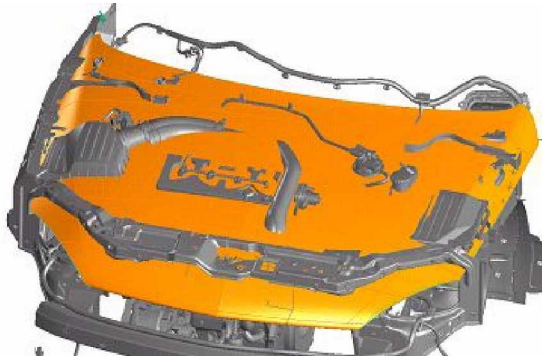


Figure 7: Penetrating Package Components

Interactions with components underneath the hood would result in a secondary acceleration peak. Whether this second acceleration peak is relevant for the HPC value depends on:

- The maximal acceleration value
- The duration
- The relative level to the first acceleration peak to the secondary peak value
- The timing distance between the first and the second acceleration peak

The acceleration characteristic varies with the impact location. A short single peak usually characterizes an impact in the center portion of the hood, as long as no component underneath the hood is contacted. The acceleration of a head impact close to the hood edge usually shows several peaks and a longer HPC relevant time frame, since many additional components (e.g. hinge) have to be deformed during the impact.

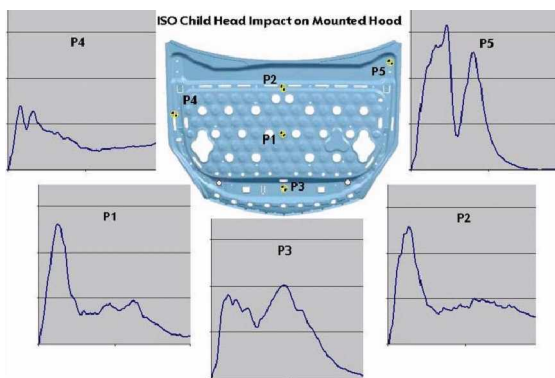


Figure 8: Variation of Acceleration Characteristic

## 2. Hood Inner Design

In the vehicle development before pedestrian protection was necessary, the hood inner was designed to meet the standard load cases as listed in the chapter “Conflicting Vehicle Requirements”. The following summarizes the main load cases derived from these standard requirements that influence the design of the hood inner panel:

- Vehicle durability
- Hood closing endurance
- Hood slam test (misuse)
- Lateral stiffness for mounted hood
- Hood stiffness for bending and torsion
- Denting and buckling
- Hood fluttering
- Manufacturing requirements for drawing
- Manufacturing requirements for single part stiffness
- Hood performance for frontal high speed crash (ODB)
- Hood performance for low speed crash (AZT)
- Hood surface quality

The exact targets for these load cases are laid down in the vehicle manufacturers technical specifications and test procedures.

The hood has to fulfill the HPC target at every single point within the impact area in the bonnet top zone. Traditionally, the hood inner panel is designed with a rib structure supporting the hood outer panel.

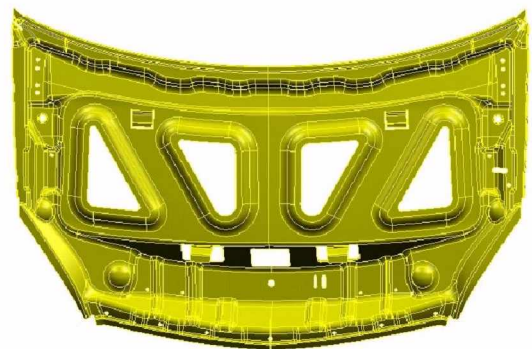


Figure 9: Traditional Hood Inner Design

Such a design usually has weak points and stiff points. For pedestrian protection, it is preferable to design the hood inner panel with a more uniform stiffness distribution. This could be achieved with:

- Increased number of ribs
- Alternative hood inner

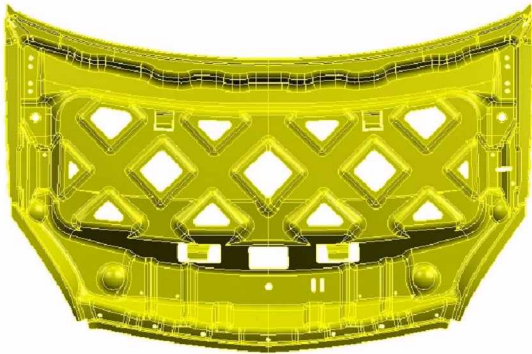


Figure 10: Hood Inner with Increased Number of Ribs

OPEL has adopted a technology from the US GM brands that was originally invented to enable the manufacturing of very thin aluminum inner panels. Multi-cones are drawn into the inner panel instead of a rib structure. These multi-cones are glued to the outer panel.



Figure 11: Hood Inner with Multi Cone Design

This technology has previously been used for weight reasons to design the vehicle hood with particular thin aluminum gages as implemented in the Cadillac Seville.



Figure 12: Cadillac Seville



Figure 13: Cadillac Seville Hood Inner Design

Since there are no ribs and no cutouts, the local stiffness does not vary as much as for a traditional hood inner design. The main advantage of such a continuous stiffness distribution is that it is easier to tune the hood to be stiffer or weaker overall. Less impact positions needs to be investigated.

The hood stiffness can be tuned by various parameters:

- Geometry of cones
  - o Upper and lower diameters
  - o Drawing depth
- Cutouts of cones
- Glue type and amount

The closed structure of the multi-cone inner panel increases the torsion stiffness of the assembled hood. In addition, the stiffness of the single inner panel is increased and enables a reduced inner panel gage. Therefore the active mass as well as the local stiffness is reduced, with benefits for head impact.

The outer frame of the inner panel mainly defines the bending stiffness of the hood and the hood reinforcements at the mounting points for hinges latch and bump stops. This frame structure of the inner panel is therefore kept and the multi-cone design replaces the inner portion of the inner panel only.

### 3. Hood Edges Design

At the hood edges, the active mass of the hood itself is reduced but other components such as the fender and the hood mountings are within the deformation zone. The influence of these components is usually more significant than that of the hood itself. Structural changes are required, such as reduced

section heights for the brace wheelhouse to provide additional deformation space or weak fender mountings.

One way to weaken the side edges of the head impact area (bonnet top zone) is to locate the cut lines between hood and fender at the vertical sides of the vehicle; out of the bonnet top zone

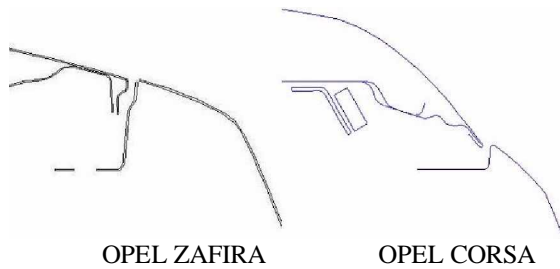


Figure 14: Inlaid Hood versus Wraparound Hood

Such a design with a so-called wraparound hood does not automatically fulfill the head impact targets. Also required is deformation space between the hood flanges and the vehicle structure (brace wheelhouse, A-pillar etc.).

For two reasons, the wraparound hood may not be a preferred design:

- The location of the cut line affects the styling. A wraparound hood design restricts the styling freedom and is not acceptable for all vehicle categories.
- A wraparound hood design increases the overall mass of the hood. Therefore, it is in conflict with the targets for fuel consumption, exhaust emission and driving dynamics (mass distribution).

Another way to weaken the side edges of the bonnet top zone is to design weak fender mountings. The description of this technology is beyond the scope of this paper. Instead the consequences for the design of the hood edges will be discussed.

If the fender mounting provides deformation space, the hood design should enable the use of this space: At the side edges, a vertical flange or a hem flange connects the hood inner and outer panels.

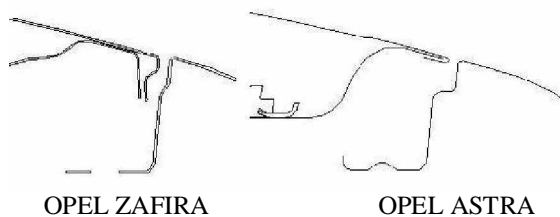


Figure 15: Vertical Flanges versus Hem Flanges

The vertical flange increases the local stiffness more than the hem flange. Shortening the height of the flange could reduce this disadvantage. The height of the flange is restricted by the clinch point diameters. The smaller the clinch point diameter, the lower the necessary flange height. Designing cut outs in the flange might reduce the local stiffness even further.

The main disadvantage of the hem flange is not the increased local stiffness, but the reduction of the deformation space. A head impacting the hood side edge would force the hood to move downwards until the bottom edge of the flange touches a rigid structure underneath. The applied forces would be too low to enable a local buckling of the flange.

Although the hem flange may be preferred from the exclusive pedestrian protection point of view, other requirements may override this to make the vehicle compliant with all requirements. The hood of the new OPEL ZAFIRA II [4] has been designed with a vertical hood flange.

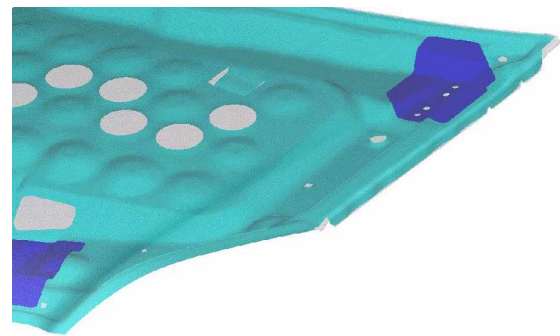


Figure 16: Hood Flange, OPEL ZAFIRA II

For the ZAFIRA II, a vertical flange is necessary for manufacturing reasons. Since the steel gages have been reduced to a minimum of 0.6mm for the outer panel and 0.5mm for the inner panel, the vertical flanges provide the required handling stiffness for the single parts before assembly.

As for many vehicle components, it is always a trade-off between different requirements that leads to the final design.

#### 4. Hood Material

The hood material affects the active mass, as well as the stiffness of the hood and therefore is an important parameter that has to be adjusted to the pedestrian protection requirements.

Around the edges of the hood and the mountings of the hood, it is most important to keep the mass and the stiffness of the hood at the lowest possible level,



since other components will add to the active mass and the overall stiffness that the head form will “see” at an impact.

In the center of the hood, a certain stiffness and mass is required to limit the intrusion and to avoid a secondary impact. Secondary impact means a second acceleration peak, which occurs when the deforming hood touches an engine bay component underneath. Depending on its maximum level and the time gap to the primary acceleration, the secondary impact might increase the resulting HPC value (see chapter “HPC and Acceleration Characteristic”). The larger the hood, the weaker it will become in the center and the more likely a secondary impact becomes. Based on investigations by simulation and physical impact tests, OPEL came to the conclusion that two options will work for an inlaid hood with a sheet metal design:

Option 1= reduced gages for a steel hood

Option 2= aluminum hood

Again, it is a necessary trade-off between pedestrian protection and deformation space on the one hand side and mass, front axle load, fuel consumption and exhaust emissions on the other side, that leads to the final, well-balanced solution for any new vehicle.

## 5. Consequences for EuroNCAP Performance

In all cases, there is a limitation in feasibility to reduce the HPC values at the outer edges below the  $HPC < 1000$  target while also satisfying the basic handling requirements for the vehicle. Therefore it is recommended to locate the less stringent head impact area with the target  $HPC < 2000$  at the left and right outer sixths of the bonnet top zone. Within the  $HPC < 2000$  zone, no points can be gained for the EuroNCAP rating. The EuroNCAP points have to be collected in the inner four sixths. Consequently, the frontal hood mounting points (latch and bump stops) should be located in front of the 1000mm wrap around distance if the vehicle concept allows.

At the 1500mm wrap around distance (WAD 1500), EuroNCAP has impacts with both head forms: the 2.5kg child head as well as the 4.8kg adult head. The more sensitive child head requires a weak hood structure. The impact at the same spot with the heavier adult head (higher energy) causes a larger intrusion. This conflict is even more difficult to be solved in the cowl area.

## HOOD HINGE CONCEPTS

It is obvious that the hood hinges, latches and bump stops are essential to mount the hood to the structure of the vehicle. It might be questionable whether hinges are always necessary, but some mountings are certainly needed.

These mounting points are usually the most difficult to fulfill head impact even for compliance with  $HPC < 2000$ . In this paper, the hinges have been selected as an example to describe the demands of pedestrian protection compliant mountings.

### 1. Vehicle Related Demands

Hood mountings such as the hinges are needed to transfer forces from hood to vehicle and vice versa under handling and driving conditions. The requirements for the hood hinges are again derived from the standard requirements listed in the chapter “Conflicting Vehicle Requirements” and listed below:

- Acceleration forces caused by driving conditions should not result in visible hood movements or material fatigue
- Aerodynamic forces should not result in visible hood fluttering or material fatigue
- Pre-stresses are applied to the hinge in the closed position to eliminate the play in its joints that might cause visible movements and/or rattle noise
- Forces are applied when the hood is pushed into the stop position that prevents the hood from being opened too wide
- Force, applied by somebody leaning against the hood in the open position or leaning on the hood in the closed position, should not cause plastic deformation or damage due to hood contacts with surrounding components as fender etc.
- Hood movement at the hinges in the low speed insurance tests has to be minimized to avoid damage at the hood and the fenders
- The hood should not intrude into the windscreen under high speed frontal crash conditions

The hinges also guide and hold the hood when opened. Their kinematics has to ensure that the hood does not contact other components. For hinges with a single joint, the choice of position is very limited. In many cases, this problem can be overcome by selecting a multi-joint hinge.

## 2. Pedestrian Protection Related Demands

The ideal acceleration as described in chapter “HPC and Acceleration Characteristic”, can usually not be achieved in the areas of the hood mountings. In these areas, the result is more likely to be a longer lasting acceleration, which needs to be kept at a lower constant level.

Most vehicles are designed with the hood hinges located at the left and right rear edges of the hood. A head impact in that area is influenced by many components:

- Hood
  - o Outer panel
  - o Inner panel
  - o Hinge reinforcement
- Hinge
- Fender
- Wiper system
- Cowl

All these components and mountings have to react together in a manner that satisfies the requirements for head impact.

A certain amount of deformation space has to be provided to fulfill the targets for head impact. Therefore, the rigid structure of the vehicle (A-pillar, brace wheelhouse, etc.) needs to be located at a certain minimum distance below the outer styling surface. Additionally, the bottoming-out depth of the deforming components needs to be considered in order to define the required distance from the styling surface to the structure.

Providing deformation space is regarded as an enabler to fulfill the head impact requirements, whereas the relevant target values depend on the mass and the stiffness of the components impacted.

A certain level of stiffness is required to fulfill the handling and driving requirements for the vehicle. These demands are contrary to the required softness for pedestrian protection. Due to these target conflicts, parts of the relaxation zones with the lower target of  $HPC < 2000$  are located at the hinge regions. The total area with  $HPC < 2000$  is limited to one third of the bonnet top zone. The amount of the  $HPC < 2000$  zone that needs to be located in the hinge region depends very much on the styling and the design of the vehicle.

## 3. Possible Concepts

Different design concepts for hinges have been found which provide the deformation space required for head impact.

Single-joint hinges:

- With joints located well outside the impact area
- Designed with deformable parts
- Designed with a collapsing mechanism

Multi-joint hinges:

- Designed with travel space in the vertical direction
- Designed with a collapsing mechanism

A single-joint hinge with its rotation point outside the head impact area could provide the required deformation space when the following additional measures are provided:

- Pivot point located with a sufficient distance to the closest head impact point
- Sufficient deformation space above and below the hood-side hinge part in the head impact zone
- Limited mass added to the active mass by the hood-side hinge part

The larger the distance of the hood-side hinge mounting to the pivot point becomes, the stiffer the hinge has to be designed. However, that is contrary to the wish of a limited hinge mass and needs to be balanced.

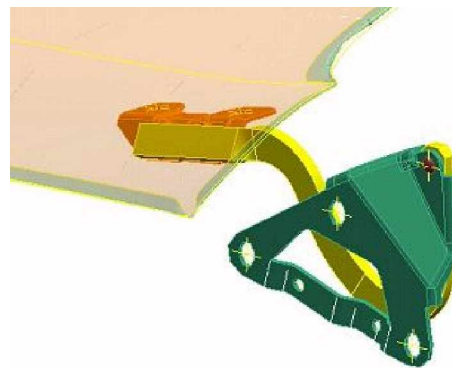


Figure 17: OPEL CORSA Hood Hinge

The current OPEL CORSA is an example of how the turning point could be located well outside the head impact deformation zone. This hinge concept provides an inertia and stiffness, which would be non-compliant.

A single-joint hinge with deformable parts could also be compliant with the head impact requirements. Its advantage is the possibility of keeping the pivot point within the head impact zone. Its disadvantage is the constant reaction force caused by the plastic



deformation of the hinge parts during the head impact.



Figure 18: OPEL ZAFIRA II Hood Hinge

The new OPEL ZAFIRA II is equipped with a deformable single-joint hinge, which complies with the EU Phase 1 requirements. Its design is described in the paper PEDESTRIAN-FRIENDLY OPEL ZAFIRA II [4].

A third possibility to design a single-joint hinge, which does comply with the pedestrian protection requirements, could be offered by a collapsible mechanism.

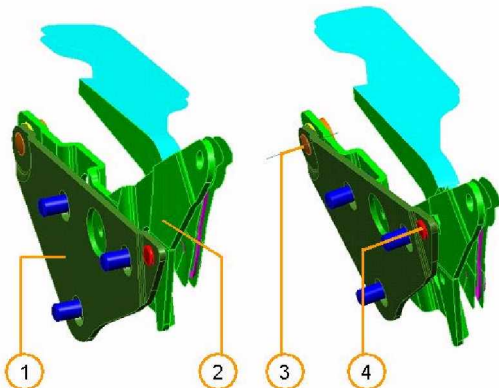


Figure 19: Collapsible Single Joint Hinge

The collapsing mechanism consists of two body-side parts (• +, ) that are combined by a pivot point  $\mathcal{F}$  and a shear pin „ . The load transmitted by the impacting head would cause a failure of the shear pin. Due to the relative rotation of the two body-side hinge parts, the required deformation space would be provided.

The failure of the shear point as well as the location of the pivot points need to be balanced for each new vehicle.

A multi-joint hinge usually consists of a body-side part and a hood-side part, both connected by two levers.

Depending on the arrangement of the levers in the closed hood position, the multi-joint hinge could provide deformation space for the head impact. The levers needed to be designed in such a way that they deform in the lateral direction to give way in the vertical direction under head impact loading.

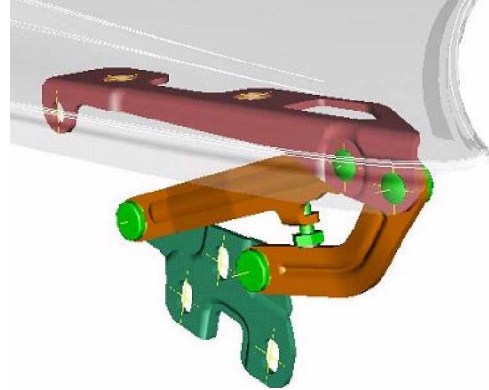


Figure 20: Multi-Joint Hinge

Such a multi-joint hinge could be located within the impact area of the head form and usually offers less resistance to the head impact than the deformable single-joint hinge. Its increased spatial requirement is a disadvantage.

If the flexibility of the multi-joint hinge itself is not sufficient, adding a collapsing mechanism could increase it. Separating one of the two hinge levers into two levers (• +, ) connected by an additional turning point  $\mathcal{F}$  and a shear pin „ could provide increased deformation space. A failure of the shear pin under head impact forces would add another degree of freedom to the kinematics of the hinge. In this way, an additional travel in the vertical direction could be provided.

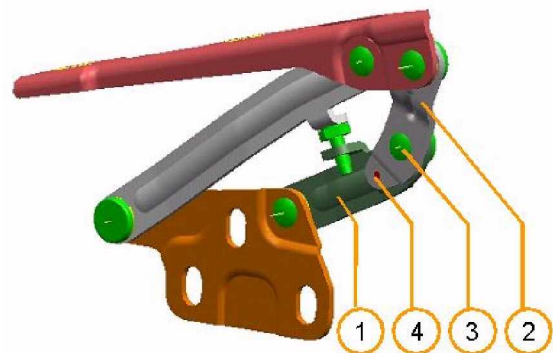


Figure 21: Collapsible Multi-Joint Hinge

The failure of the shear pin could be adjusted to the requirements for head impact, but needs to be balanced with the vehicle handling and driving requirements. Unfortunately, the larger number of parts will increase the complexity of the mechanism.

It needs to be noted, that all solutions were just able to deliver an acceptable margin for compliance with EU phase one requirements (HPC<2000, 35km/h impact speed and the given impact direction).

## CONCLUSION

This paper summarizes the concepts for vehicle hoods and hood hinges that have been developed by OPEL to fulfill the upcoming requirements for pedestrian protection. In addition, the basic theory of how to optimize the vehicle with regard to head impact is discussed. Since the measures for pedestrian protection are contrary to many other vehicle handling and driving requirements, it is obviously a challenge for the automotive industry to develop future vehicles in a sufficient balance. Many of the former valid vehicle targets for stiffness and performance will have to be modified with the focus on pedestrian protection.

Since the pedestrian protection performance of a vehicle is very styling and design dependent, the concepts presented need to be adjusted for each new vehicle and cannot be regarded as settled off-the-shelf technology to make a vehicle pedestrian protection compliant.

It is obvious that the necessary measures affect the architecture of a vehicle. Therefore, the targets have to be fixed at the very beginning of the vehicle development process and need considerable pre-development time. It would not be possible to implement pedestrian protection measures at a late stage or even within a minor facelift.

Pedestrian protection requirements cause tremendous additional workload within the vehicle development particularly for styling, design, simulation and the testing departments.

The concepts presented were developed in advance of any vehicle-related activities. The new OPEL ZAFIRA II is GM's first pedestrian protection compliant vehicle that has been developed based on the concepts shown. It has successfully been designed to meet the EU Phase 1 requirements.



Figure 22: OPEL ZAFIRA II

## REFERENCES

- [1] OECD International Road Traffic and Accident Database (IRTAD), 2002
- [2] Directive 2003/102/EC of the European Parliament and of the Council, 17<sup>th</sup> November 2003
- [3] Japanese Directive TRIAS63-2004
- [4] Pedestrian Measures for the Opel Zafira II, Wanke T. et al., 19<sup>th</sup> ESV Conference, 2005
- [5] EuroNCAP, Pedestrian Testing Protocol, Version 4.1, March 2004
- [6] Concept of Hood Design for Possible Reduction in Pedestrian Head Injury, Okamoto Y. et al., 14<sup>th</sup> ESV Conference, 1994
- [7] Dual Asymmetrical Triangle Pulse Generator, C.S. Cheng et al., GM R&D, Version 1.2, 2001

## DISCLAIMER

This presentation is solely provided for the purpose of scientific discussion of the main tasks and concepts in order to implement national and international legal requirements related to pedestrian protection efforts in automotive engineering. This presentation explicitly does not cover all and any engineering and design issues around Pedestrian Protection efforts; it is not to be construed to being an engineering manual, to provide any specific or ultimate solution nor to represent a certain engineering decision by Adam Opel AG., its subsidiaries and affiliates and / or any reasons for such decisions.

# AN INVESTIGATION OF THE POTENTIAL SAFETY BENEFITS OF VEHICLE BACKUP PROXIMITY SENSORS

**Viliam Glazduri**

Transport Canada

Canada

Paper Number 05-0408

## ABSTRACT

An increasing number of new vehicles are being equipped with backup proximity sensors. These sensors detect the presence and proximity of objects in the pathway of the reversing vehicle and warn the driver through an audible signal. This report investigates the performance capabilities and potential safety effectiveness of these systems in reducing the risks to small children and other pedestrians from reversing vehicles. These sensor systems are primarily designed and marketed as parking aids. However, some are being promoted as safety systems with the potential to reduce or prevent collisions with pedestrians, especially small children. The performance capabilities of six commercial reversing aid systems were evaluated in laboratory tests. Four systems were fitted to the vehicles as standard equipment. Two systems were purchased from aftermarket companies and installed on the test vehicles. All six systems used ultrasonic sensor technology. Laboratory tests consisted of 3-dimensional mapping of the detection zones, the system response time, and the effects of dust / dirt on sensor performance. In terms of detection area performance, parking aid systems sacrificed detection distance and height in order to suppress false or nuisance alarms. The durability and reaction time results revealed there were no substantial performance differences between the systems. The safety benefits of these devices were then estimated based on these test results.

## INTRODUCTION

There are approximately 900 (Transport Canada<sup>1</sup>) pedestrians struck and injured by reversing vehicles each year in Canada. However, this is likely an underestimate as this figure only represents those pedestrians struck in traffic situations. It does not account for pedestrians

injured or killed in private driveways or parking lots for example. Therefore, the exact number of pedestrians injured or killed in Canada is not known but studies in other jurisdictions have highlighted this problem. An Australian study by Henderson<sup>2</sup> found an average of 12 fatalities per year during the study period 1996-1999. The study also found that most of these non-traffic collisions involved toddlers. Among the recommendations made by Henderson was to investigate the potential of rear proximity sensors in detecting the presence of nearby children.

This paper reports on the performance of backup proximity sensor systems. The purpose was not to set out performance criteria but rather to investigate the capabilities of commercially available systems and to assess their potential effectiveness in reducing pedestrian collisions. The main performance parameters to be evaluated were:

- size and shape of the detection zones, with clean and dusty sensors
- lower detection zones height, with clean and dusty sensors
- sensor system's response time, with clean and dusty sensors

All six systems tested were commercially available. They are listed in Table 1. Four were installed as original vehicle equipment (OEM) and the two were aftermarket units designed to fit all types of passenger vehicles. The OEM systems had 4 sensors embedded into the bumper facias. One aftermarket system had single sensor (E) and the other had three sensors (F). The same vehicle was used to test the two aftermarket sensors.

**Table 1.**  
**Proximity sensor systems tested**

Sensor ID	Vehicle Type	Vehicle Length (m)
A (OEM)	Minivan	1.946
B (OEM)	Convertible	1.777
C (OEM)	Sedan	1.739
D (OEM)	Pickup	2.029
E (Aftermarket)	SUV	2.002
F (Aftermarket)	SUV	2.002

## PERFORMANCE TEST PROCEDURES

The performance tests were conducted in a laboratory. The ultrasonic sensors did not require relative motion between the vehicle and the test object. The engines needed to be kept running in order for the systems to operate but vehicles were stationary during the tests and with reverse gear activated the sensors.

### Detection Zones

The detection zones were mapped on a 3.60 m x 3.60 m test surface. The test surface was divided into grids. Each cell was 15 cm x 15 cm in size. The test object was a 9 cm diameter and 100 cm tall PVC tube (Figure 1).



**Figure 1.**  
**Detection zone test surface and test object.**

With the vehicle stationary, the test cylinder was moved manually and placed in each cell. Once a continuous detection signal from the system was

received, the cell was marked corresponding to the frequency of the signal.



**Figure 2.**  
**Grid cell markings**

In addition to the 100 cm test tube, tubes of different heights, ranging from 5 to 95 cm, in 5 cm increments, were used to map the bottom edge of the detection zone.



**Figure 4.**  
**Tubes used to map lower edge of detection zone**

### Response Time

The time delay between the appearance of the test object in the detection zone and the initiation of the audio signal was recorded on a chart recorder that was connected to an optical sensor and a microphone. The 100 cm test cylinder was suspended from above the detection zone just behind the rear bumper. The top of the detection zone was marked with the optical sensor. As the cylinder entered the top of the detection zone it triggered the optical sensor. The reaction time of the sensor system was the difference between this event and the audible signal given by the sensor. This test was repeated ten times for each system.

The response time was taken as the average of the 10 runs.



**Figure 5.**  
**Response time test set up**

### Dust Application

The detection zone area mapping and system response time were measured first with clean sensors and then with the sensors covered with a mixture of dust and water. The application and composition of the dust and water mixture used followed the Canadian Motor Vehicle Safety Standard 104 – *Windshield Wiping and Washing System* test procedure<sup>3</sup>.

## PERFORMANCE TEST RESULTS

### Detection Zone

The detection zone dimensions, in the horizontal plane, are shown in Table 2. The maximum detection distances from the rear of the bumper ranged from 1.05 m (system B) to 2.25 m (system E). Aftermarket system E displayed the largest detection zone size in the horizontal plane.

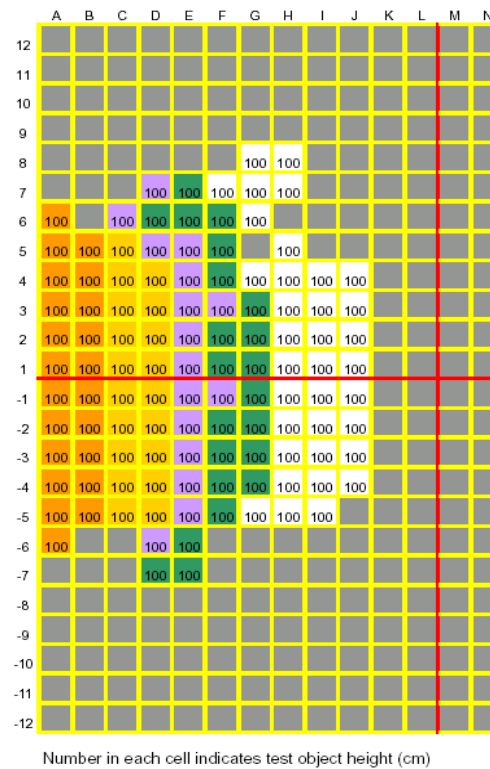
**Table 2.**  
**Detection zone dimensions in the horizontal plane**

Sensor System	Total Area (m <sup>2</sup> )	Width (m)	Depth (m)
A	3.42	2.55	1.80
B	1.53	1.80	1.05
C	2.57	2.25	1.50
D	3.38	2.70	1.80
E	5.72	3.30	2.25
F	2.07	2.40	1.20

The measured detection zone patterns for each system are set out in Appendix A. Figure 6 shows an example of a mapped detection zone in the horizontal plane using the 100 cm tall test cylinder. The number in the cell represents the height of the test object used for detection. The vehicle would have been situation on the left side with the bumper aligned with first column.

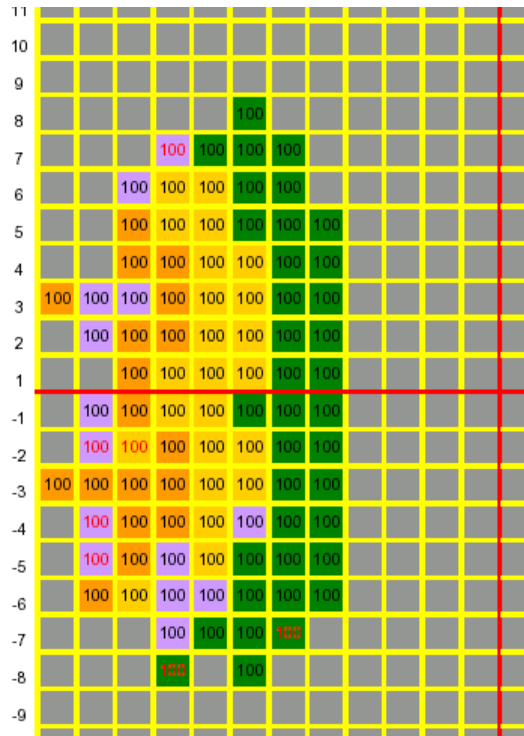
The detection zones patterns displayed two basic shapes. Systems A and D had an hourglass shape with a narrower width near the centre. The other systems had more of a teardrop shape with a gradually increasing width towards the rear.

All systems had audible signals with distinct levels of warning corresponding to distance of the test object from the rear bumper. The number of detection warning levels ranged from 3 to 5. The total frequency range of the intermittent audible warnings was 3 to 8 Hertz. The audible warning was a continuous beep for the zone closest to the bumper for all systems. System E had a 3-level led display in addition to the audible warnings.



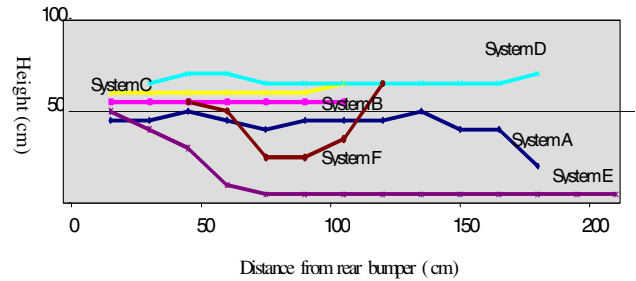
**Figure 6.**  
**Mapped horizontal detection zone using 100 cm tall test cylinder (system C)**

All sensor systems except system C had a least one cell in the row nearest to the rear bumper (row A) where there was no detection of the test object – so-called “dead spots”. System F was able to detect the 100 cm tall test cylinder in only two cells in this row (Figure 7).



**Figure 7.**  
**Mapped detection zone showing “dead cells” near bumper edge. (System F)**

Figure 8 shows a plot of the bottom edge of the detection zones measured along the central longitudinal axis. The sensors did not detect the area below the lines. All the profiles began at bumper height. System D was from a pickup truck, which had a high bumper height. The OEM systems tended to remain at bumper height level right to the end except system A, which dipped toward the ground near the end of its detection distance. The profiles of the two aftermarket systems exhibited different shapes. System E displayed the lowest cut-off. The bottom edge of the detection zone was very close to the ground at 75 cm behind the bumper. System F’s profile dipped towards the rear but then went up again at the very end of the detection zone.



**Figure 8.**  
**Average height of the lower edge of detection zones**

### Response Time

The recorded response times are listed in Table 4. These results were the averages of 10 drop tests. The times ranged from 80 milliseconds for system A to 227 milliseconds for system D. All systems displayed response times that were within the ISO recommended limit for low-speed sensor systems<sup>4</sup> of 350 milliseconds.

**Table 3.**  
**System response time results**

Sensor System	Response Time (ms)
A	80
B	187
C	135
D	227
E	199
F	105

### Dusty Sensors

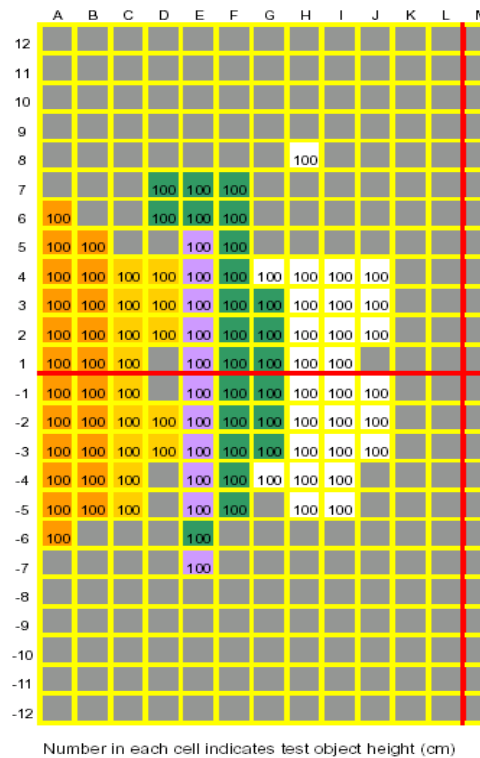
Table 4 shows the changes in sensor performance with the sensors covered with the dust and water mixture. There was no large reduction in the detection zones for any of the sensors. There was no significant change in the width of the detection zones in the horizontal plane. The maximum detection distance increased slightly for all of the systems except system C, which had a 9% reduction. The reaction times increased for all systems. The maximum increase was 25% (system A). However, all of the reaction times were still within the ISO accepted level of 350 ms.



**Table 4.**  
**Change in sensor performance with dirt application**

Sensor System	Width (%)	Depth (%)	Reaction Time (%)
A	0	5	25
B	0	1	11
C	0	1	3
D	0	-9	3
E	0	17	13
F	0	3	15

The dust application did cause some minor performance reductions that are worth mentioning. The detection zone levels were less clearly defined. That is, the stages were more dispersed with one another with one row having more than one detection level present. There were also some loss of detection in one case (system D), there was two lower priority level signals given in the row closest to the bumper – where a continuous high level signal was given with clean sensors.



**Figure 9.**  
**Mapped horizontal detection zone using 100 cm tall test cylinder with dusty sensors (system C)**

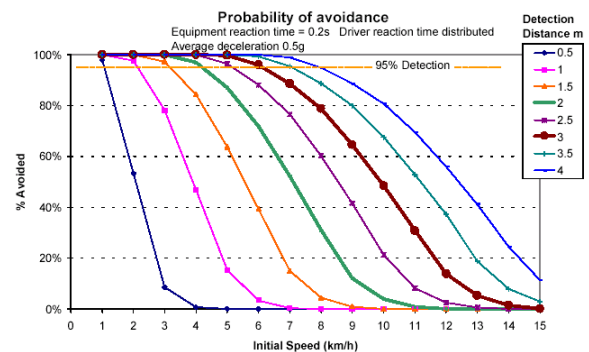
## DISCUSSION

### General Performance

The six sensor systems evaluated used similar technologies and it was not surprising then to discover that their performance was also quite similar. The performance of system E stood out the most from the others. System E displayed a larger detection zone area - in terms of both width and length - and the bottom edge of the zone started much closer to the ground.

### Estimates of Potential Effectiveness

The systems must warn the driver of the presence of a pedestrian behind the vehicle quickly enough so that the driver has enough time to react and stop the vehicle before it strikes the pedestrian. The effectiveness of these systems is dependent on a number of vehicle and human factors. NHTSA (Harpster et al<sup>5</sup>) conducted studies of driver reaction times to acoustic signals during backing maneuvers. In this experiment the drivers were alerted to the fact that an alarm would be sounded. The authors reasoned that these 'alert' driver reaction times were suitable for backing maneuvers since it is a brief maneuver and drivers would be more cautious relative to driving forward. Williams<sup>6</sup> used this data to determine the probability of avoiding a collision when a vehicle is moving at a constant speed. Paine and Henderson<sup>7</sup> calculated the percentage of collisions that would be avoided for a range of collision speeds and sensor detection distances. These are illustrated in Figure 10.



**Figure 10.**  
**Percentage of collisions avoided as derived by Paine and Henderson<sup>7</sup> for various vehicle speeds and detection distances**

Figure 10 shows that effectiveness is highly sensitive to vehicle speed. For example, a 1 km/h increase in vehicle speed can reduce the effectiveness by as much as 20%.

Applying the same analysis to the maximum detection distance and response time results obtained for the systems tested yielded the following estimates. The maximum speeds at which the systems achieve 25%, 50% and 95% avoidance levels are tabulated below.

**Table 5.**  
**Maximum vehicle speeds for 25%, 50% and 95% collision avoidance levels**

<b>Sensor System</b>	<b>25% Avoided</b>	<b>50 % Avoided</b>	<b>95% Avoided</b>
A	8 km/h	7 km/h	4 km/h
B	5 km/h	4 km/h	3 km/h
C	8 km/h	6 km/h	4 km/h
D	8 km/h	7 km/h	4 km/h
E	9/km/h	8 km/h	4 km/h
F	6 km/h	5 km/h	3 km/h

At the 50% level, the maximum vehicle speed possible ranges from 5 km/h (system B) to 9 km/h (system E). At vehicle speeds greater than 10 km/h, none of the systems tested would be very effective under ideal conditions.

At the 50% avoided level, the maximum vehicle speed ranged between 4 km/h and 8 km/h. At the 95% level there was no significant difference in maximum speeds. None of the systems would be 95% effective above a speed of 4 km/h.

Eberhard et al<sup>8</sup> estimated that 90% of backing collisions involving pedestrians were at a speed of 8 km/h or more. This would suggest that the systems would be less than 25% effective in these types of collisions due to their short detection distance capabilities.

Paine and Henderson concluded that a 4 m detection distance would be most appropriate for a vehicle traveling at 8 km/h (95% avoidance).

The above estimates are based on theoretical estimates under ideal conditions. However, there are other factors that will have an effect on the sensor system's effectiveness in preventing

collisions. For example, it is assumed that once a warning is given the vehicle driver will always react to it immediately. However, there may be scenarios such as the one raised by Huey<sup>9</sup> – where “a driver may see a vehicle eight feet behind him but not be aware that there is a child only two feet behind. The driver could receive a warning but misinterpret it to be related to the more distant object”.

Another aspect to consider is the detection height. In the analysis it is assumed that the object behind the vehicle has sufficient height so that the bottom of the sensor detection zone does not pass over it. Five of the six sensor systems tested had a minimum detection zone heights ranging from 45 to 65 cm. Sensor system E had a detection zone very close to ground level for most of its depth. Paine and Henderson recommended a minimum detection height of 60 cm in their analysis. They reasoned that the driver would have visual contact of a standing child of this height through the rear window. They also recognized that there would be some instances where a detection height of 60 cm may be insufficient (such as a child crawling or bending down) and detection would not be possible but reasoned that this was a fair trade-off against nuisance alarms. Indeed, it is very likely that sensor system E would display more false alarms than the other systems for objects close to the ground such as curbs. Nevertheless, this trade-off detection zone height still leaves the potential for the above scenario to exist thereby further reducing real world effectiveness of these sensor systems.

Overall, it would be safe to assume that the real world effectiveness of the systems would be even lower than that estimated by theoretical analysis.

## CONCLUSIONS

All of the six sensor systems tested displayed reliable performance characteristics. Their performance did not decrease significantly even with the sensors covered with dust.

However, their effectiveness in preventing pedestrian strikes appears to be low due primarily to their limited detection distances. Since most of these systems were primarily designed as parking aids they have relatively short detection distances. Even under ideal conditions, their effectiveness is limited to vehicle speeds that are likely lower than those at

which most pedestrian collision occur. The sensor systems under evaluation are unlikely to provide significant collision reduction in most situations where a reversing vehicle strikes a pedestrian.

There are other sensor technologies which could provide enough detection distance capability to be effective at higher vehicle speeds and could be worth investigating. Microwave-based sensors are capable of greater detection distances than ultrasonic sensors. However, they are also susceptible to giving false detections. Video cameras for aid in reversing are currently being made available on some vehicles as standard equipment. With the cost of video systems steadily decreasing they could become the basis of a viable countermeasure. Paine and Henderson<sup>7</sup> tested a prototype combination video camera and short-range proximity sensor with some success.

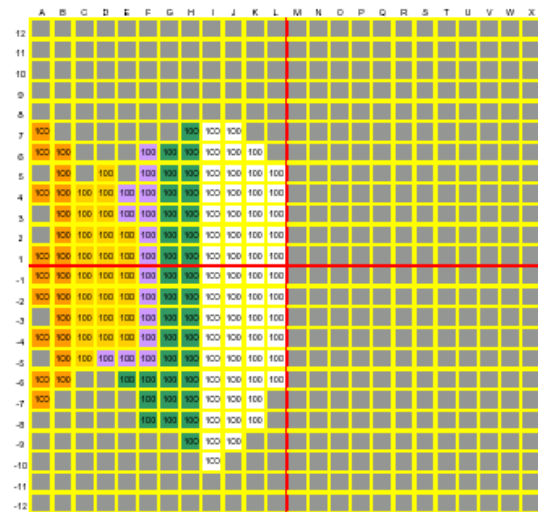
More research is needed into the causes of pedestrian collisions to more accurately determine the potential effectiveness of any type of collision avoidance system. Present Canadian national data does not provide sufficient collision detail such as vehicle speed, pedestrian action, and other human, vehicular and environmental factors to evaluate possible countermeasures thoroughly. Most studies into backing up collisions have focused only on small children. Collisions with other older and larger pedestrians may have very different dynamics. In-depth collision investigations targeting all pedestrians injured or killed of collisions could provide adequate data.

## REFERENCES

- [1] Transport Canada. 2004. "Pedestrian Fatalities and Injuries 1992-2001." Fact Sheet TP 2436E, RS-2004-01E (<http://www.tc.gc.ca/roadsafety/menu.htm>)
- [2] Henderson, M. 2000. "Child Deaths and Injuries in Driveways." Prepared for the Motor Accidents Authority of NSW Australia, October 2000.
- [3] Transport Canada, 1995. "Test Procedure for: Canadian Motor Vehicle Safety Standard No. 104: Windshield Washing and Wiping Systems." Transport Canada Reference Laboratory, January 1995.
- [4] International Organization for Standardization, 2002. "Transport information and control systems – Maneuvering Aids for Low Speed Operation (MALSO) – Performance requirements and test procedures." Draft ISO/DIS 17386
- [5] Harpster J., Huey R., Lerner N., and Steinberg G. 1996 "Backup Warning Signals: Driver Perception and Response." National Highway Safety Administration, DOT HS 808 536, August 1996.
- [6] Williams H. 1999 "Microwave Motion Sensors for Off-Road Vehicle Velocity Data and Collision Avoidance." Sensors Magazine, December 1999.
- [7] Paine M., Henderson M., 2001 "Devices to Reduce The Risk to Young Pedestrians from Reversing Vehicles.", Motor Accidents Authority of NSW Australia, March 2001.
- [8] Eberhard C., Moffa P., Young S and Allen R., 1995, "Development of Performance Specifications for Collision Avoidance Systems for Lane Change, Merging and Backing, Development of Preliminary Performance Spec., NHTSA, DOT HS 808 430, September 1995.
- [9] Huey R., Harpster J. and Lerner N., 1996, "Summary Report on In-Vehicle Crash Avoidance Warning Systems: Human Factors Considerations, NHTSA, DOT HS 808 531, September 2001.

## APPENDIX A –DETECTION ZONE PATTERNS IN THE HORIZONTAL PLANE

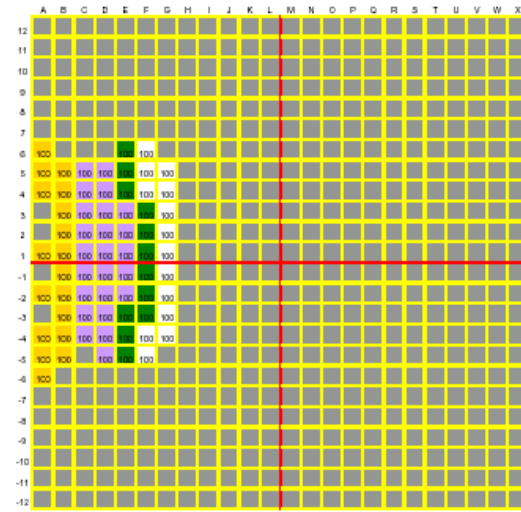
Test Number I - Detection zones with clean sensors Date 2003.10.23  
 Test obstacle GRAY PVC TUBE Height (cm) 100 Width (cm) 9  
 Detection system make/model OEM Test Location: Front ☐ Rear ☒  
 1st detection zone: Visual None audible intermittent color ☐ 2-3 Hz  
 2nd detection zone: Visual None audible intermittent color ☒ 3-4 Hz  
 3rd detection zone: Visual None audible intermittent color ☒ 4-5 Hz  
 4th detection zone: Visual None audible intermittent color ☒ 5-8 Hz  
 5th detection zone: Visual None audible continuous color ☒ DC



Number in each cell indicates test object height (cm)

### Sensor System A

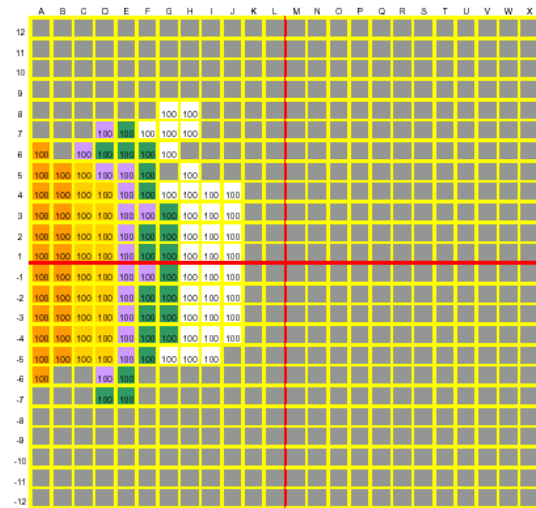
Test Number I - Detection zones with clean sensors Date 2003.11.19  
 Test obstacle GRAY PVC TUBE Height (cm) 100 Width (cm) 9  
 Detection system make/model OEM Test Location: Front ☐ Rear ☒  
 1st detection zone: Visual None audible intermittent color ☐ 3-4 Hz  
 2nd detection zone: Visual None audible intermittent color ☒ 4-5 Hz  
 3rd detection zone: Visual None audible intermittent color ☒ 5-8 Hz  
 4th detection zone: Visual None audible continuous color ☒ DC



Number in each cell indicates test object height (cm)

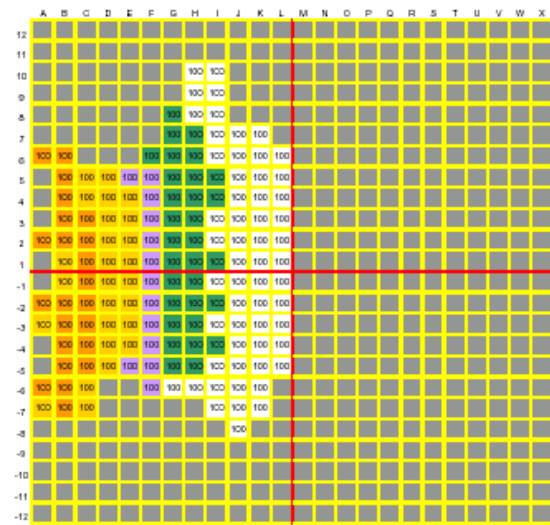
### Sensor System B

Test Number I - Detection zones with clean sensors Date 2004-01-14  
 Test obstacle GRAY PVC TUBE Height (cm) 100 Width (cm) 9  
 Detection system make/model OEM Test Location: Front ☐ Rear ☒  
 1st detection zone: Visual None audible intermittent color ☐ 2-3 Hz  
 2nd detection zone: Visual None audible intermittent color ☒ 3-4 Hz  
 3rd detection zone: Visual None audible intermittent color ☒ 4-5 Hz  
 4th detection zone: Visual None audible intermittent color ☒ 5-8 Hz  
 5th detection zone: Visual None audible continuous color ☒ DC






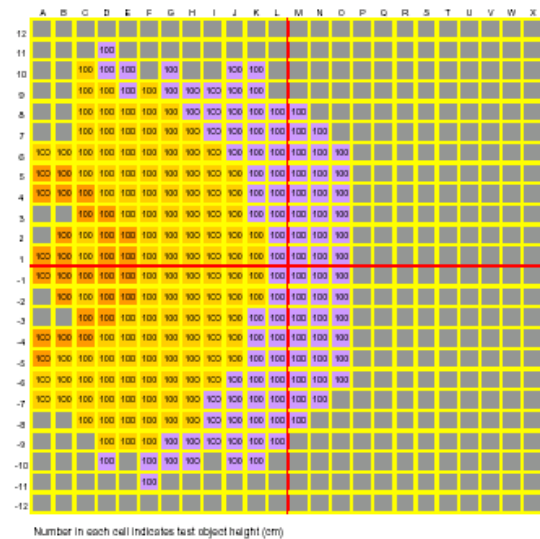
## System C

Test Number I - Detection zones with clean sensors Date 2004-02-03  
 Test obstacle GRAY PVC TUBE Height (cm) 100 Width (cm) 9  
 Detection system make/model OEM Test Location: Front ☐ Rear ☒  
 1st detection zone: Visual None audible intermittent color ☐ 2-3 Hz  
 2nd detection zone: Visual None audible intermittent color ☒ 3-4 Hz  
 3rd detection zone: Visual None audible intermittent color ☒ 4-5 Hz  
 4th detection zone: Visual None audible intermittent color ☒ 5-8 Hz  
 5th detection zone: Visual None audible continuous color ☒ DC







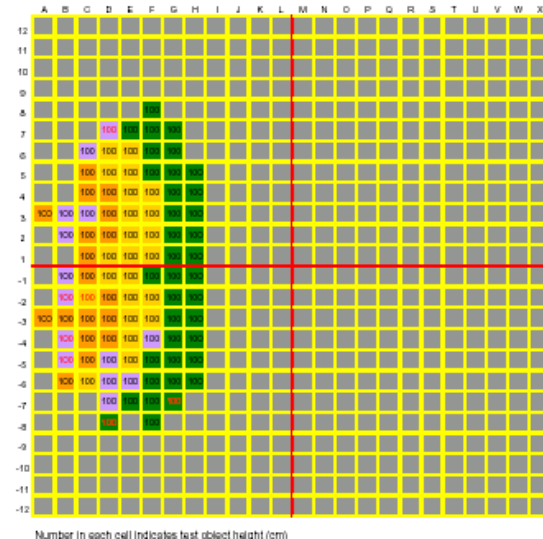
## System D

Test Number 1 - Detection zones with clean sensor Date 2003.12.15  
 Test obstacle GRAY PVC TUBE Height (cm) 100 Width (cm) 9  
 Detection system make/model C-Back Test Location: Front ☐ Rear ☒  
 1st detection zone: Visual 1 led audible intermittent color   
 2nd detection zone: Visual 2 leds audible intermittent color   
 3rd detection zone: Visual 3 leds audible continuous color 



System E

Test Number 1 - Detection zones with clean sensors Date 2003.12.08  
 Test obstacle GRAY PVC TUBE Height (cm) 100 Width (cm) 9  
 Detection system make/model SafeReverse Test Location: Front ☐ Rear ☒  
 1st detection zone: Visual None audible intermittent color  3 Hz  
 2nd detection zone: Visual None audible intermittent color  5 Hz  
 3rd detection zone: Visual None audible intermittent color  7.5 Hz  
 4th detection zone: Visual None audible continuous color  DC



System F



# VEHICLE PERFORMANCE CHARACTERISTICS AND SEAT BELT EFFECTIVENESS IN LOW SPEED VEHICLES AND GOLF CARS

**Timothy J. Long**

Collision Research and Analysis

**Thomas F. Fugger, Jr.**

**Bryan Randles**

Accident Research and Biomechanics, Inc.

United States

Paper Number 05-0431

## ABSTRACT

Low Speed Vehicle (LSV) use on public roads is currently experiencing a tremendous increase in usage in the United States. There currently exists a debate concerning the impact these vehicles will have on our roadways and the occupant injury exposure resulting from their usage. Of particular controversy are the potential safety benefits and trade offs associated with the use of seat belts in LSV's and golf cars.

In an effort to create uniform safety guidelines for these vehicles the United States National Highway Traffic Safety Administration (NHTSA) has created a new category of "Low Speed Vehicle" (LSV) to regulate small, 4-wheeled motor vehicles, other than a truck, with top speeds of 20 to 25 miles per hour. Any vehicle capable of exceeding 25 mph would fall under the Federal Motor Vehicle Safety Standards for passenger cars. LSV's, which include modified personal neighborhood vehicle (PNV), neighborhood electric vehicles (NEV) and golf cars, having a maximum speed greater than 20 mph, but not greater than 25 mph, fall under the Federal Motor Vehicle Safety Standard No. 500 (49 CFR 571.500). At present, golf cars with a maximum speed of less than 20 mph are not required to comply with the LSV standard but are still subject to state and local regulation.

Vehicle dynamic and occupant kinematics studies conducted by the authors indicate that golf cars moving at speeds as low as 11 mph are capable of rapidly producing the lateral accelerations necessary to quickly eject an unbelted occupant even with the hip restraints provided by most golf car manufacturers. The testing included a variety of LSV's and golf cars ranging from a typical golf car

with a top speed of 11 mph to an advanced LSV capable of reaching a top speed of 25 mph. In all cases the unbelted occupants were ejected in J-turn maneuvers while the belted occupants remained in the original seat. This study demonstrates that the safety benefits of seat belts in these vehicles are significant and should be required as safety devices when operated on roadways.

## INTRODUCTION

The usage of LSV's and golf cars on public roadways is currently experiencing a rapid growth. The phenomena started in the early 1990's in various resort and retirement communities across the United States. The city of Palm Desert, California was a pioneer in recognizing the rising use of LSV's and golf cars on their public roadway and the potential safety problems it could present to its citizens. In 1993 the city took the initiative to pass minimum safety requirements for the use of LSV's and golf cars on their roadways. Some of the vehicle safety requirements included front and rear turn signal indicator lights, headlights, rear lights, brake lights, mirrors, red reflectors and safety belts. The requirement for safety belts was controversial due to the fact that almost all of the golf cars available did not have safety belts as original equipment and it was the position of the National Golf Car Manufacturers Association (NGCMA), which represents the original equipment manufacturers of 95% of all golf cars manufactured and distributed in the United States, that seat belts are more of a safety detriment to the occupant than beneficial. It was the position of the NGCMA that a vehicle without a rollover protection system (ROPS) required that the occupants have the ability to jump from a moving car during a rollover event. The city of Palm Desert nevertheless went

forward with and maintained the seat belt requirement.

In 1997 NHTSA proposed a new category of motor vehicle be established called “Low Speed Vehicle”(LSV) [1]. Initially it was proposed that an LSV would be any vehicle, other than a motorcycle, whose top speed does not exceed 25 mph. The new class of vehicles would be equipped with certain basic items of motor vehicle safety equipment, including seat belts, in lieu of complying with the Federal motor vehicle safety and bumper standards that would apply if the vehicles were categorized as passenger vehicles. NHTSA indicated at this time that it did not intend to regulate “golf carts” that have a top speed of less than 15 mph and are used to carry golfers on golf courses, though “golf cars” that are used to carry golfers on golf courses and that had a top speed that exceeds 15 mph but not 25 mph would be a motor vehicle. The agency had concluded that a golf cart with a maximum speed that does not exceed 15 mph is a vehicle that is not primarily manufactured for use on public roads and is therefore is not a motor vehicle. The agency went on to state “that if a golf cart manufacturer decides to increase the maximum speed capability of its golf carts to above 15 mph in response to the decision in some states to increase their speed thresholds in their definitions of “golf carts” and to allow such vehicles to operate on certain public roads, it seems evident to NHTSA that such a manufacturer intends its vehicles to be used on public roads as well on golf courses” [1]. NHTSA was faced with the dilemma of attempting to avoid the regulation of “golf carts” whose sole use was for carrying golfers on golf courses and anticipating their eventual use of public roadways due to the increasing number of state and local laws specifically anticipating their use. It was decided at that time that NHTSA would create a new Federal motor vehicle safety standard called Standard No. 100 Low Speed Vehicles and that the proposed speed bracket for this class of vehicles would be between 15 and 25 mph. Among other requirements a seat belt of Type 1 or Type 2 would be required.

Subsequent to NHTSA’s proposed rulemaking a final rulemaking was made changing the standard to FMVSS 500 and with a significant change in the lower speed threshold from 15 to 20 mph. This change of the speed threshold was made due to a representation by the NGCMA. It was the understanding of NHTSA at the time of proposed rulemaking that an appropriate dividing line between golf cars manufactured for golf course use and those manufactured for both on-road use and golf course use was 15 mph. Subsequent to NHTSA’s proposed

rulemaking NGCMA informed NHTSA that 1% of Club Car’s fleet cars (golf cars designed solely for use on golf courses and sold to golf courses) and 75% of their personal cars (cars designed for use on golf courses and public roads) have a top speed of over 15 mph. Based on this new information NHTSA decided a better dividing line between vehicles designed for use on the golf course and vehicles designed for on road use was a minimum top speed of 20 mph. Subsequent to this decision NGCMA notified NHTSA the information regarding Club Cars was incorrect and that, in fact, Club Car does not design any fleet cars (golf cars designed solely for use on golf courses and sold to golf courses) to travel over 15 mph, nevertheless NHTSA left the final bracket at 20 to 25 mph.

The decision as to whether or not seat belts should be required was investigated by NHTSA during this rulemaking. NHTSA decided to examine the city of Palm Desert’s Golf Cart Transportation Plan. This transportation plan included the requirement of safety belts and this requirement appeared to not have any negative impact with regard to occupant safety over the years since its implementation. However, it was noted by NHTSA during its proposed rulemaking that the NGCMA viewed the seat belt requirement as “antithetical to the personal safety of drivers and occupants of golf cars” [2] and cited ANSI/NGCMA Z 130.1-1993 [3] which required a ROPS for any golf car containing seat belts. NGCMA also commented that seat belts enhance the risk of injury or even death if the occupant is restrained in the vehicle by a seat belt assembly upon rollover. NGCMA went on to explain golf cars are equipped with a standard hip or hand hold restraint located towards the outside of the seat. This restraint, according to NGCMA, does not prevent the occupant from jumping or leaping out of the golf car to avoid injury if the golf car is about to rollover. For this reason, in lieu of seat belt requirement for golf cars, the NGCMA believes a hand hold or hip restraint should be required as set forth in ANSI/NGCMA Z 130.1. NHTSA also investigated golf car injury statistics found in the Consumer Product Safety Commission’s National Electronic Injury Surveillance System (NEISS).

In its final ruling NHTSA concluded that “the conjecture by some commenters that it would be valuable to be able to jump out of an LSV are unsubstantiated speculation that is especially unpersuasive given the volume of data showing that ejection is extremely dangerous and that seat belts are remarkably effective at preventing ejection” [2]. The agency concluded that it is desirable to require seat belts in LSV’s.

NHTSA emphasized in its ruling that it has not decided or implied that vehicles with a top speed of less than 20 mph should not be subject to any safety regulation by state or local authorities. Moreover, since the agency is not treating those vehicles as passenger motor vehicles, its standard setting activities cannot pre-empt any state or local regulation. State and local jurisdictions may continue to adopt such equipment requirements as they deem appropriate for vehicles, including golf cars, with a maximum speed of 20 mph or less.

Thus, with NHTSA's final ruling it left the local communities to decide what safety devices it would require for golf cars with a top speed of less than 20 mph. A significant portion of the golf cars currently on the road today were previously leased through golf courses and subsequently turned over to dealerships for sale and rent to the general public. These relatively inexpensive vehicles are seeing a surge in demand as the popularity of golf cars on public roadways increases. The current situation has left local communities with a dilemma on how to regulate these golf cars. On one hand the NGCMA has notified them that they would not endorse the use of seat belts on their golf cars and yet parents are wondering how to put their children in the golf cars. Furthermore, some authorized golf car dealerships in California are proceeding to install seat belts in golf cars with a top speed of less than 15 mph even though the NGCMA recommend against it.

Research into the hip restraint effectiveness found standard on most golf cars today appears to be non-existent as does research into the safety benefits and potential detrimental effects of seat belts in golf cars. Current existing standards such as the ANSI/NGCMA Z 103.1-1993 [3] and the SAE Surface Vehicle "J" 2358 Standard [4] appear to be almost identical with both standards not recommending belts for golf cars with a top speed of under 20 mph. With this recommendation though is the statement "that the person operating the vehicle be qualified and trained in the proper operation of the vehicle" [4]. For general public use, however, expecting that the "operator be qualified and trained in the proper operation of the vehicle" doesn't seem to be appropriate nor realistic. The basis for the determination of not recommending seat belts for golf cars with a top speed of less than 20 mph cannot be determined.

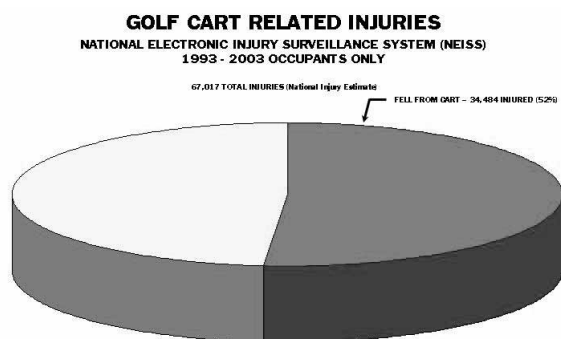
## BACKGROUND

Literature and research searches conducted by the authors revealed a dearth of information regarding golf car and LSV performance and restraint effectiveness. In fact, fewer than four papers were located concerning golf car related injuries. This is consistent with the findings completed by NHTSA. One paper, authored by Passaro et al, [5] is the most complete investigation into injuries associated with golf car use on public roadways. The paper's research was conducted in the North Carolina community of Bald Head Island and included interviews with the injured parties in an effort to ascertain the specific circumstances of each event and to ensure the injury was related to occupants involved in the usage of golf cars as transportation. The golf cars involved in the reported accidents involved the four-passenger type and none had seat belts. The mean top speed for the cars was reported to be 14 mph with two having a top speed of 18 mph. Twenty-two occupants were included in the case series. It was determined from the investigations that of the twenty-two people in the case series fifty-nine percent (59%) were injured following being ejected from a moving car and all reported injured parties were passengers. Children 10 years of age and younger were involved in thirty-two percent (32%) of the cases. It was also reported that fifty-nine percent (59%) of the injuries were sustained to the head or face and ranged in severity from scalp laceration to skull fracture. The conclusions of this study recommended installation of appropriate occupant restraints should be seriously considered.

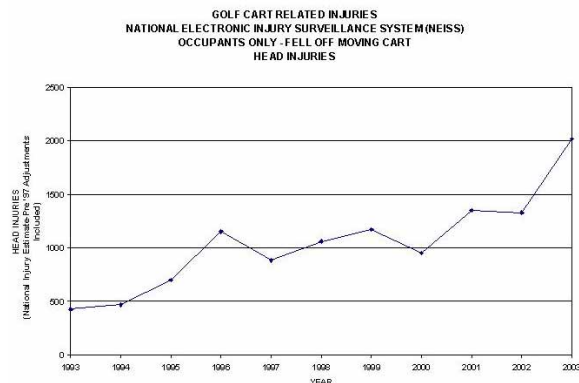
The only vehicle dynamics testing found in literature was testing completed by NHTSA in their report titled "Inspection and Testing of Low Speed Vehicles"[6]. The vehicles evaluated were the Bombardier and GEM neighborhood electric vehicles and a Yamaha gasoline powered golf car. The tests conducted included 1) measurement of the c.g. and static stability factor (SSF) for each vehicle, 2) measurement of lateral stability in a constant 50 foot radius turn, and 3) straight line braking on both a high coefficient surface and low coefficient surface. The reported SSF's for the unloaded Bombardier, GEM and Yamaha were reported to be 1.4, 1.0 and 1.3 respectively. The reported SSF's in the loaded condition for the Bombardier, GEM and Yamaha were found to be 1.2, 0.86 and 0.88 respectively. The study concluded that an LSV with a static stability factor below 1.0 with two occupants could probably tip easily in a tight turn at 20 mph. The 50 foot turning radius reported relative stability for the Bombardier and relative instability for the Yamaha,

though it should be noted the throttle linkage was adjusted on the Yamaha to achieve 20 mph during the testing. The stability on the GEM at 20 mph could not be determined.

Injury statistics for golf cars can be found through the Consumer Product Safety Commission's National Electronic Injury Surveillance System (NEISS). The system allows a search for injuries involving various product codes and one of the codes available is "golf carts". NEISS is a probability sample of hospitals in the U.S. and its territories that have at least six beds and an emergency department. Patient information is collected nightly from each NEISS hospital for every patient treated in the emergency department for an injury associated with consumer products. National estimates are made of the total number of product related injuries treated in U.S. hospital emergency departments based on the NEISS data collected from these hospitals. Each incident contains a brief description of the event and circumstance surrounding the injury producing event. The authors have obtained and filtered the data for the years 1993-2003 for occupants contained in a golf cart. The summary of reported injuries for golf cart occupants can be seen in Figure 1. As seen in Figure 1, there were 67,017 total estimated injuries for occupants riding in a golf cart over this time period. Of this total 52% were due to occupants falling from a moving cart. Examining the data regarding the injuries to those occupants that fell from the moving cart (34,484 occupants) indicated that approximately 35% of those individuals (11,976) sustained head injuries over this time period. This data also indicates a steady increase in the estimated number of head injuries occurring each year, as shown in Figure 2.



**Figure 1 – NEIS data for golf car occupants, 1993-2003**



**Figure 2 – NEISS data for occupants sustaining a head injury**

## TEST PROCEDURES

Four vehicles were obtained for testing, three of the vehicles can be categorized as golf cars (top speed less than 20 mph) and one can be categorized as a Low Speed Vehicle (LSV – top speed less than 25 mph). Each vehicle would be run through a series of tests as follows:

1. Acceleration test with driver only (both directions on track)
2. J-Turn test (straight approach followed by a counter-clockwise steering maneuver) with a belted driver and dummy passenger in a belted and unbelted condition.
3. In-line brake tests with a belted driver and dummy passenger in a belted and unbelted condition.

The test vehicles are depicted in Figures 3 through 6. The vehicles have designated seating positions for two or four occupants and all came equipped with either lap belts (Type 1) or lap/shoulder seat belts (Type 2) as original equipment or had been installed by the dealership. The dummy utilized in the series of test is a 50<sup>th</sup> percentile Alderson dummy.

Two methods of collecting performance data for the tests were employed. A triaxial array of accelerometers (IC Sensors 3031-050) was affixed to the vehicle's approximate static center of gravity. The accelerometers attached to the test vehicles were gain adjusted for a  $\pm 10$  g range. All accelerometer data were collected following the general theory of SAE Recommended Practice: Instrumentation for Impact Test - J211/1 Mar95. The axis systems were in accordance with SAE J1733 Information Report with the positive X, Y and Z axes forward, rightward

and downward, respectively. All accelerometer data were collected at 1000 Hz and filtered using a SAE Class 60 filter (TDAS Pro, Diversified Technical Systems, Inc., Seal Beach, CA). In addition to accelerometer data, vehicle performance data were measured using a GPS-based system (VBOX, Racelogic Ltd., Buckingham, England). Three-dimensional speed and positional data were collected at 100 Hz.



**Figure 3 – Test vehicle 1, 2002 Ford Think**



**Figure 4 – Test vehicle 2, 2003 Club Car**



**Figure 5 – Test vehicle 3, 1998 EZGO golf car**



**Figure 6 – Test vehicle 4, 2000 EZGO golf car**

## TEST RESULTS

Vehicle test results from the GPS-based VBOX system can be found in Table 1. The results include top speed, peak acceleration and acceleration to peak velocity. The peak acceleration for this data is the average of the sustained peak acceleration and not a single peak acceleration value. The acceleration to peak velocity is the average acceleration from the

initiation of movement until the peak velocity was attained.

**Table 1.**

### VBOX Acceleration Test Results

Cart	Test	Top Speed (mph)	Peak Acceleration (g)	Acceleration to Peak Velocity (g)
1T	1_1	12.47	0.15	0.08
	1_2	12.77	0.16	0.10
1D	1_3	24.10	0.26	0.08
	1_4	24.20	0.27	0.07
2	2_1	16.60	0.19	0.07
	2_2	dl	dl	dl
3	3_1	11.50	0.23	0.05
	3_2	12.88	0.37	0.04
4	4_1	14.30	0.26	0.11
	4_2	14.50	0.28	0.12
	4_3	14.50	0.27	0.13
	4_4	14.40	0.30	0.13

Accelerometer data for all the tests can be found in Tables 2 through 4. Table 2 shows the peak accelerations for the top speed tests. Table 3 presents the average peak sustained lateral acceleration attained when completing the J-turn maneuver. The J-turn tests resulted in an average peak lateral acceleration of approximately 0.7 g's with a turning radius of approximately 14'. In each of the unbelted occupant tests the passenger dummy was ejected over the hip restraint and onto the ground whereas each of the belted occupant tests resulted in the occupant remaining within the confines of the passenger's seat. The resulting occupant kinematics from each test is located in Appendix A. The results of braking tests for each LSV and golf car are shown in Table 4. The values in Table 4 represent the average peak deceleration values. In braking test 1\_7 the unbelted passenger dummy came out of the seat and struck it's head on the windshield header, as seen in Figure 7.



**Figure 7 – Dummy occupant head strike on windshield header**

**Table 2.****TDAS Acceleration/Top Speed Results**

Cart	Test	Peak Acceleration (g)
1T	1_1	0.20
	1_2	0.19
1D	1_3	0.31
	1_4	0.31
2	2_1	0.23
	2_2	0.24
3	3_1	0.33
	3_2	0.42
4	4_1	0.30
	4_2	0.33
	4_3	0.33
	4_4	0.33

**Table 3****TDAS J-Turn Lateral Acceleration Tests**

Cart	Test	Average Peak Lateral Acceleration (g)
1	1_5	0.67
	1_6	0.70
2	2_3	0.67
	2_4	0.64
3	3_3	0.63
	3_4	0.56
4	4_5	0.74
	4_6	0.65

**Table 4****TDAS Braking Results**

Cart	Test	Average Peak Deceleration (g)
1	1_7	0.88
	1_8	0.87
2	2_5	0.53
	2_6	0.52
3	3_5	0.54
	3_6	0.47
4	4_7	0.46
	4_8	0.44

## CONCLUSIONS

The research contained in this paper provides a part of the critical data required for agencies (both national and state) and local communities to make informed decisions regarding their LSV/golf car transportation plans. Previous decisions in some communities relied on simply anecdotal evidence and testimony.

The data from the testing supports the implementation of rules and regulations requiring seat belts in LSV's and golf cars which are to be utilized on roadways by the general public, regardless of whether or not their top speed is less than 20 mph. The potential for ejection is significantly higher for an unbelted occupant during a cornering maneuver as opposed to a rollover event, even for vehicles with a maximum speed of only 11 mph. The potential for a rollover event decreases at the lower speeds, thereby significantly decreasing the theoretically detrimental effects that a belted could present over an unbelted occupant. The theory that an occupant is better off jumping from a moving cart on a roadway is simply speculation and fails to consider, among other factors, the age and health of the occupants. Observations made from the J-turn tests demonstrate how ineffective the hip restraints become to an unbelted occupant due in part to the forward migration of the occupant resulting from the longitudinal accelerations occurring during the turns. The high slip angle on the front wheels not only produce high lateral accelerations but also significant longitudinal accelerations. During this forward migration the high lateral accelerations tend to pull the occupant up and over the hip restraint which acts as tripping mechanism. This trip orients the ejected occupant into a head first dive into the ground as shown in Figures 8 and 9. The ejection process

**Figure 8 – Ejected occupant kinematics resulting from the J-turn maneuver during test 1\_5**





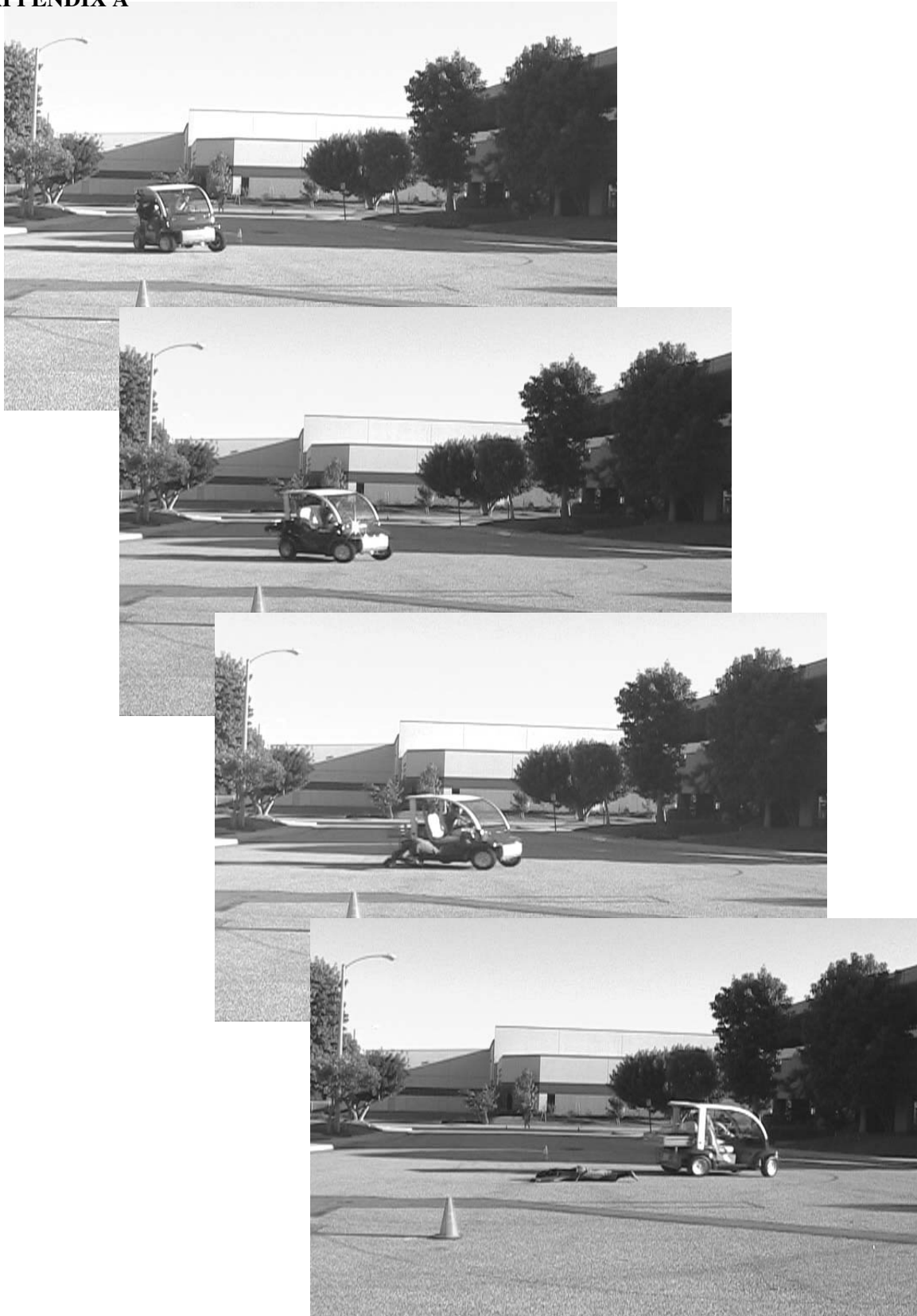
**Figure 9 – Ejected occupant kinematics resulting from the J-turn maneuver during test 4\_5**

occurred rapidly with the time from initiation of the turn to the ejected occupant contacting the ground averaging between approximately one and two seconds. Thus, an unanticipated turn presents little time for an occupant to brace themselves prior to ejection. Additionally, in the case of vehicles that have rear facing seating positions, the exposure to an unanticipated turn and therefore ejection is significantly increased. It should be noted that during the J-turn steer inputs the driver of the vehicle noted little difficulty controlling the vehicle during the entire duration of the turn. It should be also be noted that the lower speed vehicles have a significantly lower tendency to roll over and in fact if the vehicle did roll the energy dissipated getting the vehicle to the roll position would likely only produce a  $\frac{1}{4}$  roll. This scenario would limit the protection offered by a ROPS. Furthermore, a rollover event presents a scenario in which an occupant is likely to be injured, potentially seriously, regardless of whether they are belted or not belted in the vehicle. The theory that injuries will be mitigated by allowing the occupants to jump from a moving LSV or golf car during a rollover, thereby justifying the lack of belts, cannot be supported by this research.

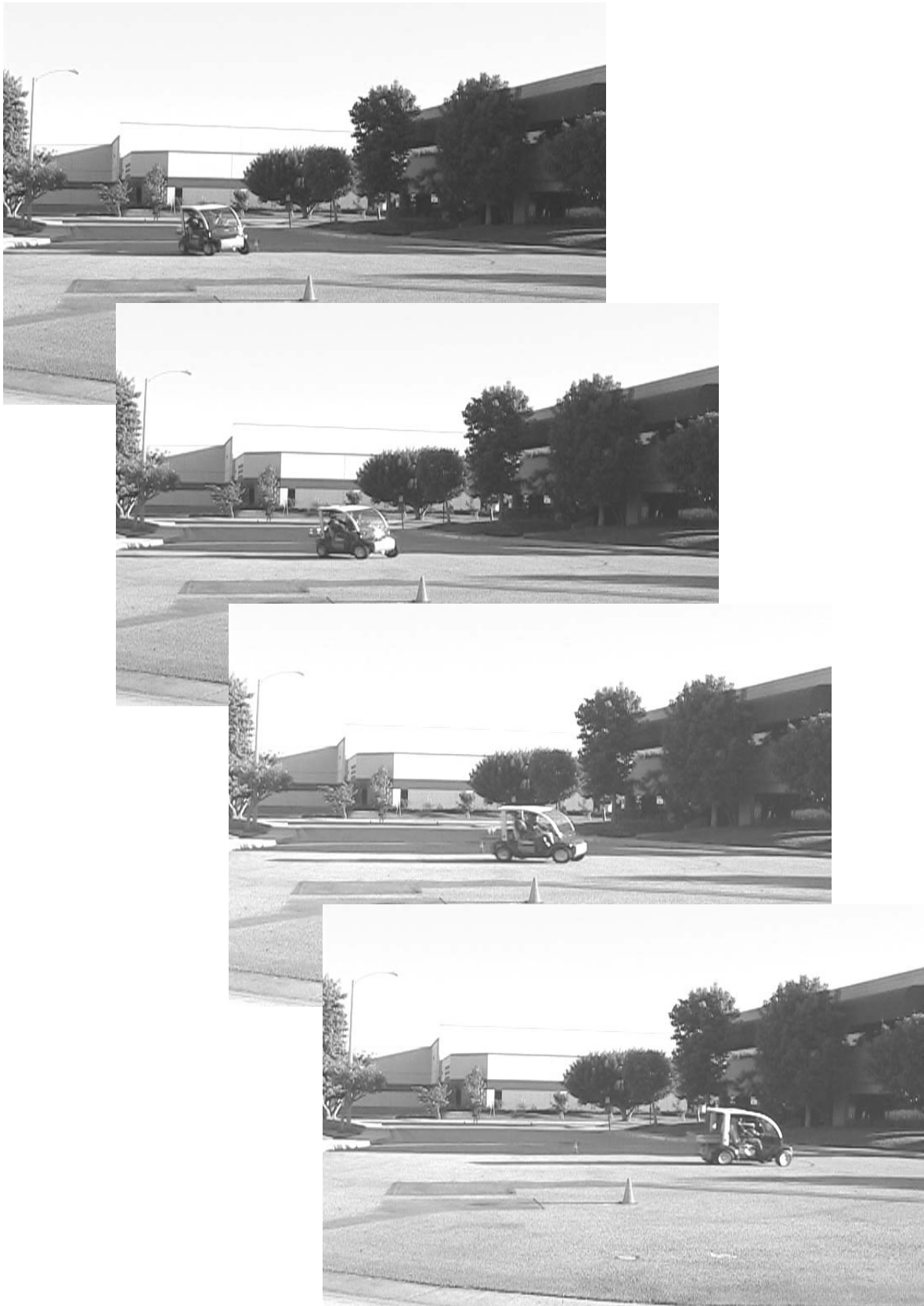
## REFERENCES

- [1] National Highway Traffic Administration, 49 CFR Part 571, Docket No. 96-65; Notice 2.
- [2] National Highway Traffic Administration, 49 CFR Part 571, Docket No. 98-3949
- [3] ANSI/NGCMA Z130.1-1993, "American National Standard for Golf Cars – Safety and Performance Requirements"
- [4] SAE J2358, 2002-03, "Surface Vehicle Standard – Low Speed Vehicles"
- [5] Passoro K., Cole T., Morris P., Mathews D., MacKenzie W., 1996. "Golf Cart Related Injuries in a North Carolina Island Community, 1992-4", Injury Prevention
- [6] Elias J., 1998. "Inspection and Testing of Low Speed Vehicles" NHTSA Report No. VRTC-83-0461.

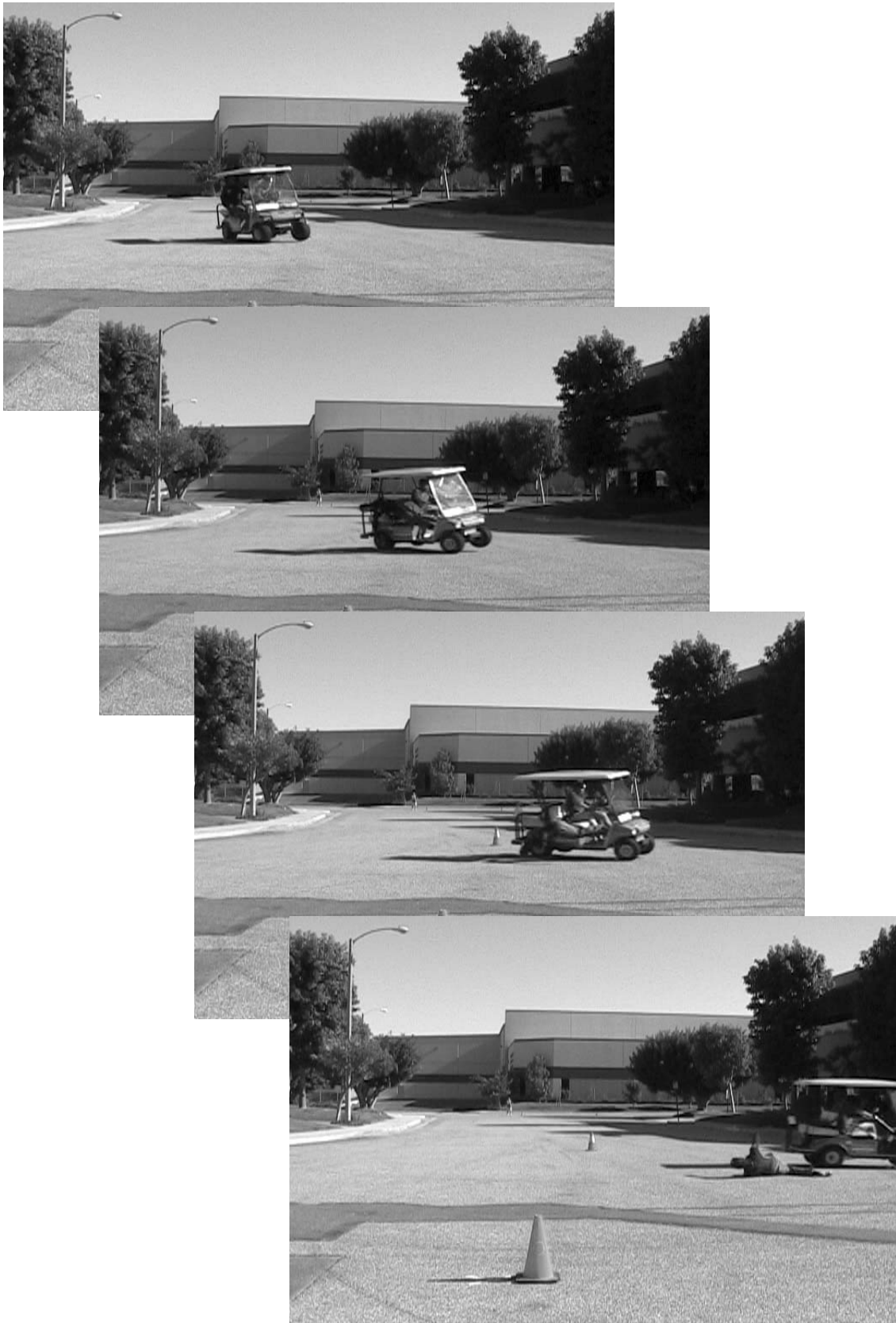
## APPENDIX A



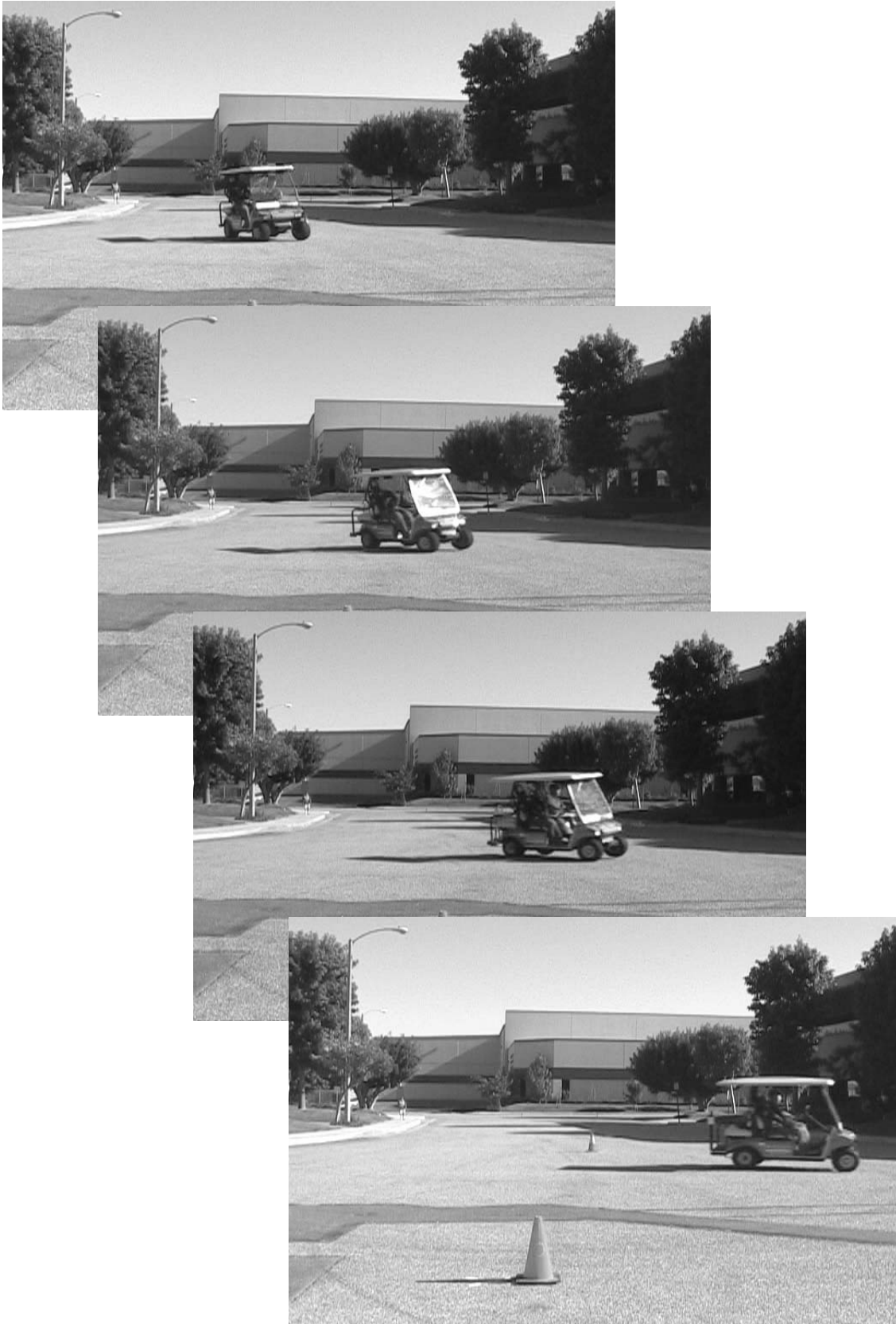
**Figure A1 – Test 1\_5 ejection of unbelted occupant during J-Turn maneuver**



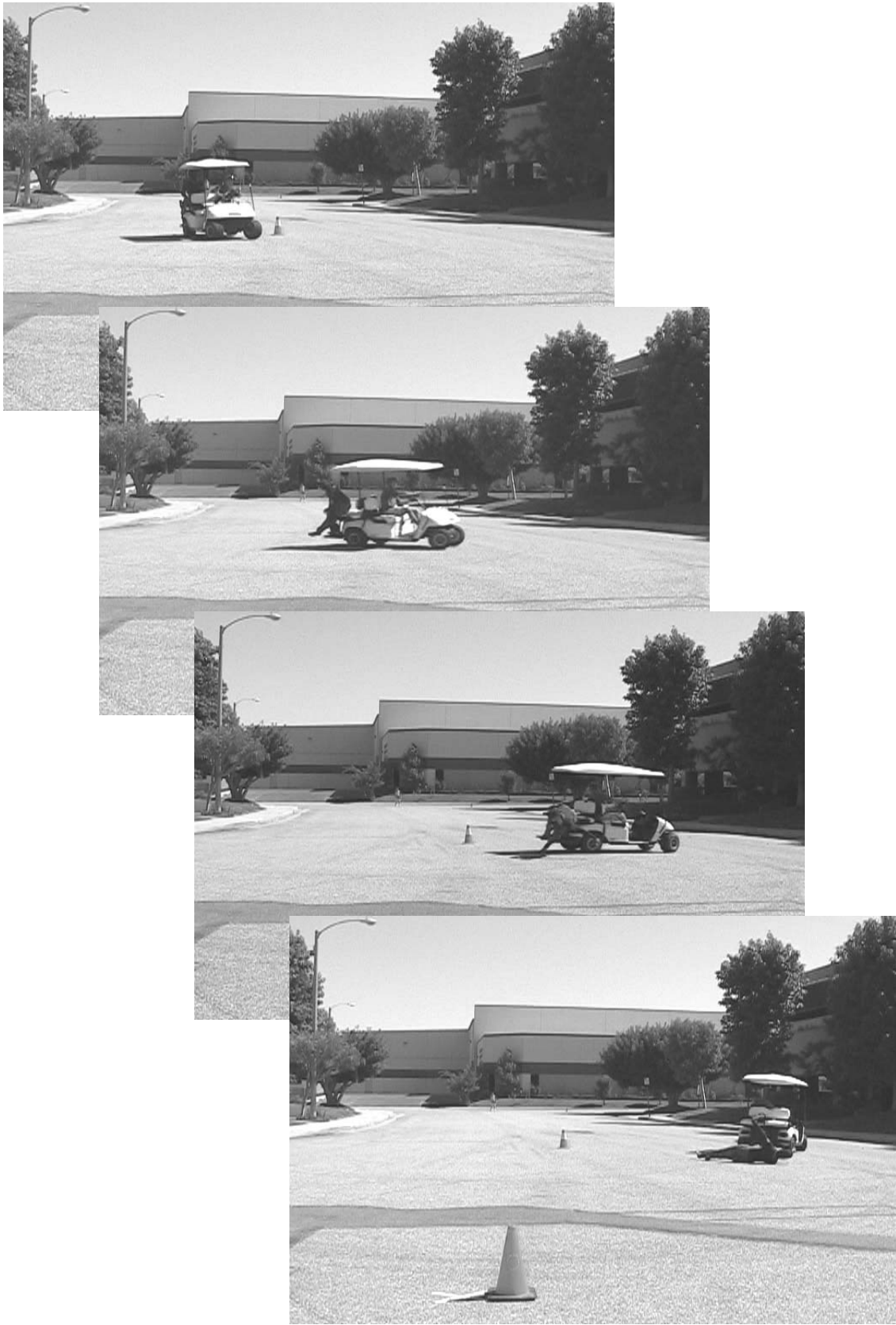
**Figure A2 - Test 1\_6 retention of belted occupant during J-Turn maneuver**



**Figure A3 – Test 2\_3 ejection of unbelted occupant during J-Turn maneuver**

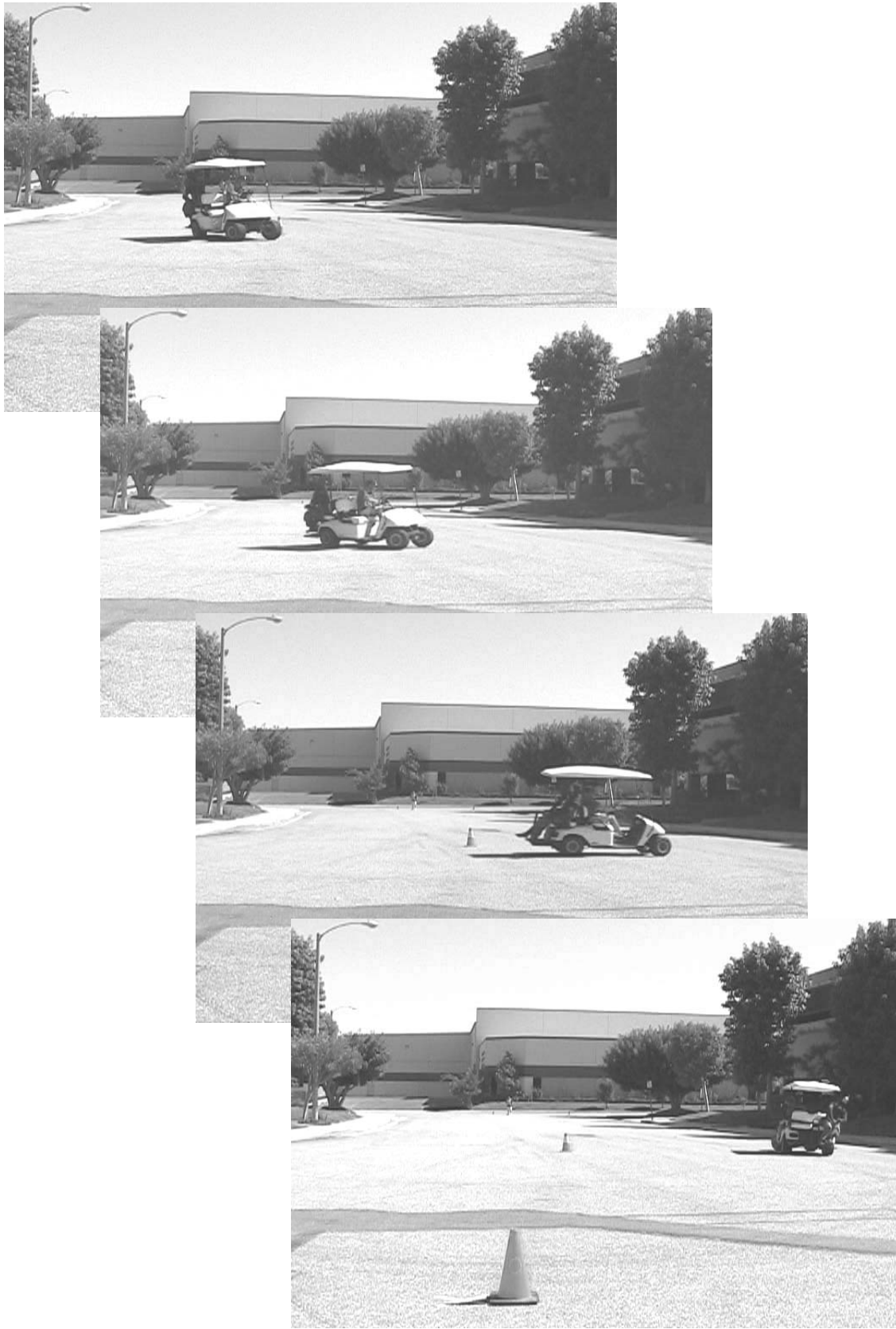


**Figure A4 – Test 2\_4 retention of belted occupant during J-Turn Maneuver**

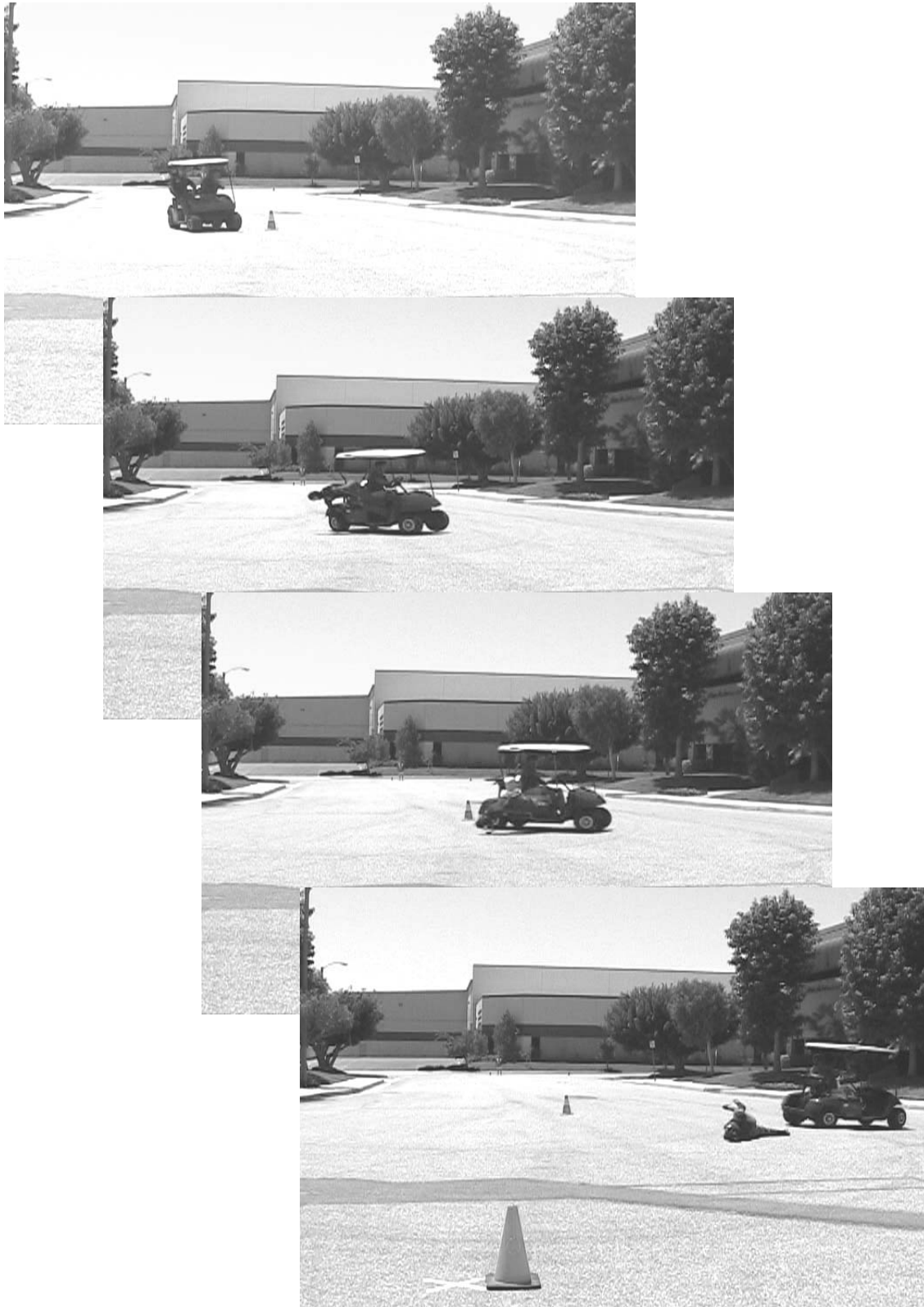


**Figure A5 – Test 3\_3 ejection of unbelted occupant during J-Turn maneuver**

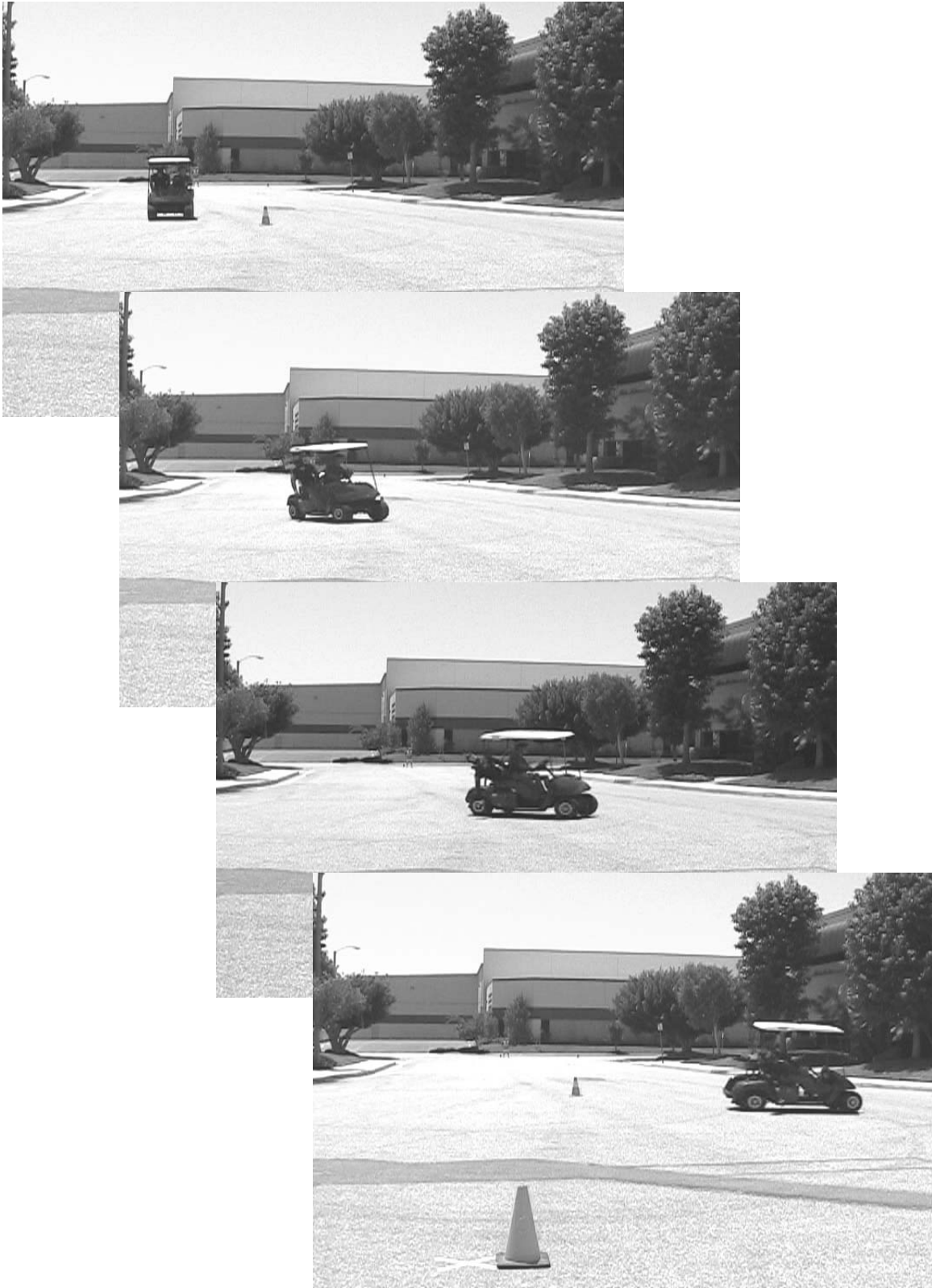




**Figure A6 – Test 3\_4 retention of belted occupant during J-Turn Maneuver**



**Figure A7 – Test 4\_5 ejection of unbelted occupant during J-Turn Maneuver**



**Figure A8 – 4\_6 retention of belted occupant during J-Turn Maneuver**